



PHOTOSENSITIVE POLYMERS AND THEIR APPLICATION.

Anna Trojanowska

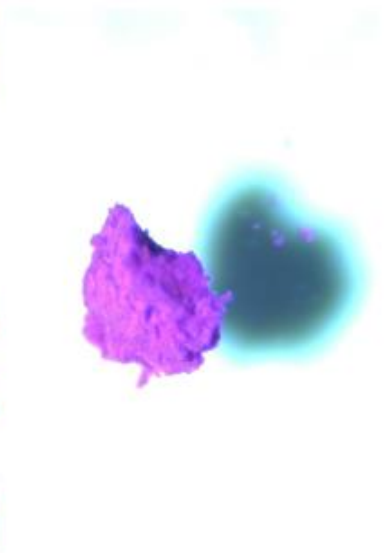
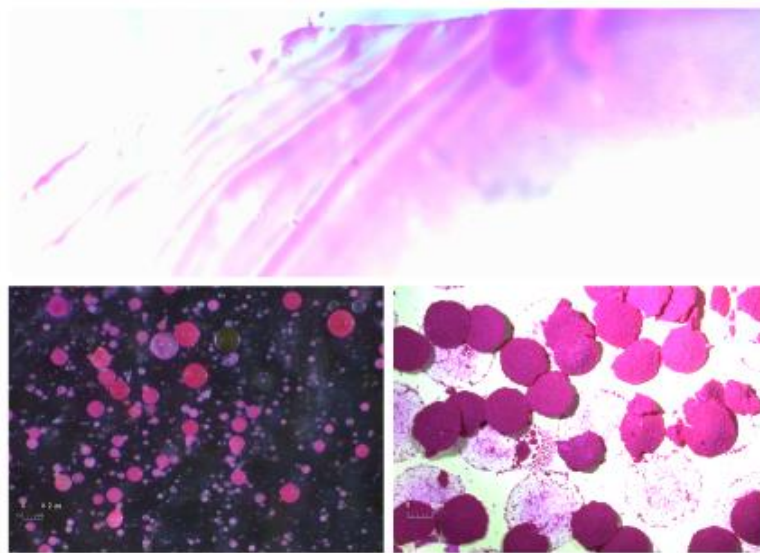
ADVERTIMENT. L'accés als continguts d'aquesta tesi doctoral i la seva utilització ha de respectar els drets de la persona autora. Pot ser utilitzada per a consulta o estudi personal, així com en activitats o materials d'investigació i docència en els termes establerts a l'art. 32 del Text Refós de la Llei de Propietat Intel·lectual (RDL 1/1996). Per altres utilitzacions es requereix l'autorització prèvia i expressa de la persona autora. En qualsevol cas, en la utilització dels seus continguts caldrà indicar de forma clara el nom i cognoms de la persona autora i el títol de la tesi doctoral. No s'autoritza la seva reproducció o altres formes d'explotació efectuades amb finalitats de lucre ni la seva comunicació pública des d'un lloc aliè al servei TDX. Tampoc s'autoritza la presentació del seu contingut en una finestra o marc aliè a TDX (framing). Aquesta reserva de drets afecta tant als continguts de la tesi com als seus resums i índexs.

ADVERTENCIA. El acceso a los contenidos de esta tesis doctoral y su utilización debe respetar los derechos de la persona autora. Puede ser utilizada para consulta o estudio personal, así como en actividades o materiales de investigación y docencia en los términos establecidos en el art. 32 del Texto Refundido de la Ley de Propiedad Intelectual (RDL 1/1996). Para otros usos se requiere la autorización previa y expresa de la persona autora. En cualquier caso, en la utilización de sus contenidos se deberá indicar de forma clara el nombre y apellidos de la persona autora y el título de la tesis doctoral. No se autoriza su reproducción u otras formas de explotación efectuadas con fines lucrativos ni su comunicación pública desde un sitio ajeno al servicio TDR. Tampoco se autoriza la presentación de su contenido en una ventana o marco ajeno a TDR (framing). Esta reserva de derechos afecta tanto al contenido de la tesis como a sus resúmenes e índices.

WARNING. Access to the contents of this doctoral thesis and its use must respect the rights of the author. It can be used for reference or private study, as well as research and learning activities or materials in the terms established by the 32nd article of the Spanish Consolidated Copyright Act (RDL 1/1996). Express and previous authorization of the author is required for any other uses. In any case, when using its content, full name of the author and title of the thesis must be clearly indicated. Reproduction or other forms of for profit use or public communication from outside TDX service is not allowed. Presentation of its content in a window or frame external to TDX (framing) is not authorized either. These rights affect both the content of the thesis and its abstracts and indexes.

Photosensitive polymers and their applications

Anna Trojanowska



DOCTORAL THESIS
2020

UNIVERSITAT ROVIRA I VIRGILI

PHOTOSENSITIVE POLYMERS AND THEIR APPLICATION.

Anna Trojanowska

UNIVERSITAT ROVIRA I VIRGILI

PHOTOSENSITIVE POLYMERS AND THEIR APPLICATION.

Anna Trojanowska

UNIVERSITAT ROVIRA I VIRGILI

PHOTOSENSITIVE POLYMERS AND THEIR APPLICATION.

Anna Trojanowska

Anna Trojanowska

Photosensitive polymers and their applications

DOCTORAL THESIS

supervised by

Dr. Marta Giamberini

Dr. Bartosz Tylkowski

DEPARTMENT OF CHEMICAL ENGINEERING



Universitat Rovira i Virgili

Tarragona 2020

UNIVERSITAT ROVIRA I VIRGILI

PHOTOSENSITIVE POLYMERS AND THEIR APPLICATION.

Anna Trojanowska



UNIVERSITAT
ROVIRA I VIRGILI

Department d'Enginyeria Química
Av. Paisos Catalans, 26
43007 Tarragona, Spain

I STATE that the present study, entitled "Photosensitive polymers and their applications", presented by Anna Trojanowska for the award of the degree of Doctor, has been carried out under my supervision at the Department Chemical Engineering of this university

Tarragona, 13 of March 2020

Doctoral Thesis Supervisors


Dr. Marta Giamberini


Dr. Bartosz Tylkowski

UNIVERSITAT ROVIRA I VIRGILI
PHOTOSENSITIVE POLYMERS AND THEIR APPLICATION.
Anna Trojanowska

I Acknowledgements

Firstly, I would like to express my deepest sincere gratitude to my incredible advisers Dr. Marta Giamberini and Dr. Bartosz Tylkowski for the opportunity to join the doctoral programme under their supervision, for the continuous support of my PhD study and related research, for their patience, motivation, and immense knowledge. Their guidance helped me in all the time of research and writing of this thesis. I could not have imagined having better and friendlier advisers and mentors for my PhD study.

This thesis was possible thanks to the strong collaboration between industry and academia. Thanks must be given to the following Procter & Gamble Company employees: Luke Zannoni, Calum Macbeath, Johan Smets, Todd Underiner. I would like to give a special thanks to Susana Fernandez Prieto for counseling and the time she dedicated to this PhD project.

Moreover, I would like to thank professors of Chemical Engineering Department of Organic Chemistry and Chemical Engineering for their help and word of advice. I am also thankful to technicians of Department of Chemical Engineering. As well, I would like to thank Josep Maria Montornes and Núria Juanpere for their help in all the administrative issues.

My sincere thanks also goes to all technicians of Servei de Recursos Científics i Tècnics for kindly helping me in my sample analysis, especially Mariana Stefanova, Mercè Moncusí, Rita Marimon, and Ramón Guerrero.

I would like to thank Memtec group, full of extraordinary and smart people. Thank you for your help: Professor Ricard Garcia Valls, Professor Tània Gumí, Professor José Antonio Reina,

Josefa Lázaro, Xavier, Monika, Kamila, Adrianna, Magda, Cristina, Krzysiu, Rubén, Cinta, Mario, Rita, Mimmo, Gianmarco.

My stay in Tarragona would not be so fantastic without special people I met on my way. I could never imagine that I would find such a special group of friends.

I would like to thank to students, which worked with me: Michalina Wroblewska, Mikolaj Podlewski, Michalina Jezierska, Lukasz Marciniak, Jaime Gascon Puente, and Amadeusz Wos.

You were these people, who gave me an important lesson - how to share my knowledge and how to be a tutor. Each one of you was different and special for me. Thank you for that!

Thank you does not seem enough for all what we went through together.

A special thanks goes to my incredible family. I am truly grateful for my incredible daughter Nina. She uplifts me, comforts me and brings joy to my soul. She gives me strength to overcome any challenges. I am also truly thankful to my parents and my siblings for support, understanding, help and love. This would not be possible without my lovely family. I love you!

Finally, financial support from Martí-Franquès Research grants Programme from Universitat Rovira i Virgili are gratefully acknowledged.

Thank you all for your advices, guidance and support!

II Table of contents

I	Acknowledgements.....	I
II	Table of contents.....	III
III	Figure index	V
IV	Table index.....	XI
V	List of abbreviations	XII
VI	List of publications resulting from the thesis.....	XIV
VII	Summary	XVI
1	Introduction.....	1
1.1	Photosensitive compounds - state of art	1
1.1	Capsules.....	4
1.1.1	Chemical Methods	7
1.1.2	Physico-Chemical Methods	8
1.1.3	Physico-Mechanical Methods	12
2	Objectives & hypothesis	16
3	Preparation of photoactive compound	17
3.1	Introduction	17
3.2	Materials and methods.....	22
3.3	Results and discussion.....	26
3.4	Conclusions	29
4	Polymer modification	30
4.1	Introduction	30
4.2	Materials and methods.....	34
4.3	Results and discussion.....	38
4.4	Conclusions	54

5	Photosensitivity studies	56
5.1	Introduction	56
5.2	Materials and methods	61
5.3	Results and discussion.....	63
5.4	Conclusions	72
6	Applications.....	73
6.1	Membranes	73
6.1.1	Introduction.....	73
6.1.2	Materials and methods	74
6.1.3	Results and discussion	76
6.1.4	Conclusions.....	89
6.2	Capsules	90
6.2.1	Introduction.....	90
6.2.2	Materials and methods	91
6.2.3	Results and discussion	96
6.2.4	Conclusions.....	114
7	Acrylates	116
7.1	Introduction	116
7.2	Materials and methods	117
7.3	Results and discussion.....	121
7.4	Conclusions	128
8	Overall conclusions	130
9	References	133

III Figure index

Figure 1. Transformation between two chemical species of different absorption spectra: A and B. Reverse reaction occurs photochemically (type P photochromism) (a); or thermally (type T photochromism) (b).	1
Figure 2. Graphical representation of a capsule.....	4
Figure 3. Schematic representation of structures of the capsules. From left: continuous core/shell microcapsule, polycore capsule, continuous core capsule with more than one layer of shell material, and matrix capsule type.....	5
Figure 4. Publications per year on Encapsulation (tool used: Web of Science, February 2020).	6
Figure 5. Schematic presentation of the complex coacervation process.....	9
Figure 6. Schematic presentation of the spray drying process...	11
Figure 7. Schematic presentation of the co-extrusion process...	13
Figure 8. Graphical representation of SCIII polymers structure.	18
Figure 9. Graphical representation of the synthetic approach to achieve the photosensitive poly(styrene-malic anhydride) modified with donor-acceptor adducts (SCIII).	19
Figure 10. Knoevenagel condensation of an aldehyde with Meldrum's acid.	20
Figure 11. Meldrum's acid structure (a); Meldrum's acid in a boat conformation (b); unoccupied orbital pictures of reaction center of Meldrum's acid was reprinted from [1] (c).	20
Figure 12. Michael addition of Meldrum's acid to 5-alkenyl-2,2-dimethyl-1,3-dioxane-4,6-dione.....	22
Figure 13. ^1H NMR spectra for 5-alkenyl-2,2-dimethyl-1,3-dioxane-4,6-dione. ^1H NMR (400 MHz, $(\text{CD}_3)_2\text{SO}$) δ 1.72 (s, 6H),	

6.95 (dd, $J = 3.9, 1.5$ Hz, 1H), 8.12 (s, 1H), 8.27 (d, $J = 3.7$ Hz, 1H), 8.33 (d, $J = 1.5$ Hz, 1H).....	26
Figure 14. Synthetic approach to achieve the photosensitive poly(styrene-maleimide) modified with donor-acceptor adducts (SCIII).....	31
Figure 15. Schematic representation of the malic anhydride reaction with nucleophiles.	32
Figure 16. Schematic representation of Amberlyst® 15 structure.	33
Figure 17. Schematic representation of thermal 4- π conrotatory electrocyclization transformation of Stenhouse salts.....	34
Figure 18. SMA structure (a); experimentally collected data of C7 carbon integrations (b); and corresponded ^{13}C NMR spectra (c).	41
Figure 19. SMA reaction with n-methyl ethylene diamine.....	45
Figure 20. Schematic representation of interactions between resin and SMA.....	46
Figure 21. FT-IR spectra recorded at RT in absorption mode of SMA FLAKE 1000 (black line) and modified FLAKE 1000 (red line)(a); FT-IR spectra recorded at RT in absorption mode of five different modifications of poly(styrene-maleimide) (b) ; table of bonds assignments of SMA and modified SMA, SCII (c).....	47
Figure 22. Two-dimensional separated local field spectrum shows a signal for the ^{15}N - ^1H dipolar interaction.	49
Figure 23. Reaction scheme between 5-(furan-2-ylmethylene)-2,2-dimethyl-1,3-dioxane-4,6-dione and poly(styrene-co-maleimide).	50
Figure 24. ^1H NMR spectra of SCIII (a); SCIII generic structure (b); table of chemical shifts assignments of SCIII (c).	51
Figure 25. SMA modified with DASA photoswitching scheme.	56
Figure 26. DASA photoswitching mechanistic proposal. Reprinted from [2].	59

Figure 27. UV-Vis spectra of SCIII polymers in chloroform at RT.	64
Figure 28. Photoswitching degree of SCIII polymers.....	65
Figure 29. UV-Vis spectra of SCIII EF 40 polymer before (black line) and after (red line) light excitation.	66
Figure 30. Table with the rate constants of SCIII EF 60 at different temperatures (a) with corresponding spectra (b).....	67
Figure 31. Arrhenius plot with a fitting $R^2=0.95$, (a) and Eyring plot with a fitting $R^2=0.94$ (b) for relaxation of SCIII EF 60 ...	69
Figure 32. UV-Vis spectra of SCIII in different mediums.	70
Figure 33. FT-IR spectra recorded at RT in absorption mode of SCIII Flake 1000 before (black line) and after (orange line) illumination.	71
Figure 34. Optical microscope images of the SCIII membranes surfaces.....	77
Figure 35. AFM topographic images of membranes that were not exposed to light (a-e) and after 30min of samples irradiation with visible light (a'-e').	79
Figure 36. Roughness average change before (dark) light exposure and after (light) for each SCIII membrane.	80
Figure 37. RMS roughness obtained for each SCIII membranes before (dark) light exposure and after (light) (a); Table specifying the content of DASA in each membrane (b).....	81
Figure 38. FT-IT spectra of membrane made with SCIII FLAKE 1000. Blue line (dark) corresponds to spectra collected for the membrane before light exposure; and green line (light) for the spectra of the irradiated sample.....	82
Figure 40. The differences between the average roughness before and after light exposure plotted against the degree of photoisomerization in respect to SCIII polymer modification...	84
Figure 39. Degree of SCIII membranes photoswitching versus DASA content in each membrane.....	84

Figure 41. Photoisomerization degree of SCIII polymers plotted against corresponding molecular weight.	85
Figure 42. CA images of the SCIII FLAKE 1000 membranes. Image left: water drop on the sample not exposed to light (a); image right: water drop on the irradiated sample (b).....	86
Figure 43. CAs were plotted against the SCIII polymers modifications.....	87
Figure 44. Difference in CAs before and after light exposure were plotted against the SCIII polymers modifications.	88
Figure 45. Phase-inversion precipitation technique set-up.	96
Figure 46. MC1 capsules with encapsulated THF made by PIP method.....	98
Figure 47. Voyager Zen encapsulated by SCIII EF 80 in PIP method at 20°C (top, red frame) and 0°C (bottom, green frame).	99
Figure 48. ESEM micrographs of MC3 capsules and corresponding size distributions data.....	100
Figure 49. MC3 capsules cross-section ESEM micrograph. ...	101
Figure 50. MC3 capsules size distributions and ESEM micrographs before light exposure (left side of the Figure), and afterlight exposure (right side of the Figure).	102
Figure 51. ESEM microscope images of MC4 capsules.....	103
Figure 52. Terpolymer of molar ratio ST-styrene, MA-maleic anhydride, MI-maleimide; 4ST : 1MA : 2MI.	104
Figure 53. Scheme of the reaction between SMA/DASA terpolymer and 1.8-diaminooctane.	105
Figure 54. Scheme of MC4 encapsulation process.....	105
Figure 55. Optical microscope images of MC5 capsules with corresponding size distribution data.	106
Figure 56. Optical microscope images of MC5 capsules after 4 days of their preparation.	107
Figure 57. Scheme of MC6-10 encapsulation process.....	107

Figure 58. Optical microscope images of MC6 capsules with corresponding size distribution data.....	108
Figure 59. Optical microscope images of MC6 capsule upon irradiation.	109
Figure 60. Scheme of MC11 encapsulation process.	109
Figure 61. Optical microscope images of MC11 capsules with corresponding size distribution data.....	110
Figure 62. Optical microscope images of MC11. During preparation process; emulsion (a), immediately after amine addition (b), after completion of the process (c).	111
Figure 63. Optical microscope micrographs of MC11 capsules taken at 0min (a) and 80min (b).	111
Figure 64. Optical microscope micrographs of MC11 capsule taken during 0min and 80min light irradiation.	112
Figure 65. Confocal laser scanning microscop images of MC11 capsule.	113
Figure 66. Reaction between 2-(tert-butylamino)ethyl methacrylate and SCI.	121
Figure 67. ¹ H NMR spectra for Acrylate/DASA. ¹ H NMR (400 MHz, (CDCl ₃) (a); generic structure of Acrylate/DASA (b); table of chemical shifts assignments of Acrylate/DASA (c). Additional peaks not include in (c) are assigned to residual solvents.....	122
Figure 68. Acrylate/DASA suspected behaviour upon light exposed and corresponding thermal relaxation.	123
Figure 69. UV-Vis spectra of Acrylate/DASA polymers in chloroform at RT.	123
Figure 70. Scheme of NH ₂ functionalized capsules modification with SCI.	124
Figure 71. Scheme of the Acrylate/DASA capsules preparation.	125
Figure 72. Optical micrographs of NH ₂ functionalized capsules modified with SCI.	125

Figure 73. Optical microscope images of Acrylate/DASA capsules with corresponding size distribution data..... 126

Figure 74. Release of encapsulated perfume analysed by dynamic headspace (DHS) gas chromatography results for Acrylate/DASA capsules. Sample subjected to visible light (light) and sample kept in dark (dark)..... 127

IV Table index

Table 1 Capsule's size range obtained by each technique.	5
Table 2. Condition variables for large scale reactions.	25
Table 3. Condition variables for small scale reactions.	25
Table 4. SMA characteristics supplied by Cray Valley Total....	30
Table 5. SMA compositions supplied by Cray Valley Total and calculated by means of NMR and titration.	39
Table 6. SMAs Run numbers values.....	42
Table 7. SMAs number average sequence lengths.....	43
Table 8. Probability for diads and triads arrangement within the copolymer chain.	44
Table 9. SMA modification percentage results.....	48
Table 10. ¹ H NMR quantitative analysis of SCIII polymers.	50
Table 11. DSC analysis of the starting copolymers and polymers before and after modifications.	52
Table 12. RMS roughness of SCIII membranes before light exposure (dark) and after (light).	78
Table 13. Photoisomerization degree of SCIII membranes.	83
Table 14. CAs of SCIII membranes measured before (CA dark) and after (CA light) light exposure with corresponding standard deviations.	86
Table 15. GC analysis of the free perfume content in the MC11 capsules slurry.	112

V List of abbreviations

^1H , ^{13}C , ^{15}N NMR	proton, carbon and nitrogen nuclear magnetic resonance
A_∞	absorption at the photostationary state.
AFM	atomic force microscope
A_vS	number average sequence length
CA	contact angle
DASA	Donor-Acceptor Stenhouse adducts
DHS–TD	dynamic headspace–thermal desorption
DMF	dimethylformamide
DSC	differential scanning calorimetry
ESEM	environmental scanning electron microscope
FT-IR	Fourier transform infrared spectroscopy
GC–MS	gas chromatography–mass spectrometry
PIP	phase inversion precipitation
PVA	poly(vinyl alcohol)
$R_{n \text{ exp}}$	experimentally calculated Run Number
$R_{n \text{ random}}$	Random Run Number
RT	room temperature
SCI	5-(furan-2-ylmethylene)-2,2-dimethyl-1,3-dioxane-4,6-dione

SCII	poly(styrene-maleimide)
SCIII	poly(styrene-maleimide) modified with DASA
SMA	poly(styrene-co-maleic anhydride)
TBA	2-(tert-butylamino)ethyl methacrylate
T _g	glass transition temperatures
THF	tetrahydrofuran
TLC	thin layer chromatography

VI List of publications resulting from the thesis

PATENT:

Inventors: Bartosz Tylkowski, Anna Trojanowska, Luke Zannoni, Marta Giamberini, Calum Macbeath, Johan Smets, Todd Underiner

Title: Photosensitive microcapsules

Title holder entity: Procter & Gamble International Operations SA,

European Patent Application Number: 17382567.0-1468

United States Patent Application: 20190049838

PUBLICATIONS:

1. Anna Trojanowska, Nuno A.G. Bandeira, Adrianna Nogalska, Valentina Marturano, Marta Giamberini, Pierfrancesco Cerruti, Veronica Ambrogi, Bartosz Tylkowski, Squeezing release mechanism of encapsulated compounds from photo-sensitive microcapsules, published in Applied Surface Science, 2019, 472, pp. 143-149.
2. Anna Trojanowska, Valentina Marturano, Nuno A.G. Bandeira, Marta Giamberini, Bartosz Tylkowski, Smart microcapsules for precise delivery systems, published in Functional Materials Letters, 2018, 11(5), Article number 1850041.
3. Rita Del Pezzo, Nuno A.G. Bandeira, Anna Trojanowska, Susana Fernandez Prieto, Todd Underiner, Marta Giamberini, Bartosz Tylkowski, Ortho-substituted

- azobenzene: Shedding light on new benefits, published in Pure and Applied Chemistry, 2018, article in press.
4. Bartosz Tylkowski, Anna Trojanowska, Valentina Marturano, Martyna Nowak, Lukasz Marciniak, Marta Giamberini, Veronica Ambrogi, Pierfrancesco Cerruti, Power of light – Functional complexes based on azobenzene molecules, published in Coordination Chemistry Reviews, 2017, 351, pp. 205-217.
 5. Anna Trojanowska, Adrianna Nogalska, Ricard G. Valls, Marta Giamberini, Bartosz Tylkowski, Technological solutions for encapsulation, published in Polymer Engineering, 2017, pp. 171-201.
 6. Anna Trojanowska, Marta Giamberini, Irene Tsibranska, Martyna Nowak, Lukasz Marciniak, Renata Jatrزاب, Bartosz Tylkowski, Microencapsulation in food chemistry, published in Journal of Membrane Science and Research, 2017, 3(4), pp. 265-271.

VII Summary

This thesis focuses on synthesis of novel photosensitive polymers and their successive application in photo-triggered microcapsules preparation. In particular, the project aims at incorporation of photosensitive moiety - Donor-Acceptor Stenhouse adducts (DASA) within polymeric matrixes. Mainly two distinct approaches were followed in this thesis.

First approach involves incorporation of DASA within the side chain of commercially available polymers, specifically five types of poly(styrene-co-maleic anhydride) (SMA) with different molecular weights and molar ratio compositions. As prepared modified polymers were then applied to obtain microcapsules containing active agents, such as perfumes provided by Procter & Gamble Company.

Second approach involves modification of a methacrylate (2-(tert-Butylamino)ethyl methacrylate (TBA)) monomer with DASA and then its subsequent application for microcapsules preparation by interfacial polymerization method. Both approaches lead to our final goal which is preparation of capsules with phototriggered controlled release of encapsulated cargo.

In order to reach the objectives, the following studies were performed:

- I. Preparation of DASA precursor;
- II. SMA modification with DASA moieties to obtain photoactive polymers (SCIII);
- III. Studies of SCIII polymers behaviour upon light exposure;
- IV. Application of SCIII polymers to obtain membrane and capsules. Subsequent characterization of prepared material;

- V. Modification of TBA with DASA moieties and its characterization;
- VI. Preparation of photosensitive polyacrylates capsules containing DASA moieties within its matrix and their performance evaluation.

During first year of this PhD thesis, an optimization of the synthesis of 5-(furan-2-ylmethylene)-2,2-dimethyl-1,3-dioxane-4,6-dione was carried out. This molecule serves as DASA precursor required for the modification of the polymeric matrix. Optimization of preparation procedure, previously reported in the literature, was successfully performed. Results obtained from this part provide a more robust and a practical method to gain a high yield of 5-(furan-2-ylmethylene)-2,2-dimethyl-1,3-dioxane-4,6-dione in water without the need of a catalyst, making the process more economically efficient, less tedious, sustainable and environmentally friendly.

In the second stage, the modifications of the five commercially available SMA copolymers were studied. Within this task, first the maleic anhydride group of the SMA copolymers were modified with 2°amines. Despite the fact that, the reaction between maleic anhydride group and primary amines is known in the literature; investigation on the reaction conditions was required to get poly(styrene-co-maleimide)s (SCII). Then, the purified SCIIs were used in the reaction with previously synthesised DASA – precursor to create copolymers with photosensitive properties (SCIII).

In the third part, the photosensitive performance of the final SCIII polymers was exhaustively investigated. The negative type T photochromism as well as the solvatochromism of DASA molecules were retained after its incorporation within SMA structure. It was conjectured that the mechanism of the photoswitching was preserved after polymer modification, as

described previously in the literature. The alternation of the photoisomerization kinetics between parent DASA and modified polymers containing DASA moieties in their structures was investigated and deeply analysed. Two separate models were applied: Eyring and Arrhenius to describe changes in a rate of chemical transition against temperature.

In the fourth stage, membranes and series of microcapsules containing SCIII polymers were fabricated. The membranes were prepared in order to facilitate the investigation of the SCIII polymers physicochemical properties. It was assumed that SCIII membranes will mimic the behaviour of the photosensitive microcapsules shell. Thus, the membranes were obtained by solvent evaporation method. Four techniques were used to prepare the capsules: 1) phase inversion precipitation; 2) emulsion crosslinking of partially modified SCIII copolymer (DASA modified polymer, molar ratio ST-styrene, MA-maleic anhydride, MI-maleimide; 4ST : 1MA : 2MI; 3) SMA/SCIII emulsion precipitation in different non-solvents; 4) emulsion crosslinking of SCIII with SMA blend. Membranes modification upon light exposure were analysed by means of AFM, CA and FT-IR analysis. SCIII polymers capsules behaviour upon light exposure were analysed by means of ESEM, optical microscope and GC analysis.

In the fifth stage synthesis Acrylate/DASA molecule was performed, in order to use it for microcapsule shell preparation employing a protocol developed by scientists from P&G Company. Indeed, during the next step of the thesis the Acrylate/DASA molecule was used together with 2 other acrylate resins (provided by P&G) for capsules preparation.

Furthermore, during the sixth stage of the PhD thesis, surfaces of acrylate capsules provided by P&G Company were modified with DASA precursor. Obtained capsules were characterized by means

of optical microscope and dynamic headspace–thermal desorption (DHS–TD) combined with gas chromatography–mass spectrometry (GC–MS).

UNIVERSITAT ROVIRA I VIRGILI
PHOTOSENSITIVE POLYMERS AND THEIR APPLICATION.
Anna Trojanowska

1 Introduction

1.1 Photosensitive compounds - state of art

This Chapter will explain the basic concepts of organic photochromism and will give an overview of the organic photochroms reported up to date.

Photochromism is defined by IUPAC as “a reversible transformation of a molecular entity between two forms, A and B, having different absorption spectra, induced in one or both directions by absorption of electromagnetic radiation” [3]. In most cases the thermodynamically stable form A is colourless or pale yellow, and then upon absorption of electromagnetic radiation it transforms to coloured form B. This phenomenon is known as a positive photochromism in opposite to inverse or negative photochromism, where form A is coloured and it fades upon irradiation with light into form B. As mentioned in its definition this transformation from A to B is reversible. Commonly, the transformation from A to B is called “switch on”, while the back reaction is called “switch off”. The latter can occur in two ways: thermally (type T) or photochemically (type P). The reaction scheme between A and B from is presented in Figure 1.

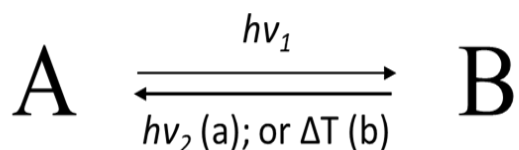


Figure 1. Transformation between two chemical species of different absorption spectra: A and B. Reverse reaction occurs photochemically (type P photochromism) (a); or thermally (type T photochromism) (b).

There is a number of parameters that are useful in describing the performance of organic photochromes, such as:

- fatigue – describes a loss of switching on-off performance over time. Organic photochromes performance can be affected by side reactions that cause their degradation, for instance: photooxidation, electron-transfer to organic and inorganic acceptor, trapping of free radical species, and reactions with nucleophiles [4, 5];
- number of cycles – is a number of switching-on and switching-off transformation that a molecule can perform before its total degradation [5];
- half-life – is an unit of time that is required to lower in half the intensity of absorbance maximum of the coloured chemical specie [6];
- rate of the transformation – is a speed at which a transition between A to B proceeds; etc.

Nature of the chemical transformation that occurs between form A and form B depends on the photochrom class. According to the literature, there are thirteen families of photochromic organic compounds. Among them are: spiropyrans, spirooxazines, chromenes, fulgides and fulgimides, diarylethenes, spirodihydroindolizines, azo compounds, polycyclic aromatic compounds, anils, polycyclic quinones, perimidinespirocyclohexadienones, viologens, triarylmethanes[6]. In general, each class of photochroms will differ in photoswitching mechanisms. However, five main process can be singled out:

- *E-Z* isomerization of double bonds occurs mainly for stilbenes, azo compounds;
- Electron transfer can be detected in cell chlorophyll, viologens;
- Intramolecular hydrogen transfer is found in anils, benzylpyridines;
- Dissociation processes occur in triarylmethanes;

- Pericyclic reactions are found in spiropyrans, spirooxazines, fulgides.

One of the most extensively studied class of photochromic compounds are azobenzene and its derivatives. It was extensively employed for its remarkable change in volume, resulting from a *trans* to *cis* isomerization, upon irradiation [7]. Other photochromes that were of interest are spiropyrans and diarylethenes. Their unique changes in spectral properties upon photoswitching were exploited in a number of applications. Moreover, spiropyran exhibiting the added benefit of a solubility switch, or a conversion from a hydrophobic to a hydrophilic form, upon irradiation [8-10]

Despite their ubiquity and broad utility, these special classes of photochromes typically all require the use of high-energy UV light to trigger their photochemical reactions. This hinders their potential use in biomedical applications and material science because UV light can be damaging to healthy cells and results in degradation for many macromolecular systems. Fatigue resistance is also a primary concern for UV-based photochromic switches. A common design principle to address this problem is to make synthetic modifications to these known classes of photochromic compounds that enable the use of visible light [11, 12].

The photochrome that was used in this PhD thesis is Donor Acceptor Stenhouse adduct (DASA). Its preparation will be described in details in Chapter 3 and 4, while its photosensitive behaviour will be addressed in Chapter 5. Structurally DASA molecules are similar to merocyanine dyes. Both can be described as a polymethine dyes i.e. chromophoric systems consist of conjugated double bonds (polyenes) located between two end groups: an electron acceptor and an electron donor [13]. What distinct DASA molecules from other polymethine dyes is that they consist of a hydroxy group within polyenes chain [14]. The

photoswitching in case of DASA was discovered to have at least two key steps: 1) photoinduced *Z-E* isomerization within the triene chain; 2) 4π thermal electrocyclization followed by a proton transfer and tautomerization [2].

1.1 Capsules

In general, capsules are a circular cross-section shape particles with certain free volume inside, where a core material can be allocated. Figure 2 provides a graphical illustration of a single capsules. Encapsulation may be also explained in the frames of supramolecular chemistry as a process where a guest molecule is confined inside the cavity of a host and leads to formation of a capsule. Capsules can exhibit different morphologies dependent on the material used to prepare them. Although, also the preparation technique has a huge impact on their final outcome [2]. Microcapsules diameter sizes varies in the range of 1-

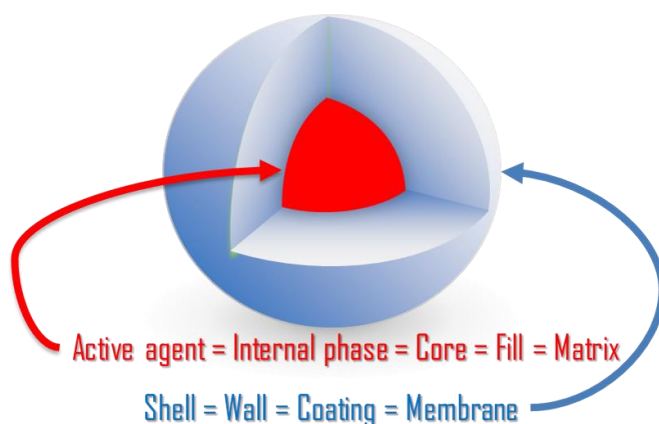


Figure 2. Graphical representation of a capsule.

1000 μm , if its below 1 μm they are called nanocapsules and above 1000 μm – macrocapsules.

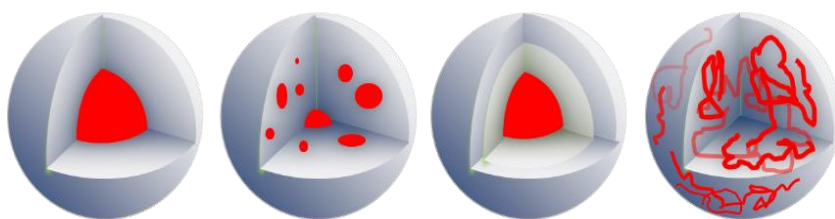


Figure 3. Schematic representation of structures of the capsules. From left: continuous core/shell microcapsule, polycore capsule, continuous core capsule with more than one layer of shell material, and matrix capsule type.

Depending on the structure of the capsules, they can be characterized as: continuous core/shell microcapsule; polycore capsule; continuous core capsule with more than one layer of shell material; and the matrix type; where encapsulated agent is incorporated within the shell material. Representation of aforementioned structures of the capsules is shown in Figure 3 [5].

Relying on the preparation method used different morphologies of the capsules will be expected. Rough approximation of the capsule's size range obtained by each technique is presented in Table 1.

Table 1 Capsule's size range obtained by each technique.

Chemical methods	Interfacial polymerization						
	In situ polymerization						
Physico-chemical methods	Coacervation						
	Layer by Layer						
	Sol-gel encapsulation						
Physico-mechanical methods	Suspension crosslinking						
	Spray drying						
	Co-extrusion						
	Spinning disk						
	Fluidized bed spray coating						
	Phase inversion precipitation						
		0,1	1	10	100	1000	10000
		Size Range [μm]					

Encapsulation is a dynamic research field, over the last decades research regarding encapsulation expanded due to novel technologies, production paths and demand for innovative applications. Running a search on “encapsulation” over 100,000 records can be found from 1920 to 2010, as it is illustrated in Figure 4, by the use of Web of Science tool. Taking into account the data provided in this figure it is an obvious that encapsulation technology is a prominent and augmenting topic.

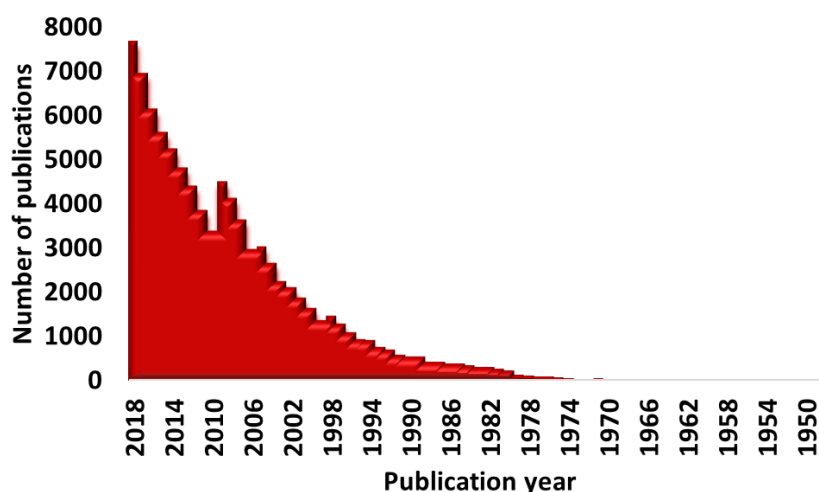


Figure 4. Publications per year on Encapsulation (tool used: Web of Science, February 2020).

Numerous methods were developed for the preparation of nano-micro- and mili-capsules. First, chemical methods will be described, such as interfacial polymerization, in situ polymerization (suspension, emulsion, dispersion polymerization). Then, information about physico-chemical methods will be provided, namely coacervation, layer-by-layer assembly, sol-gel encapsulation, suspension crosslinking. Finally, we will describe physic-mechanical methods, such as spray drying, co-extrusion, centrifugal techniques, phase inversion precipitation.

1.1.1 Chemical Methods

Chemical methods involve sphere fabrication along with various polymerization reactions. This indicates that the starting materials in these cases will be monomers or prepolymers. Further subdivision of these techniques along with a short description is detailed below.

Interfacial polymerization - takes place at the interface between two immiscible liquids, each of the liquids contain reactive monomers that polymerize when get in contact with each other [15]. One of its major advantages is its controllable character. Capsule mean size and membrane thickness can be directly designed [16]. Interfacial polymerization's tuneable conditions make it applicable to various camps e.g. agrochemicals, self-healing, pharmaceuticals and cosmetics. As far as it is reported in patents and publication, mainly four groups of polymers were consider by researchers utilizing this technique: polyamides, polyurethanes, polyureas and polyesters. This technique can be classified as a relatively simple, flexible and of low cost, thus it is a valid method for industrial capsules manufacturing. Nevertheless, it seems that the process is still not well understood e.g. the effect of the temperature, catalyst, surfactant and active ingredient is not entirely clear [17, 18].

In situ polymerization - is a broad concept that includes suspension, emulsion and dispersion polymerization. The literal translation of *in situ* means "in place", what in terms of polymer science means in reaction mixture. Both of the chemical methods presented in this Chapter, interfacial polymerization and *in situ* polymerization include polymerization reaction. The main differences between them is that regarding *in situ* polymerization, monomer or prepolymer are present only in the single phase of the

reaction mixture, whereas in interfacial polymerization each of the liquids contain reactive monomers [15].

Suspension polymerization - happens when miscible liquids of monomers and initiator form a droplets by mechanical agitation in the continuous liquid phase which is a bad solvent for monomers and initiator. Then polymerization reaction is induced and solid polymeric beads are fabricated [19, 20].

Emulsion polymerization - occurs when monomer is added dropwise to the solution of core material and surfactant (emulsion). Then polymerization is being induced and the core solution is being encapsulated. Katampe et al. used this type of encapsulation technique to fabricate microcapsules by enwrapping an oily core material in an amine-formaldehyde condensation product formed by in situ polymerization. Their invention includes addition to the aqueous phase of the oil-in-water emulsion a synthetic viscosity modifier. They used a carboxyvinyl polymer, more specifically, a crosslinked polymer of acrylic acid. According to them this component allows production of a more uniform, controlled, small size microcapsules [21, 22].

Dispersion polymerization - happens when monomer, initiator and dispersant are present in the same batch. Great influence in this process have a solvent, which need to be good for all aforementioned substrates but will not dissolve produced polymer, thus the polymer will precipitate [23-25].

1.1.2 Physico-Chemical Methods

Physico-chemical methods involve procedures where chemical interaction occur along with various physical transformation to shape the capsules.

Coacervation – it was the first encapsulation process patented in 1953 by Green & Schleicher working in the laboratories of the National Cash Register Company, Dayton, USA [26]. They encapsulated trichlorodiphenyl inside microscopic gelatine capsules by coacervate forces. We can speak about coacervation when an active agent is distributed within the homogenous polymer solution, and by triggering coacervation colloidal polymer aggregates (coacervates) are formed on the outer surface of an active agent droplet. Initiation of the coacervation can be achieved by varying some parameter of the system such as temperature, pH, or the composition of the reaction mixture (addition of water-miscible nonsolvent or salt). In the work of Green & Schleicher coacervation was initiated by the addition of salt, in this case sodium sulphate.

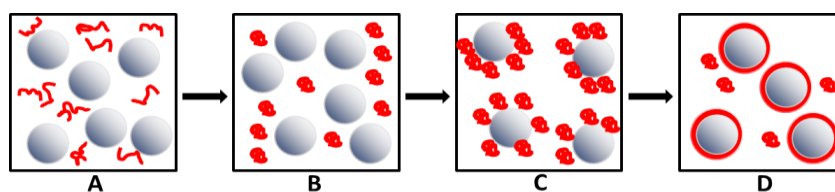


Figure 5. Schematic presentation of the complex coacervation process.

Coacervation techniques are divided into two groups simple and complex coacervation. They differ in the mechanism of the phase separation. Simple coacervation occurs when used polymer is salted out or desolvated, whereas complex coacervation is achieved by the complexation of two or more oppositely charged polyelectrolytes. The simple technique was mentioned above, while Green & Schleicher patent was discussed, and the complex one will be described here in more detail. Phases of complex coacervation method are presented schematically on Figure 5. Briefly, it can be presented as a four step process: (A) dispersion of the core material in homogenous two-different-polymer

solution, (B) initial agglomeration of polyelectrolytes after triggering the coacervation, (C) coacervation of polymer on the surface of the core, and (D) wall hardening [27-29]. To summarize, coacervation processes became a widely used encapsulation methods, because of their simplicity, low cost, reproducibility, moreover those methods can be easily scale-up to fabricate microcapsule at the industrial set-up. Nevertheless, those techniques need a constant attention and the adjustment of operating conditions (such as: stirring, viscosity, pH, and temperature), also unwanted agglomerated microcapsules were commonly observed.

Layer by Layer assembly (LbL) - includes self-assembly of oppositely charged polyelectrolytes on the outer surface of colloidal particles. By use of this technique multilayer thin films surrounding core materials are formed. Layers are prepared sequentially, substrate is added to positively or negatively charged polyelectrolyte solutions alternately. This technique can offer capsules with a broad permeability coefficients spectrum that can be tailored depending the desired application. Therefore, obtained material can be used as a drug carrier, biosensor, catalyst, among others, and also its selective permeability makes it suitable to become microreactors [30] LbL assembly is an extremely valuable, economic and versatile technique for capsules formation. Final material properties can be easily tailored through the thoughtful selection of the active agent, coating material, assembly conditions. Following the conventional methodology two oppositely charged polyelectrolytes are used, nevertheless recently three-component method fuelled much interest. New feature of this approach includes alternate deposition of a blend made of two-component polyelectrolyte and a third polyelectrolyte. This innovation opens an easy way to tune film thickness, chemical composition, wettability, stability and biological interaction by alternating the ratio of a blended

polyelectrolytes [31]. LbL as much as it is beneficial, has a one current limitation which is the standard manual, where numerous time-consuming centrifugation and resuspension are needed to perform the layering steps [32].

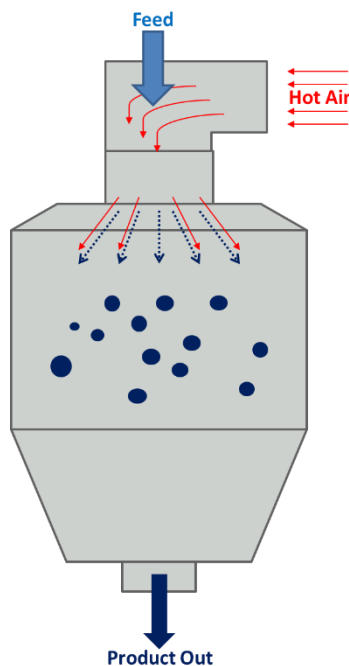


Figure 6. Schematic presentation of the spray drying process.

Sol-gel encapsulation - is an abbreviation for “solution-gelling”. The term stands for the process where sol is added to the precursor solution, and by alternating physico-chemical factors the material is gelled and hardened into the shape of the capsules [33]. Broadly speaking sol-gel processes can be divided into six steps: hydrolysis, condensation, gelation, ageing, drying and densification [34]. Sol-gel encapsulation techniques are widely used methods, therefore there are many reviews and books which describe in details variations of those techniques [34-41].

Suspension crosslinking - occurs if aqueous solution of the polymer is mixed with immiscible organic solution of core material, this suspension need to be stabilized by appropriate

agent. Core material which takes form of a sphere in suspension will be encapsulated by polymer when to suspension will be added crosslinking agent or the crosslinking will be induced thermally [42-45].

1.1.3 Physico-Mechanical Methods

Physical methods do not involve any polymerization reactions considering that the starting materials in these cases are polymers, thus broadly speaking only the formation of shape occur. Few examples of these techniques are listed below.

Spray drying – it is a process where liquid phase (emulsion, suspension or solution) is forced to form droplets by an atomizer or spray nozzle. In the further part of the device droplets are dried by the hot air and solidified capsules are created and collected. Schematic representation of this technology is shown in Figure 6. This method is widely used since 19th century in the industry because of its simplicity, flexibility, consistent particle size distribution and system can be fully automated [46]. Nevertheless, spray drying operation presents several drawback such as: low thermal efficiencies, nozzles clogging, high maintenance costs. Moreover, product loss was commonly observed, due to the agglomeration of capsules and material sticking to the internal chamber walls. Also it is highly unlikely to obtain capsules of smaller size than $\sim 100\mu\text{m}$. [47-49] Therefore, the process calls for various optimizations [50, 51].

Co-extrusion - it is a technique where dual fluid stream is pumped through the nozzle. One of the liquids contains core material and the other wall material. Droplet is formed by the vibrations applied at the exit of the concentric tubes. Then the droplet undergoes solidification by chemical crosslinking, cooling or solvent evaporation [52-54]. Schematic representation of co-extrusion is shown in Figure 7.

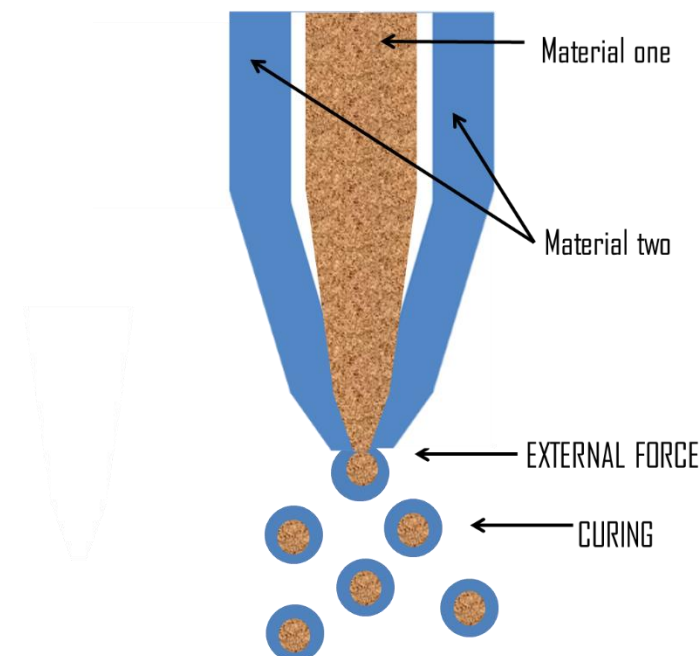


Figure 7. Schematic presentation of the co-extrusion process.

Spinning disc – it is a technique where a mixture of both core and wall material is casted onto rotating disk. By the action of centrifugal force encapsulation process occurs. Then capsules are solidified, usually by cooling. Capsules made by this technique generally feature narrow size distribution, nevertheless majority of the equipment available in the market cannot produce capsules of the sizes smaller than 10 μ m. This method is often applied in the industry since it is easily scaled-up. It also allows for the feed solution to be of various viscosities, what makes it applicable and

versatile. However, to collect undamaged capsules the set-up needs large surface or volume to receive produced material. Moreover, spinning disk involved with complex and costly hardware design [55-57].

Fluidized bed spray encapsulation - involves spraying a coating solution into a fluidized bed of solid particles. Several cycles of wetting and subsequent drying are necessary to form a continuous film around the spheres. For a coating material may serve a solution, suspension or melt. Depending from which direction the particles are being sprayed, coating can be divided into four groups: (i) top spray, (ii) tangential spray, (iii) bottom spray, (iv) Wurster process or rotor process [58]. These methodologies are a convenient solution for coating relatively large in size solid particles. This technique is appealing for the industry due to its low cost and simplicity. To efficiently operate the equipment that one should pay attention to flow-rate and pressure of the spraying liquid, flow-rate and temperature of the fluidizing air. Moreover, the composition of the spraying liquid is a key parameter, if it is poorly selected during the process liquid bridges tend to form, what leads to undesirable agglomeration [59, 60].

Phase inversion precipitation method - comprises mass transfer and phase separation processes which occur when polymeric solution in form of droplet get in contact with a non-solvent and the polymer precipitates. Phase inversion or immersion precipitation is usually isothermal, ternary system. This technique includes involvement of three components: solvent, nonsolvent and polymer. Process begins by dissolving polymer in its solvent and confining it in the wanted shape, for example film or droplet. Then, the solution is immersed into a nonsolvent bath, to activate an exchange between molecules of solvent and nonsolvent. Transfer between the solvents inevitably forces precipitation of

the polymer, resulting in the final porous structure of the obtained membrane or capsule [61-63].

There are number of parameters that are useful in describing the encapsulation performance, such as:

- capsules morphology – size distribution and shapes of obtained particles are of great importance;
- encapsulation efficiency - amount of an active entrapped within a colloidal system after a formulation process;
- encapsulation yield - is determined by dividing the total weight of capsules with the total weight of the material used to create capsules wall and active agent;
- leakage – usually slow release of an encapsulated material during storage. It leaves the active moiety unprotected by capsule shell, what potentially decreases final product performance;
- controlled release of encapsulated cargo – occurs when an application of a designed external stimuli upon capsules causes an active material to permeate through the pores of the capsules shell in desired location and time.

2 Objectives & hypothesis

The objectives of this dissertation can be summarised as follows:

1. Side chain modification of polymers with DASA as a photosensitive moiety towards a material highly receptive to light.
2. Synthesis of photosensitive polymers containing DASA within its matrix.
3. Preparation and characterisation of membranes based on photosensitive polymers containing DASA. Their in-depth physicochemical characterization to estimate their further application as shell materials in photosensitive microcapsules.
4. Preparation and characterisation of microcapsules based on photosensitive polymers containing DASA. Their assessment in potential applications in P&G products.

The main hypotheses of this work are:

1. To prepare polymers with photosensitive moiety that will allow the formation of membranes and microcapsules.
2. DASA incorporation in polymeric matrix will alter its properties.
3. The presence of DASA moiety within polymeric matrix will gain photo-sensitive properties of the final material.
4. Physicochemical properties of membranes based on the photosensitive polymers with DASA will mimic behaviour of the shell in photosensitive microcapsules.

3 Preparation of photoactive compound

3.1 Introduction

Photo-sensitive molecules are receiving a considerable amount of attention. Among the classes of organic photochromic materials, azobenzenes, spiropyrans and diarylethenes have gotten most interest because of their excellent performance and broad utility. Specifically, azobenzene has been extensively employed for its change in volume, resulting from a *trans* to *cis* isomerization, upon irradiation [7]. Similarly, the change in spectral properties of spiropyrans and diarylethenes upon photoswitching has been exploited in a number of applications with spiropyran exhibiting the added benefit of a solubility switch, or a conversion from a hydrophobic to a hydrophilic form, upon irradiation [8-10]. Despite their ubiquity and broad utility, these special classes of photochromes typically all require the use of high-energy UV light to trigger their photochemical reactions. This hinders their potential use in biomedical applications and material science because UV light can be damaging to healthy cells and results in degradation for many macromolecular systems. Fatigue resistance is also a primary concern for UV-based photochromic switches. A common design principle to address this problem is to make synthetic modifications to these known classes of photochromic compounds that enable the use of visible light [11, 12].

Recently a versatile new class of organic photochromic molecules that offers an unprecedented combination of physical properties including tuneable photo-switching using visible light, excellent fatigue resistance and large polarity changes, named Donor – Acceptor Stenhouse Adducts (DASA) was discovered by Prof. Javier Read de Alaniz's group from the Materials Department at the University of California, Santa Barbara, USA [64]. According

to the authors, these derivatives switch from a conjugated, coloured and hydrophobic form to a ring-closed, colourless and zwitterionic structure on irradiation with visible light. A number of important contributions helped Prof. Read de Alaniz's group establish the basis for the discovery of DASAs as a photoswitching platform.

As the photosensitive moiety we selected donor-acceptor Stenhouse adducts (DASA). This molecule is composed of donor and acceptor part with a triene chain in between. In this Chapter we focused on synthesis of (5-alkenyl-2,2-dimethyl-1,3-dioxane-4,6-dione) which is an acceptor part of DASA.

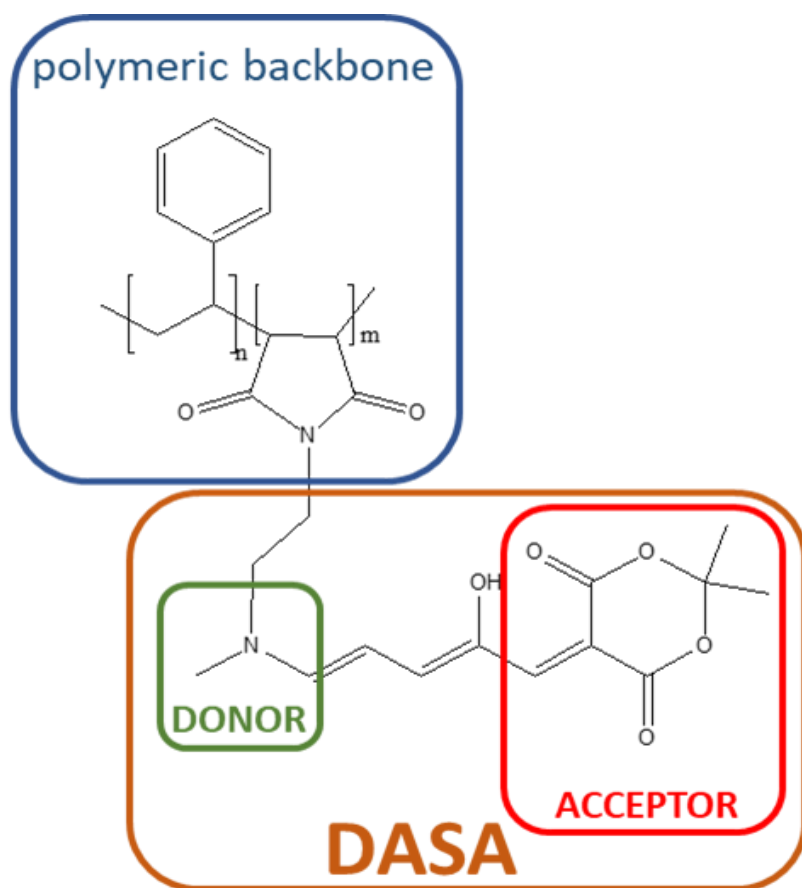


Figure 8. Graphical representation of SCIII polymers structure.

A photosensitive material that we designed for the purpose of this thesis was poly(styrene-malic anhydride) modified with donor-acceptor adducts (SCIII). As it is shown in Figure 8, SCIII is composed of two separated parts:

- polymeric backbone,
- DASA photosensitive moiety.

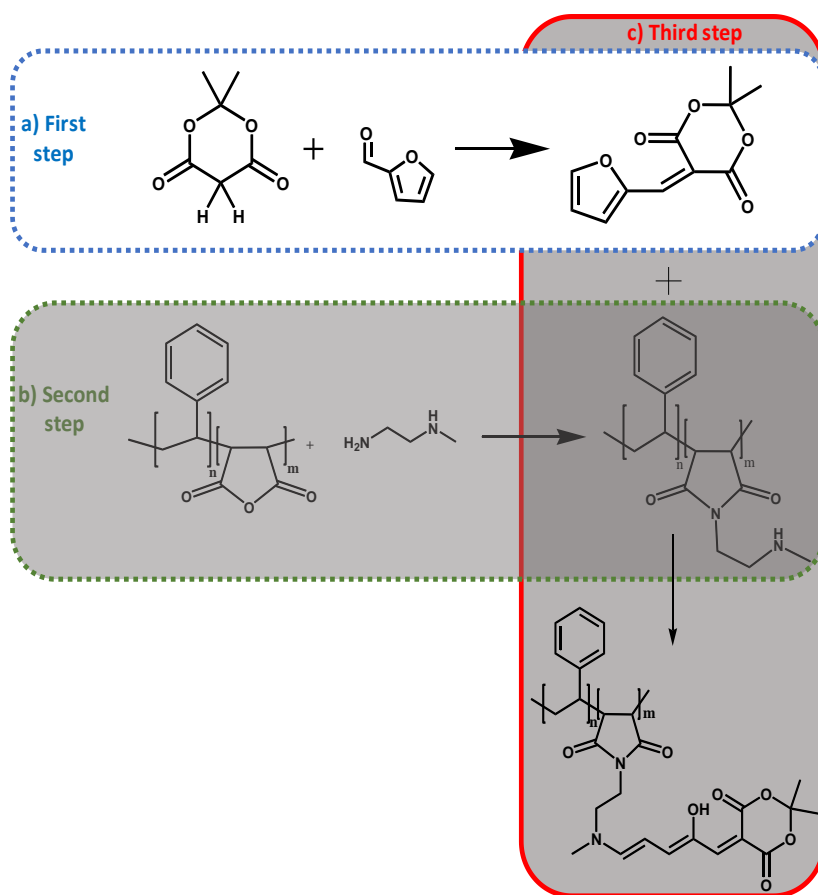


Figure 9. Graphical representation of the synthetic approach to achieve the photosensitive poly(styrene-malic anhydride) modified with donor-acceptor adducts (SCIII).

In order to synthesise a photosensitive poly(styrene-malic anhydride) modified with donor-acceptor adducts (SCIII), first a photoactive moiety has to be prepared. A graphical representation of a synthetic path to achieve this polymer is presented in Figure 9.

We established that to obtain the SCIII polymers three synthetic steps need to be followed. In this Chapter, a first step (Figure 9(a)) of the synthesis route is addressed.

There are numerous procedures to obtain 5-alkenyl-2,2-dimethyl-1,3-dioxane-4,6-dione. The most convenient preparation method to get this mono-substituted 5-(1-arylmethylidene) Meldrum's acids is the Knoevenagel condensation of an aldehyde with a Meldrum's acid. Figure 10 shows the reaction scheme.

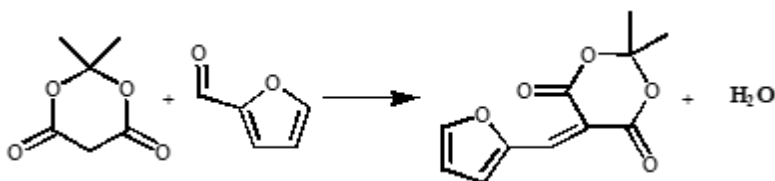


Figure 10. Knoevenagel condensation of an aldehyde with Meldrum's acid.

2,2-dimethyl-1,3-dioxane-4,6-dione also known as the Meldrum's acid is a substrate of the photoactive compound reaction.

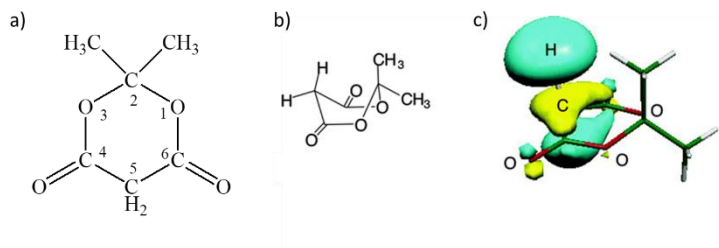


Figure 11. Meldrum's acid structure (a); Meldrum's acid in a boat conformation (b); unoccupied orbital pictures of reaction center of Meldrum's acid was reprinted from [1] (c).

Meldrum's acid was thoughtfully studied since its discovery in 1908 [65]. It is a heterocyclic molecule with two oxygen and four carbons atoms in its structure (Figure 11) [1].

Meldrum's acid remarkable reactivity origin in its susceptibility to both: 1) electrophilic attack at C₅, and 2) nucleophilic attack at C₄ and C₆. Moreover, it is highly receptive towards ring opening reactions, as such it is a reagent of tremendous usefulness in organic synthesis. It was applied in various types of reactions: Diels-Alder; hetero Diels-Alder; alkylation reaction with alkyl halides; Michael-type addition of electrophilic olefins to afford functionalized alkyl derivatives; enantioselective ring opening reactions; condensation with Mannish bases; catalytic C-C bond forming reactions; mono-selective per- and polyfluoroarylation; etc [66-69].

Commonly, the condensation of an aldehyde with the Meldrum's acid is catalysed by bases in organic solvents [70-72]. Moreover, this process was excessively studied and carried out in various conditions. For example, Hedge et al. performed this reaction in DMSO and DMF without any catalyst [73]. Recently, another protocol for an uncatalyzed Knoevenagel condensation of Meldrum's acid was reported in the literature, and it was carried out in ionic liquids at room temperature [74, 75].

Our approach was inspired by Bigi et al. who proposed method of clean synthesis in water. The investigators demonstrated that the reaction does not require a catalyst and it is seemingly simple to carried out. Besides, the authors highlighted that due to a high dielectric constant of water, Meldrum's acid dissociation is promoted. Therefore, a nucleophilic attack on aldehydic carbon is favoured, hence there is no need to use a catalyst [76].

It is imperative to mention that the reaction rate is disturbed by a Michael addition of Meldrum's acid to the 5-alkenyl-2,2-dimethyl-1,3-dioxane-4,6-dione forming bis-Meldrum's acid adducts (Figure 12).

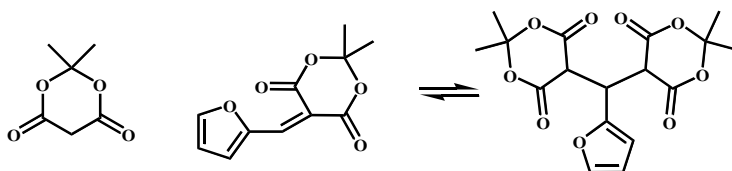


Figure 12. Michael addition of Meldrum's acid to 5-alkenyl-2,2-dimethyl-1,3-dioxane-4,6-dione.

The resulted by-products are relatively easily separated from the main product. The purification can be achieved by a simple washing with different saturated inorganic salts, such as: sodium bicarbonate, sodium bisulfite, sodium chloride. Nevertheless, a considerable loss in reaction yield can be noted. It is highlighted in the literature that alkylidenes affinity to Michael addition is strongly dependent on the condensation conditions. For instance, it is reported that if the by-product precipitation was prevented, the reaction shifts its selectivity towards the desired product. To avoid the unwanted precipitation a mixture of solvents might be used [76].

3.2 Materials and methods

- **Materials**

2,2-dimethyl-1,3-dioxane-4,6-dione, 2-furaldehyde, trichloromethane, sodium bisulfite, sodium bicarbonate, sodium chloride, and anhydrous magnesium sulfate were purchased from Sigma Aldrich with purity higher than 98%. N-hexane and ethyl acetate were purchased from Fisher Chemicals. All reactants were

used without further purification. Milli-Q water was used in all aqueous solutions.

- **Procedure of photoactive compound synthesis**

5-(furan-2-ylmethylene)-2,2-dimethyl-1,3-dioxane-4,6-dione was synthesized by modification of reported procedure. [64] Following the standard procedure, 2,2-dimethyl-1,3-dioxane-4,6-dione (1.5 g, 10.5 mmol) and 2-furaldehyde (0.96g, 10.5 mmol) were added sequentially to 25 mL of H₂O. The heterogeneous mixture was heated up to 75°C and stirred at that temperature for 2 h. During the course of the reaction a yellow precipitate was formed. Reaction progress was monitored by TLC, as a mobile phase mixture of hexane:ethyl acetate (3:1) was used. At the completion of the reaction, the mixture was cooled down to room temperature (22 ±2°C).

The precipitated black solid was collected by a vacuum filtration and washed twice with 30 mL of cold H₂O. The collected solid was dissolved in dichloromethane, washed sequentially with 90 mL of saturated aqueous NaHSO₃, 90 mL of H₂O, 90mL of saturated aqueous NaHCO₃, and 90 mL of saturated NaCl.

The organic layer was dried over anhydrous MgSO₄, and the solvent was removed by rotary evaporation to give 5-(furan-2-ylmethylene)-2,2-dimethyl-1,3-dioxane-4,6-dione as a bright yellow powder.

The reaction yield reported by Helmy et al. was 99% [64]. It was not in good agreement with our experimentally gathered results, following exactly the same protocol reported by the authors, five times. The yield obtained by us, under those specific conditions was 56 ±2%. Thus, the high level of discrepancy in obtained yields compelled us to carefully study the aforementioned procedure. Therefore, the effects of reaction duration, temperature, stirring

method and molar ratio between the substrates were deeply investigated.

The reaction was performed at a small scale and a larger one. Tables 2 and 3 give the variable conditions of the reactions and the corresponding yields. The small scale refers to the amounts of 2,2-dimethyl-1,3-dioxane-4,6-dione and 2-furaldehyde (1.5 g, 10.5 mmol) and (0.96g, 10.5 mmol), respectively, as it was described previously in general procedure (S1-S6 reactions). The larger scale refers to 5g (35 mmol) and 3.25g (35 mmol) of 2,2-dimethyl-1,3-dioxane-4,6-dione and of 2-furaldehyde, respectively (L1-L9 reactions).

- **Characterization**

Obtained products were characterized by means of ^1H NMR spectroscopy, using deuterated dimethyl sulfoxide ($(\text{CD}_3)_2\text{SO}$) as a solvent with a Varian Gemini 400 MHz spectrometer (^1H – 400 MHz, tetramethylsilane), at room temperature, using a pulse delay time of 5s.

Table 3. Condition variables for small scale

entry	small scale conditions			error
	time (h)	T (°C)	yield (%)	
S1	0.5	75	33	4
S2	1	75	80	6
S3	1.5	75	80	2
S4	2	75	56	4
S5	1.5	80	51	4
S6	1.5	70	62	2

Table 2. Condition variables for large scale reactions.

entry	large scale conditions					error
	time (h)	molar ratio	T (°C)	stirring method	yield (%)	
L1	1.5	1	75	magnetic stirrer	67	8
L2	1.5	1	70	magnetic stirrer	65	1
L3	1.5	1	65	magnetic stirrer	50	3
L4	1.5	1	RT	magnetic stirrer	59	4
L5	2	1	RT	magnetic stirrer	66	4
L6	2.5	1	RT	magnetic stirrer	70	2
L7	3	1	RT	magnetic stirrer	85	6
L8	3	1.1	RT	magnetic stirrer	91	2
L9	3	1	RT	overhead stirrer	65	6

3.3 Results and discussion

The synthesis of photosensitive precursor was achieved by Knoevenagel condensation of Meldrum's acid with a formaldehyde (Figure 10, Chapter 3). The yields of all the products obtained under different conditions are reported in Tables 2 and 3. Their structures were confirmed by ^1H NMR spectroscopy. As the matter of fact, Figure 13 provides a representative example of ^1H NMR spectra of 5-alkenyl-2,2-dimethyl-1,3-dioxane-4,6-dione, synthesised during the reaction S3, along with peak assignments.

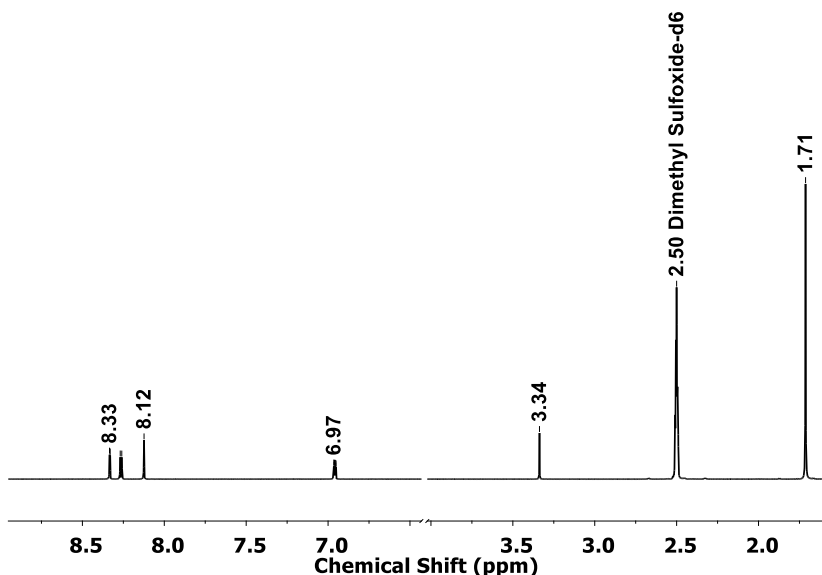


Figure 13. ^1H NMR spectra for 5-alkenyl-2,2-dimethyl-1,3-dioxane-4,6-dione. ^1H NMR (400 MHz, $(\text{CD}_3)_2\text{SO}$) δ 1.72 (s, 6H), 6.95 (dd, $J = 3.9, 1.5$ Hz, 1H), 8.12 (s, 1H), 8.27 (d, $J = 3.7$ Hz, 1H), 8.33 (d, $J = 1.5$ Hz, 1H).

The influence of S1-S6 reaction times and the temperature on the reaction yield were studied. At the small scale, it resulted that the highest yields 80% was achieved at 75°C in 1h. Prolonging the duration of the reaction time from 1h to 2h at the same temperature 75°C (S2-S4) the reaction yield did not increase, quite

the opposite: the yield dropped significantly from $80 \pm 2 \%$ to $56 \pm 4 \%$. The reason of this occurrence might be due to the secondary reaction that takes place in this system.

The photosensitive precursor reacts with Meldrum's acid thus forming bis-Meldrum's acid adducts. ^1H NMR put into evidence the multi-peaks of compound impurities. The low yield of S1 (33%) could be explain by insufficient reaction time. Indeed, by increasing the reaction time 30min, at the same temperature (75°C), the value of the reaction yield increased 2.42 times (S2). Furthermore, the synthesis was additionally performed at 80°C (S5) and 70°C (S6). In both cases, the 5°C temperature changes negatively affected the reaction yields, $51 \pm 4 \%$ (S5), and $62 \pm 2 \%$ (S6). Moreover, a colour heterogeneity of synthesised products (S1, S4-S6) was observed. While the compounds S2 and S3 were obtained as yellow powders, the S1, S4-S6 compounds were black. Therefore, the need of washing sequence of each precipitate from the S1-S6 reactions is essential. To get the pure 5-alkenyl-2,2-dimethyl-1,3-dioxane-4,6-dione compounds, a protocol for the impurity separation from the reaction mixtures was developed basing on the main and by-products solubility in different organic solvents. Preliminary results showed that the desired photosensitive precursor is soluble in both: dichloromethane and chloroform; however only 100 mL of chloroform was sufficient to purify the reaction mixture, while at least 900 mL of dichloromethane was needed to get the same results. Finally, it is important to underline that our procedure leads to remarkable difference observed during the separation procedure; a significant decrease in amount of solvent used makes the process more economically efficient, less tedious, sustainable and environmentally friendly.

In order to produce the photo-sensitive SCIII polymers a high amount of DASA precursor is required. For this reason, the next

goal of the first step of the SCIII synthesis was focused on a scale-up of 5-alkenyl-2,2-dimethyl-1,3-dioxane-4,6-dione.

Firstly, the conditions of reaction S3 were repeated, except that increased amounts of the starting substrates were used (reaction L1). The increase in Meldrum's acid went from 1.5g to 5g. To maintain the molar ratio between the others substrates and Meldrum's acid, corresponding amount were recalculated and used. Conducting the L1 reaction under the same conditions as S3 but at larger scale did not result in expected high yield. S3 reaction yield is 80 ± 2 %, whereas L1 gives the value of 67 ± 8 %. As if often happens when upscaling, the optimization/adjustments of reaction conditions is advised. Consequently, the reactions at the larger scale but at lower temperatures were carried out. The temperatures 70 °C (L2) and 65 °C (L3) did not result in yield improvement; they give 65 ± 1 % and 50 ± 3 %, respectively. Basing on the careful analysis of the small scale reactions results we learned that increasing of the temperature promotes the competing reaction (forming bis-Meldrum's acid adducts (see Figure 5)), thus impoverishing the yield of desired product. Therefore, we decided that the reaction temperature should not be higher than 75 °C. Instead, we performed a number of reactions at room temperature, while increasing the reactions duration from 1.5 h up to 3 h (L4-L7). It was observed that by extending the experiment time, the yield increased from 59 ± 4 % (L4) to 85 ± 6 % (L7). The highest yield of 85 ± 6 % was obtained for the reaction L7, conducted at room temperatures for 3 h.

It was mentioned in the literature, that the slight excess of furfural might unfavored the side reaction, thus results in yield enhancement.[71] In consequence, the reaction L8 was performed applying the same protocol like in L7, with the exception of the variation of the molar ratio between furfural and Meldrum's acid. The slight excess of furfural (5.5 ± 0.5 %) was added. In our case,

it gave the desired outcome, resulting in 91 ± 2 % of yield, which was the highest yield obtained for this procedure.

Finally, by following the suggestion of our industrial collaborators from P&G, we changed the experimental set up, and performed the reaction by stirring it with an overhead stirrer instead of a magnetic one (L9). The rest of the reaction's conditions were repeated as for the L7 reaction, nevertheless it gave poor yield of 65 ± 6 %, in comparison of the 85 ± 6 % for L7.

3.4 Conclusions

We reported on the synthesis 5-(furan-2-ylmethylene)-2,2-dimethyl-1,3-dioxane-4,6-dione, which in our case serves as a photosensitive precursor used to modified the polymeric matrix. Optimization of preparation procedure previously reported in the literature was successfully performed. Results obtained from this Chapter provide a more robust and a practical method to gain a high yield of 5-(furan-2-ylmethylene)-2,2-dimethyl-1,3-dioxane-4,6-dione in water without the need of a catalyst. At the small scale the highest reaction yield of 80 ± 2 % was archived at 75 °C while at the larger scale the yield of 91 ± 2 % was obtained at room temperature after 3h.

4 Polymer modification

4.1 Introduction

In this Chapter the second and the third steps (Figure 14(b), 14(c)) of the synthesis route will be addressed. In order to synthesise the photosensitive SCIII a commercially available poly(styrene-maleic anhydride) (SMA) will be modified with the photosensitive precursor obtained according to the procedure described in Chapter 3. Figure 14 shows a synthetic path carried out to achieve this product.

Particularly, five types of commercially available SMAs with different molecular weights and molar ratio compositions (Table 4), an amine and DASA precursor 5-(furan-2-ylmethylene)-2,2-dimethyl-1,3-dioxane-4,6-dione will be applied to synthesize the SCIII copolymers with different properties.

Table 4. SMA characteristics supplied by Cray Valley Total.

Designation	M_n [g/mol]	M_w [g/mol]	m% Styrene content	m% Anhydride
FLAKE 1000	2000	5500	50%	50%
FLAKE 2000	3000	7500	67%	33%
EF 40	4500	10500	80%	20%
EF 60	5500	11500	86%	14%
EF 80	7500	14400	89%	11%

Polymer modifications are common strategy to obtain a material of desired properties. Typically, the modifications lead to materials of enhanced thermal stability, resistance, rigidity or degradability, etc [77]. Modification of the polymers can be divided into two groups:

- Physical modifications - those include entanglement, entrapment and radiation induced changes;

- Chemical modifications - where a transformation occurs via chemical reactions [78].

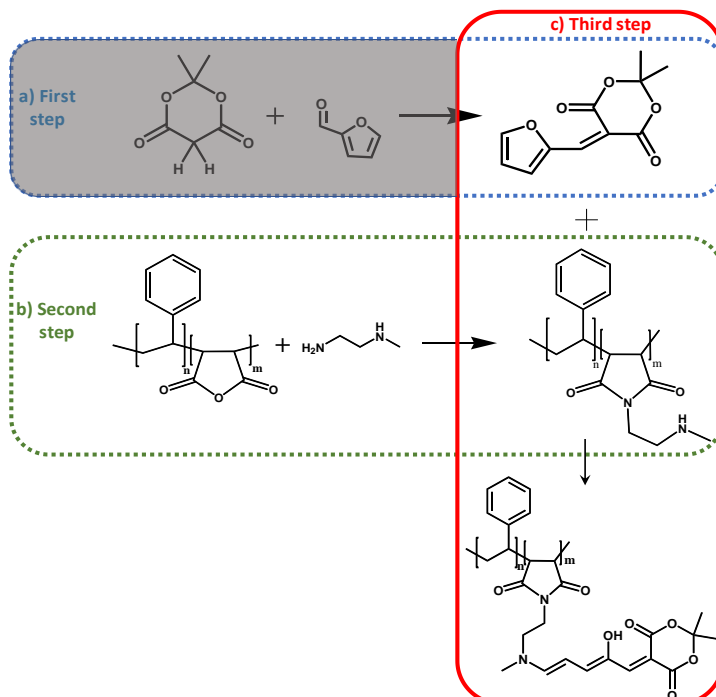


Figure 14. Synthetic approach to achieve the photosensitive poly(styrene-maleimide) modified with donor-acceptor adducts (SCIII).

Chemical modifications can occur: (i) on the polymers or (ii) they can be done to the monomers before the polymerization process. Furthermore, new moiety can be added to the side chain of the polymer or it can be incorporated within the polymeric back bone [79].

During this PhD thesis, to achieve the set objective as the starting block SMA was chosen. Within its structure (Figure 14(b)) it contains a maleic anhydride group which is highly reactive. Maleic anhydride can react doubly while subjected to primary amines. It can either lead to addition or substitution reaction [80]. Whether it will be former or latter depends on reaction parameters, such as: temperature, solvent, reaction time, and addition of

catalyst. Schematic representation of the malic anhydride reaction with nucleophiles is shown in Figure 15.

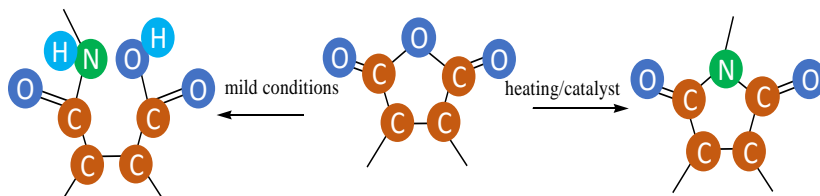


Figure 15. Schematic representation of the malic anhydride reaction with nucleophiles.

During the second step of the process we carried out a substitution reaction between maleic anhydride and an amine to get a maleimide (see step 2, Figure 14(b)). Literature studies put into evidence that most of researchers chose an acidic catalyst for this type of reaction, such as: zinc bromide or acetic anhydride [81, 82]. However, according to the patent investigation, very promising results were achieved performing this reaction with a heterogenous catalysis such as ion-exchange resins (US Patent 4,812,579). They offer stability of reaction mixture, easy separation and reutilizability. Reactions performed in liquid phases are strongly dependent on the solvent used. Recent studies demonstrated that a compatibility between the solvent and the resin dictates the effectiveness of the catalyst [83, 84]. In our study, we used a cation-exchange resin containing a sulfonic acid - Amberlyst® 15. Its structure is schematically shown in Figure 16.

It is a conventional, macroreticular acid type resin, in which the sulfonated polystyrene chains are crosslinked by divinylbenzene. Usually, it is added into a reaction in a form of pellets, thus it creates heterogenous reaction mixture. When the resin enters to the process, it adsorbs its components. However, in a multi-component mixture the affinity of reagents to the resin differ. This phenomenon might be used as an advantage. For example, if the

product of the reaction is preferably adsorbed by the resin, the rate of the inverse reaction is minimized [85].

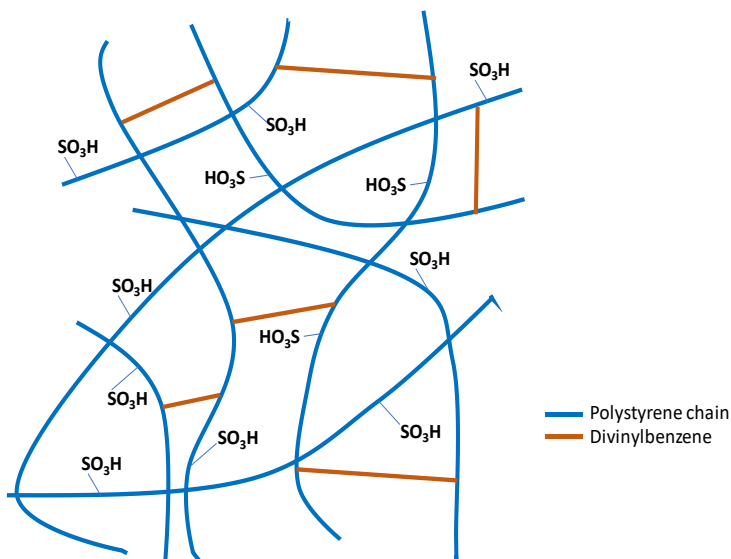


Figure 16. Schematic representation of Amberlyst® 15 structure.

According to the literature, the reaction between the maleic anhydride and primary amines is mainly carried out in organic, nonpolar solvents, like benzene or xylene [86]. Due to the macroreticular and rigid structure, the Amberlyst® 15 resin could be applied in both polar and non-polar solvents [87].

Then, within the third step of the process, to introduce the photosensitive moiety within the copolymer structure, its styrene-maleimide, obtained in the 2nd step, was modified with Donor-Acceptor Stenhouse Adduct (DASA) (Figure 14(c)). The product obtained in a reaction of an amine with DASA precursor is known as Stenhouse salt and it was firstly mentioned in 1850 [88]. Doctor John Stenhouse was the first to publish reaction that occurs between furfural and aniline and the product was named after him. Due to the conjugated triene structures of Stenhouse salts they are characterized by rich tint. Therefore, this reaction resulted useful in the industry to identify amino acids in food products [89].

Further studies reveal that Stenhouse salts undergo a thermal $4-\pi$ conrotatory electrocyclic transformation. Hence, they transform from prolonged, triene conjugated, coloured form to cyclic, zwitterionic, colourless structure. The difference between the form before and after transformation is highlighted in Figure 17. Recently the interest in the mechanism of this transformation revived, it will be described in more detail in next Chapter [90].

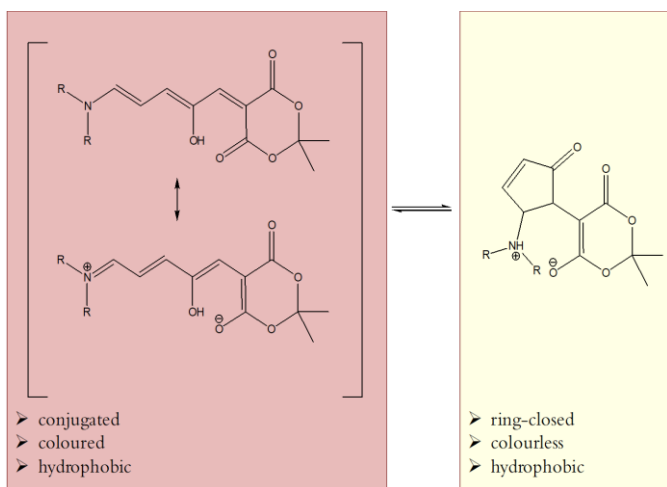


Figure 17. Schematic representation of thermal $4-\pi$ conrotatory electrocyclic transformation of Stenhouse salts.

4.2 Materials and methods

• Materials

Five poly(styrene-co-maleic anhydride) (SMA) with different molecular weight and styrene:maleic anhydride ratio (Table 4) were donated from Cray Valley Total. 5-(furan-2-ylmethylene)-2,2-dimethyl-1,3-dioxane-4,6-dione was synthesized applying the procedure explained in previous Chapter. N,N-Dimethylformamide (DMF), N-methylethylenediamine, Amberlyst® 15, tetrahydrofuran (THF), n-heptane, and diethyl

ether were purchased from Sigma Aldrich with purity higher than 98%. All reactants were used without further purification.

- **Procedure of photosensitive polymer preparation**

Into a 250 mL round-bottom flask equipped with a reflux condenser with a water-separator, a thermometer, a stirrer and a dropping funnel(optional), were placed: 5 g of poly(styrene-co-maleic anhydride) and 80 mL of DMF and the resulting mixture was stirred. Then, separately a mixture of 1.1 mL of N-methylethylenediamine and 2.3 mL of DMF was prepared, and it was added dropwise from the dropping funnel to the above mixture over a period of about 5 min. After completion of the dropwise addition, the reaction mixture was heated at 60°C for 2 hours to complete the reaction.

Next, the reaction mixture was refluxed at 130°C and 0.987 g of a strongly acidic ion exchange resin (Amberlyst® 15) was added to it. The reaction mixture was kept under reflux and continuous stirring for 20 hours to effect the reaction. During this period 0.22g of water was separated by means of the water-separator. After completion of the reaction, the ion exchange resin of the catalyst was filtered off and the filtrate was stripped of the solvent under a reduced pressure to yield solid. The product was purified by means of precipitation. First it was dissolve in THF, and then precipitated in 10-fold excess of n-heptane. Precipitated poly(styrene-co-maleimide) (SCII) was dried and stored. Then, into a 250 mL round-bottom flask equipped with a reflux condenser, a thermometer, a stirrer, an oil bath, and 5g of SCII and 75mL of THF was placed. Separately, 2.63g of 5-(furan-2-ylmethylene)-2,2-dimethyl-1,3-dioxane-4,6-dione (SCI) was dissolved in 40 mL of THF. When both mixtures were

homogenously dissolved, SCI was added to SCII. As prepared reaction mixture was stirred at room temperature for 5 min. Then, the reaction mixture was heated up to 60°C and kept stirring for 60min at 60°C to complete the reaction. After that, the reaction mixture was precipitated in 10-fold excess of n-heptane. Next, it was filtered to collect the precipitated solid. The solid was washed with cold diethyl ether, and dried to afford SCIII.

- **Characterization**

Titration of SMA was performed to confirm the styrene maleic anhydride ratio provided by the donating company.

Three weighed portions of dried SMA copolymer were placed in conical flasks, and dissolved in 20mL of THF. Then, 20 mL of 0.5 M NaOH solutions were added to each of them. As prepared mixtures were titrated with 0.5 M solution of hydrochloric acid using phenolphthalein as an indicator. This procedure was employed to analyse all five polymer modifications. To calculate the content of maleic anhydride (% by weight, and mole) in copolymer basing on the volume of NaOH and HCl used in titrations, it was assumed that all of maleic anhydride groups in the polymer were hydrolysed to maleic acid when mixed with NaOH. The content of maleic anhydride (% by weight, and mole) was calculated following the equations given below.

$$n_{MA} = 0.5 \cdot (n_{NaOH} - n_{HCl}) \quad (1)$$

where: n_{MA} - number of moles of maleic anhydride in the titrated sample; n_{NaOH} – number of moles of NaOH contained in 20mL added to the sample; n_{HCl} - number of moles of HCl consumed in the titration of excess NaOH.

$$m_{MA} = 0.5 \cdot (n_{NaOH} - n_{HCl}) \cdot M_{MA} \quad (2)$$

where: m_{MA} - mass of maleic anhydride in a sample; M_{MA} – molar mass of maleic anhydride (98.057g/mol).

$$\%m_{SMA} = \frac{m_{MA}}{m_{SMA}} \cdot 100\% \quad (3)$$

where: m_{SMA} – mass of SMA weighed portion taken to analysis.

$$\%mole_{SMA} = \frac{n_{MA}}{n_{SMA}} \cdot 100\% \quad (4)$$

where: n_{SMA} – moles of SMA weighed portion taken to analysis.

Investigated polymers were characterized with ^1H NMR, ^{13}C NMR and ^{15}N NMR spectroscopy, using deuterated chloroform (CDCl_3) as a solvent with a Varian Gemini 400 MHz spectrometer (^1H – 400 MHz, tetramethylsilane; ^{13}C – 100 MHz, tetramethylsilane; ^{15}N – 40 MHz, nitromethane) at room temperature with proton noise decoupling for ^{13}C NMR and using a pulse delay time of 5 s for ^1H NMR. Measurements were carried out at room temperature on 10–15% (w/v) sample solutions. Homonuclear correlation of resonances via through bond J coupling (correlated spectroscopy, COSY) and heteronuclear single quantum correlation (gHSQC) experiments were performed according to standard procedures.

Fourier transform infrared (FT-IR) spectra of polymer powders were obtained at room temperature with a FT-IR

spectrophotometer (Vertex 70, Bruker) with a resolution of 4 cm^{-1} and scanning speed of 2 mm s^{-1} , in absorbance mode. An attenuated total reflection (ATR) accessory with thermal control and a diamond crystal a Golden Gate heated single reflection diamond ATR from Specac-Teknokroma) was used to obtain FT-IR spectra. Spectra were elaborated by means of Origin Pro8.

Thermal transitions of SMA and modified SMA polymers were detected with Differential Scanning Calorimetry (DSC) Mettler-Toledo mod. 822 in dynamic mode at a heating or a cooling rate of $10^\circ\text{C}/\text{min}$ in cycle: 1st heating from -10°C to 150°C , followed by cooling to -10°C and 2nd heating to 300°C . Nitrogen was used as the purge gas. The calorimeter was calibrated with an indium standard (heat flow calibration) and an indium-lead-zinc standard (temperature calibration).

4.3 Results and discussion

Five of the SMA copolymers were thoughtfully analyzed in order to gain insight regarding molar composition of the copolymers as well as sequence distributions. Investigated copolymers contained from 50% to 89% of styrene units in the copolymer structure according to supplier data. Molar composition was confirmed via ^1H NMR, ^{13}C NMR and titration. As it is shown in Table 5 the copolymer composition measured by mentioned methods are in good agreement. The results generated by titration and ^{13}C NMR show the closest similarities to the supplier data, while the results obtained by ^1H NMR variate $\pm 3\text{-}10\%$ comparing to the values given by the provider. These differences could be caused by integration error during ^1H NMR spectra elaboration.

Table 5. SMA compositions supplied by Cray Valley Total and calculated by means of NMR and titration.

supplier ref.	composition							
	SMA supplier		SMA H NMR		SMA C NMR		SMA titration	
	ST content	MA content	ST content	MA content	ST content	MA content	ST content	MA content
FLAKE 1000	0.50	0.50	0.56	0.44	0.54	0.46	0.57	0.43
FLAKE 2000	0.67	0.33	0.70	0.30	0.67	0.33	0.69	0.31
EF 40	0.80	0.20	0.88	0.12	0.80	0.20	0.79	0.21
EF 60	0.86	0.14	0.89	0.11	0.85	0.15	0.85	0.15
EF 80	0.89	0.11	0.98	0.02	0.88	0.12	0.87	0.13

In order to understand copolymer structure a determination of triad sequence distribution was made via ^{13}C NMR spectra analysis basing on the finding published by Hieu Ha [91]. The author made a clear assignment for triad sub-peaks basing on the comparison made of the styrene homopolymer and styrene copolymers, among others poly(styrene-maleic anhydride). High sensitivity of a quaternary aromatic carbon (C7, Figure 18(a)) was used to describe the distribution of copolymers sequences. The peak assigned to C7 exhibits chemical shift splitting depending on the sequences distribution that it is in. Thus, detail analysis of this split signal is of use to describe the distribution of the styrene (S) and maleic anhydride (M) sequences in the poly(styrene-maleic anhydride) copolymer.

SMA structure is shown in the Figure 18(a). It is known that also the carbon C1 shows sensitivity towards sequence distribution, nevertheless in our case the chemical shift of this carbon overlaps with the peaks assigned to carbons C4 and C2, thus the collected results were not reliable. Experimentally collected data of C7 carbon integrations are gathered in Figure 18(b) and the corresponded spectra is shown in Figure 18(c). Basing on these data we were able to establish the run number for each polymer, therefore allowing a discussion regarding sequence distribution.

The run number can be defined as an average number of monomer sequences occurring in copolymer per 100 monomer units. The run number is widely used to describe the degree of alternation of the co-monomers in the copolymer chain. [92] It can be calculated by use of the experimentally collected data by applying the equation shown below. In our study, the run numbers of the copolymers were obtained from the ^{13}C NMR results [93].

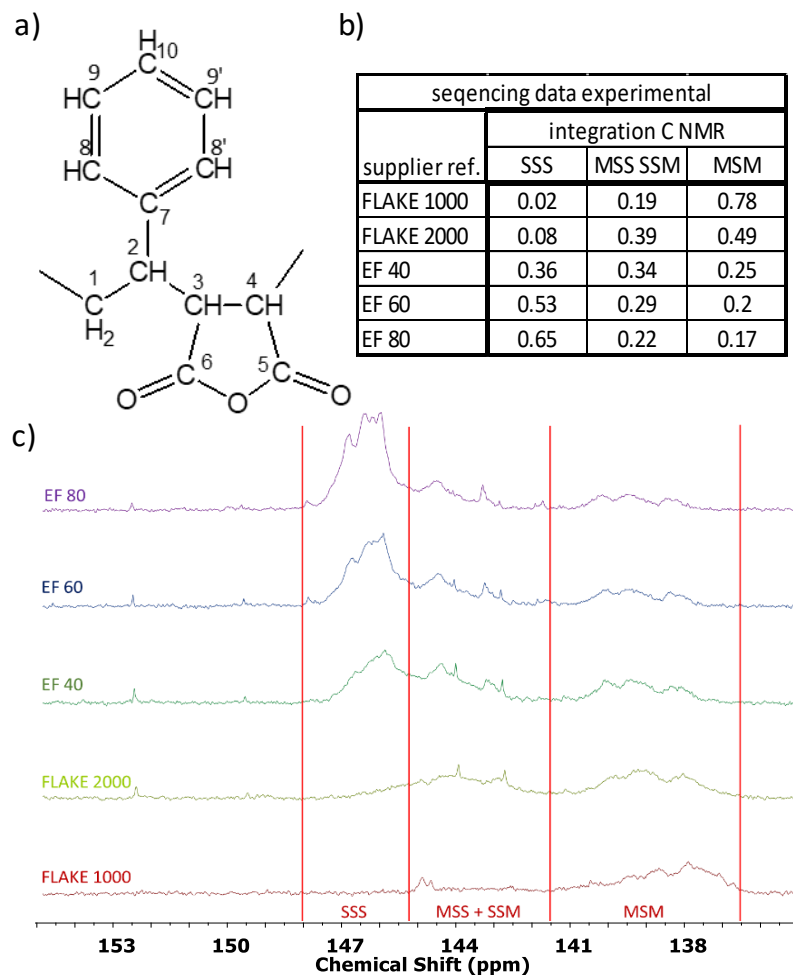


Figure 18. SMA structure (a); experimentally collected data of C7 carbon integrations (b); and corresponded ^{13}C NMR spectra (c).

$$R_{n \text{ exp}} = \text{MSM} + (\text{MSS SSM})/2 \quad (5)$$

The resulted values can be compared with a random run number ($R_{n \text{ random}}$) which can be described by the following expression.

$$R_{n \text{ random}} = (\%S \cdot \%M) / 2 \quad (6)$$

Relationship between $R_{n \text{ exp}}$ and $R_{n \text{ random}}$ can be describe as the tendency of the copolymer to alternate or cluster in blocks in like units. Essentially, when $R_{n \text{ exp}}$ is higher than $R_{n \text{ random}}$ for the same copolymer it tends to alternate, whereas if $R_{n \text{ exp}}$ is lower than $R_{n \text{ random}}$ monomers tend to cluster in blocks within the polymeric chain [94]. The SMA copolymers microstructure were deduced from the analysis of run numbers. As it is given in Table 6, in all investigated copolymers modifications, the calculated values of $R_{n \text{ exp}}$ are higher than the $R_{n \text{ random}}$. These results brought us to the conclusion that the copolymers have an inclination towards alternating structures.

Table 6. SMAs Run numbers values.

supplier ref.	Run number experimental	Run number random
FLAKE 1000	0.88	0.50
FLAKE 2000	0.71	0.44
EF 40	0.44	0.32
EF 60	0.34	0.25
EF 80	0.27	0.21

To gain more information regarding the styrene arrangement within the polymeric chain, a number average sequence length ($Av S$) was calculated for all the SMA copolymers (Eq.7). The $Av S$ describes the average number of corresponding monomer in one run. Calculated results are given in Table 7.

$$Av S = \%S / R_{n \text{ exp}} \quad (7)$$

As it is provided in Table 7, the number average sequence length of investigated polymers is in the range from 1.13 to 3.71. As a matter of example the polymer EF 60 has the AvS value of 2.96. It means that on average 3 units of styrene are repeated in one run, while in the case of FLAKE 1000 (AvS=1.13) on average approximately 1 units of styrene is repeated in one run.

Table 7. SMAs number average sequence lengths.

supplier ref.	Av S
FLAKE 1000	1.13
FLAKE 2000	1.40
EF 40	2.26
EF 60	2.96
EF 80	3.71

Finally, probability values for diads and triads arrangements within the copolymer chain were studied (Table 8). The values highly depend on the content of each monomer in the polymeric chain, therefore the calculation was performed for amounts provided by supplier, ^1H NMR study results, ^{13}C NMR study analysis and titration. Table 8 collects all possible diads and S-centered triads arrangements. As a matter of example, the diads probability, calculated using the content ratio between styrene to maleic given by supplier, for S-M or M-S sequence in the FLAKE 1000 copolymer (formed by styrene and maleic anhydride units in the molar ratio 1:1) is 0.88 for both diads; while in the case of copolymer EF 80 (formed by styrene and maleic anhydride units in the molar ratio 8:1) the probability of diads S-M and M-S sequence is 0.15 and 1.22, respectively.

Table 8. Probability for diads and triads arrangement within the copolymer chain.

SMA supplier		diads					S-centered triads		
supplier ref.	styrene content	maleic content	$P_{S-M} = (R_{\text{Resp}}/2) / \%S$	$P_{M-S} = (R_{\text{Resp}}/2) / \%M$	$P_{S-S} = (\%S - R_{\text{Resp}}/2) / \%S$	$P_{M-M} = (\%M - R_{\text{Resp}}/2) / \%M$	$P_{M-S-M} = P_{S-M}^2$	$P_{S-S-S} = P_{S-S}^2$	$(P_{S-S-M} + P_{M-S-S}) = \frac{2 \cdot P_{S-S-M} \cdot P_{M-S-S}}{P_{S-S-S} + P_{M-S-S}}$
FLAKE 1000	0.50	0.50	0.88	0.88	0.12	0.12	0.78	0.01	0.21
FLAKE 2000	0.67	0.33	0.53	1.08	0.47	-0.08	0.28	0.22	0.50
EF 40	0.80	0.20	0.28	1.11	0.72	-0.11	0.08	0.52	0.40
EF 60	0.86	0.14	0.20	1.21	0.80	-0.21	0.04	0.65	0.32
EF 80	0.89	0.11	0.15	1.22	0.85	-0.22	0.02	0.72	0.26
SMA ¹ H-NMR									
supplier ref.	styrene content	maleic content	P_{S-M}	P_{M-S}	P_{S-S}	P_{M-M}	P_{M-S-M}	P_{S-S-S}	$(P_{S-S-M} + P_{M-S-S})$
FLAKE 1000	0.56	0.44	0.80	0.99	0.20	0.01	0.63	0.04	0.33
FLAKE 2000	0.70	0.30	0.51	1.20	0.49	-0.20	0.26	0.24	0.50
EF 40	0.88	0.12	0.25	1.86	0.75	-0.86	0.06	0.56	0.38
EF 60	0.89	0.11	0.19	1.58	0.81	-0.58	0.04	0.66	0.31
EF 80	0.98	0.02	0.14	5.52	0.86	-4.52	0.02	0.74	0.24
SMA ¹³ C-NMR									
supplier ref.	styrene content	maleic content	P_{S-M}	P_{M-S}	P_{S-S}	P_{M-M}	P_{M-S-M}	P_{S-S-S}	$(P_{S-S-M} + P_{M-S-S})$
FLAKE 1000	0.54	0.46	0.82	0.96	0.18	0.04	0.67	0.03	0.30
FLAKE 2000	0.67	0.33	0.53	1.08	0.47	-0.08	0.28	0.22	0.50
EF 40	0.80	0.20	0.28	1.12	0.72	-0.12	0.08	0.53	0.40
EF 60	0.85	0.15	0.20	1.14	0.80	-0.14	0.04	0.64	0.32
EF 80	0.88	0.12	0.15	1.13	0.85	-0.13	0.02	0.72	0.26
SMA titration									
supplier ref.	styrene content	maleic content	P_{S-M}	P_{M-S}	P_{S-S}	P_{M-M}	P_{M-S-M}	P_{S-S-S}	$(P_{S-S-M} + P_{M-S-S})$
FLAKE 1000	0.57	0.43	0.78	1.03	0.22	-0.03	0.60	0.05	0.35
FLAKE 2000	0.69	0.31	0.52	1.15	0.48	-0.15	0.27	0.23	0.50
EF 40	0.79	0.21	0.28	1.05	0.72	-0.05	0.08	0.52	0.40
EF 60	0.85	0.15	0.20	1.13	0.80	-0.13	0.04	0.64	0.32
EF 80	0.87	0.13	0.15	1.04	0.85	-0.04	0.02	0.71	0.26

During the next step of this PhD thesis, having the detailed analysis of SMA copolymers we proceeded with their modifications. Firstly, SMA (FLAKE 1000, FLAKE 2000, EF 40, EF 60, EF80) were reacted with n-methyl ethylene diamine following the method described in US Patent 4,812,579 to obtain poly(styrene-co-maleimide).

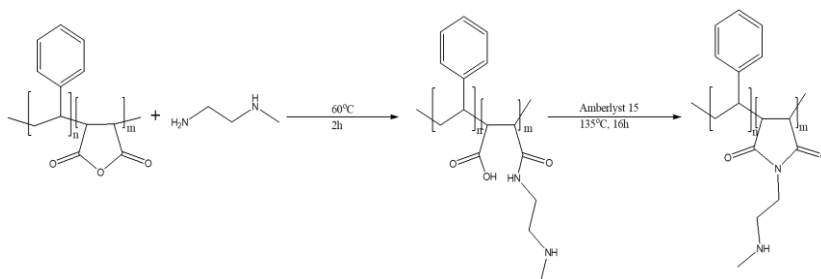


Figure 19. SMA reaction with n-methyl ethylene diamine.

Reaction pathway is represented in Figure 19. It is a well-known transformation that occurs via maleamic acid intermediate [95]. The maleic anhydride ring opening step of the reaction takes place under mild conditions. Then, to close the ring and allow imide transformation, an adjustment of the conditions is required. To promote cyclic imide transformation catalyst needed to be added to reaction mixture. We chose strongly acidic cation exchange resin Amberlyst® 15 [84]. When it enters the reaction mixture it swells in order to reach the equilibrium with the liquid phase. As the reaction mixture is a multi-component mixture we can assume that each component is adsorbed onto the surface of the catalyst, nevertheless adsorption occurs to different extent. For example, it was recorded that the Amberlyst 15 has a higher affinity towards water than some organic molecules [85, 96]. In our case, the resin acts as a heterogenous catalyst and due to its acidity it can protonate the carboxyl group of the copolymer. Hence, cyclic imide transformation is promoted. Figure 20 provides a scheme of the resin interaction with the copolymer. We have to keep in mind that the reaction is nonetheless partial, as carboxyl groups could

still be accounted for in the resulting modified copolymer. Therefore, thoughtful analysis of the modification degree was needed.

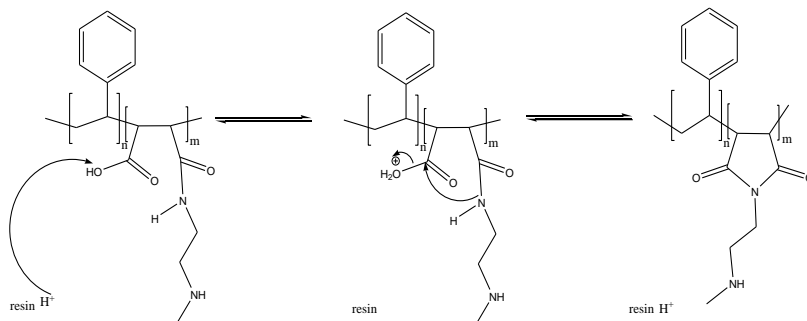


Figure 20. Schematic representation of interactions between resin and SMA.

The products of the second step of the synthetic path (Figure 14(b)) were characterized by means of FT-IR (Figure 21) and ^{15}N NMR (Figure 22).

Figure 21(a) shows spectra of SMA FLAKE 1000 (black line) and modified SCII FLAKE 1000 (red line). Characteristic band that is assigned to maleic anhydride ($1910\text{-}1814\text{cm}^{-1}$ and $1814\text{-}1647\text{cm}^{-1}$) was detected in SMA spectra (black line). Aforementioned band was not present in modified SCII FLAKE 1000 spectra.. Moreover, bands at $1780\text{-}1745\text{cm}^{-1}$ and $1743\text{-}1614\text{cm}^{-1}$ that correspond to maleimide were found in the modified SCII FLAKE spectra. Those results suggest that the SMA modification reaction with amine was successful. Figure 21(b) shows spectra collected for all five SCII polymers. Band assignment for both: SMA and SCII are presented in Figure 21(c)[97-100]. As mentioned before the determination of the degree of modification was imperative. FT-IR absorption analysis was employed to estimate the composition of absorbing species in multicomponent systems.

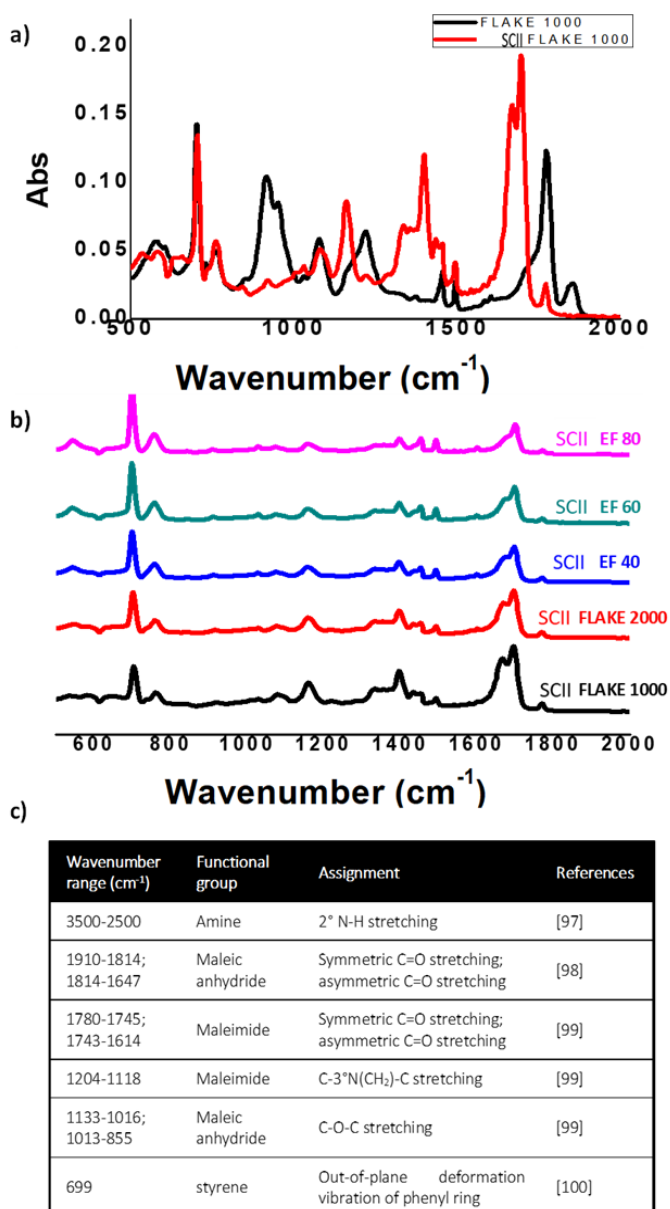


Figure 21. FT-IR spectra recorded at RT in absorption mode of SMA FLAKE 1000 (black line) and modified FLAKE 1000 (red line)(a); FT-IR spectra recorded at RT in absorption mode of five different modifications of poly(styrene-maleimide) (b) ; table of bonds assignments of SMA and modified SMA, SCII (c).

Quantitative spectroscopic analysis is based on the Lambert-Beer law (Eq.8) where the absorbance ($A(\tilde{\nu})$) is related to a molar absorption coefficient at chosen wavenumber ($\epsilon(\tilde{\nu})$), a concentration (c) and an optical path length (l) [101-103].

$$A(\tilde{\nu}) = \epsilon(\tilde{\nu}) \cdot c \cdot l \quad (8)$$

Spectroscopic spectra can be examined quantitatively by integrating absorbance relying on the Eq.9 presented below.

$$Int = \int A(\tilde{\nu}) d\tilde{\nu} \quad (9)$$

Table 9. SMA modification percentage results.

labels	SMA integration data			MODIFIED SMA integration data (SCII)			results	
	integration limits	area		integration limits	area	unmodified	modified	
FLAKE 1000	1642	1813	5.35	1749	1817	0.26	5%	95%
FLAKE 2000	1618	1813	3.53	1737	1799	0.24	7%	93%
EF 40	1694	1817	2.22	1743	1802	0.18	8%	92%
EF60	1724	1817	1.92	1755	1793	0.14	7%	93%
EF 80	1707	1813	1.47	1755	1790	0.09	6%	94%

Each of the spectra obtained for unmodified and modified copolymer were normalized using as a reference band that corresponds to styrene (699cm^{-1}). The styrene peak integral value is constant before and after modification within the same copolymer. Thus, it was an obvious choice for the internal standard [104]. Then signal that corresponds to maleic anhydride symmetric C=O stretching ($\approx 1788\text{cm}^{-1}$) was integrated in spectra recorded before and after modification reaction. This characteristic band was easily identified for each of the copolymers, however the wavelength limits for this specific band differ slightly in each case. Results are gathered in Table 9.

The modification for each copolymer was successful and it was calculated that 92-95% of the maleic anhydride groups were converted into maleimide.

To further examine the structure of modified copolymers and confirm that the modification was successful, As it is illustrated in Figure 20, in order to obtain the SCII copolymers, we carried out reactions of SMA with diamine (N-methylethylenediamine). This diamine possesses 2 amine groups in its structure: primary (R-NH₂) and secondary (R-NH-R₂). Our goal was to create the side chain modification of the copolymer. To confirm that during the synthesis, the maleic anhydride groups reacted only with the primary amine forming maleimide, as it is draw in the Figure 20, the ¹⁵N NMR analysis of SCII copolymers were carried out.

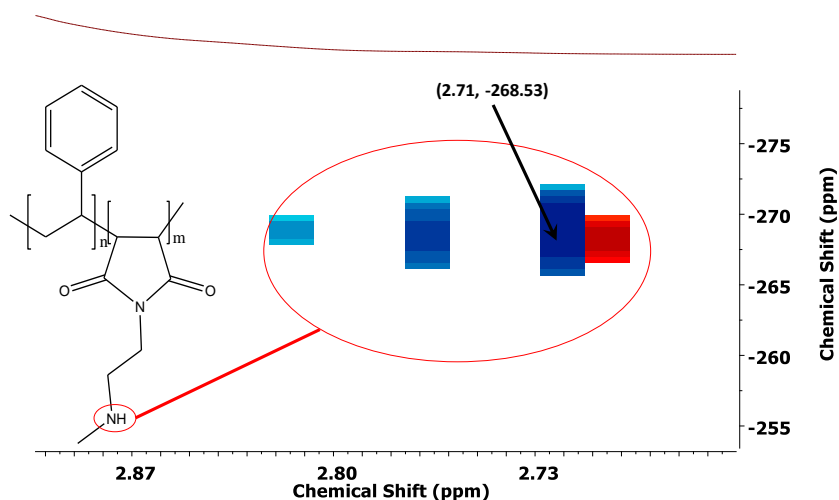


Figure 22. Two-dimensional separated local field spectrum shows a signal for the ¹⁵N-¹H dipolar interaction.

Furthermore, obtained SCII polymers were dissolved in different organic solvents, such as: DMF, THF, chloroform . The solubility experiments confirmed that the SMA polymers were not cross-linked with the diamine, and only primary amine groups of N-methylethylenediamine reacted with the maleic anhydride groups.. There was a slight possibility that the secondary amine might react with the maleic anhydride to form maleamic acid. If it occurred, we would create crosslinked system that posed two 3°

amine. We would have to discard as modified copolymer as it would not sever our purpose in the subsequent step. Therefore, establishing if the 2° amine is presented in the modified copolymer was a significant step of characterization.

Table 10. ¹H NMR quantitative analysis of SCIII polymers.

composition				
supplier ref.	SMA supplier		SCIII ¹ H NMR	
	styrene content	maleic content	DASA content	SMA content
FLAKE 1000	0.50	0.50	0.28	0.67
FLAKE 2000	0.67	0.33	0.23	0.70
EF 40	0.80	0.20	0.10	0.82
EF 60	0.86	0.14	0.06	0.87
EF 80	0.89	0.11	0.05	0.89

As a matter of example spectra recorded for SCII FLAKE 1000 is shown in Figure 22, where a two-dimensional separated local field spectrum shows a signal for the ¹⁵N-¹H dipolar interaction at -269ppm that in the literature is assign to 1° or 2° amines [105]. It confirms the presence of the 2° amine in the side chain of the copolymer. It means that the obtained polymers SCII do not contain a tertiary amine group into their structures, so the reaction between the secondary group (R-NH-R1) of N-methylethylenediamine did not occur under the selected reaction conditions.

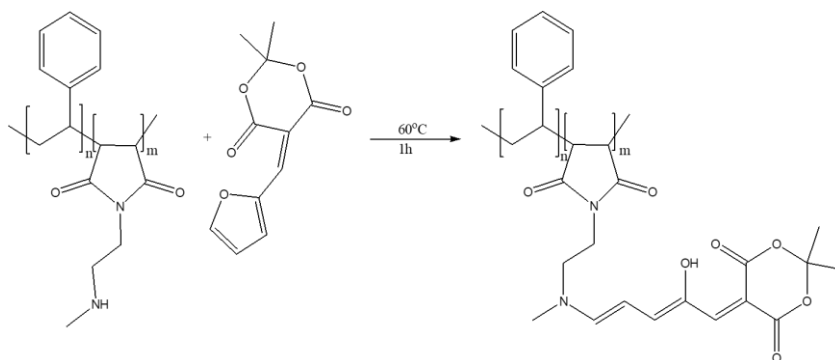


Figure 23. Reaction scheme between 5-(furan-2-ylmethylene)-2,2-dimethyl-1,3-dioxane-4,6-dione and poly(styrene-co-maleimide).

As prepared copolymers were subjected to subsequent step that involve 5-(furan-2-ylmethylene)-2,2-dimethyl-1,3-dioxane-4,6-dione reaction with poly(styrene-co-maleimide) to provide poly(styrene-co-maleimide)-5-(furan-2-ylmethylene)-2,2-dimethyl-1,3-dioxane-4,6-dione (SC III). Reaction pathway is represented in Figure 23.

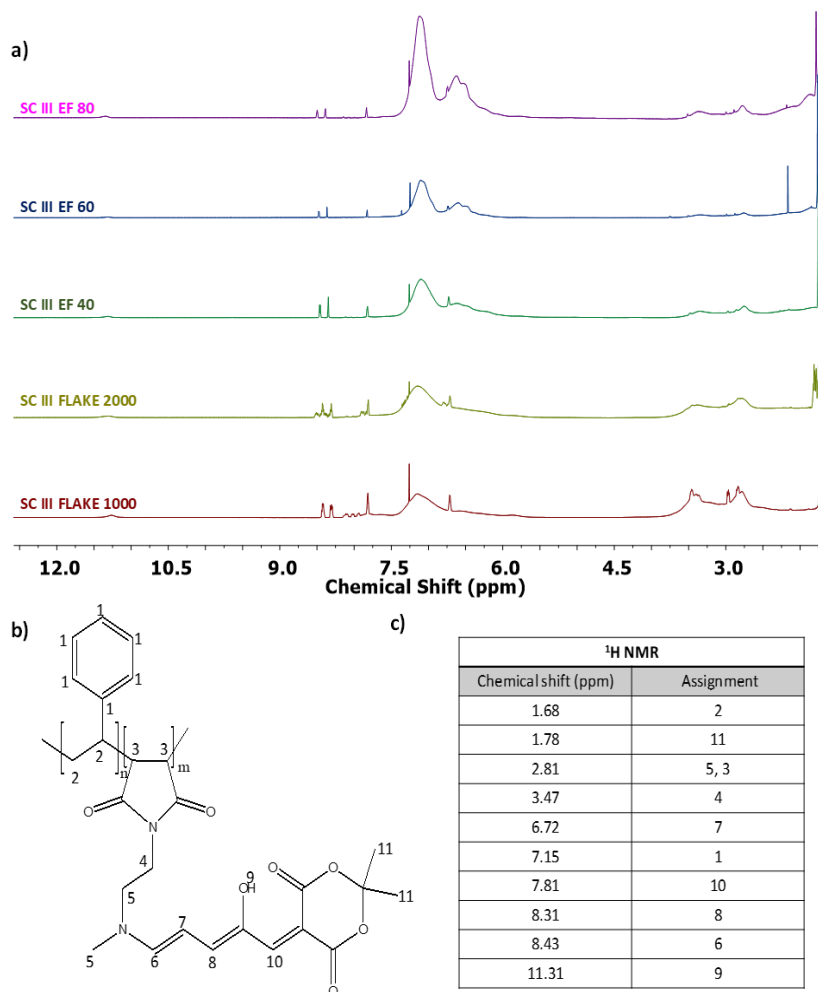
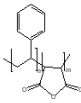
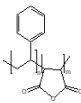
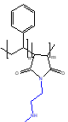
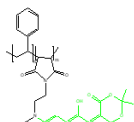


Figure 24. ¹H NMR spectra of SCIII (a); SCIII generic structure (b); table of chemical shifts assignments of SCIII (c).

Figure 24(a) represents ^1H NMR spectra of all obtained SCIII copolymers. The corresponding assignments are reported in Figure 24(c). Basing on obtained spectra, compositions of copolymers were calculated. An integration of a band that was assigned to backbone of the polymer (Figure 24(c) band 2) was compared with an integration of a band assigned to DASA moiety (Figure 24(c) band 11). Resulted data is show in Table 10, and as presented DASA modification of poly(styrene maleimide) varies between 5 % and 28 % according to ^1H NMR quantitative analysis.

Table 11. DSC analysis of the starting copolymers and polymers before and after modifications.

Structure				
Label	SMA Tg [°C] supplier data	SMA Tg [°C] experimental data	SCII Tg [°C] experimental data	SCIII Tg [°C] experimental data
FLAKE 1000	155	149	114	131
FLAKE 2000	135	129	127	134
EF 40	115	111	126	131
EF 60	106	103	119	120
EF 80	104	103	121	126

Basing on the above discussed results, it was concluded that desired material was successfully obtained. To gain insight regarding thermal transitions associated with a SMA and modified SMA materials, differential scanning calorimetry (DSC) was employed. DSC analysis of the polymers were performed before and after modifications and results are collected in Table 11. All of the studied polymers possess an amorphous structure with Tg values between 149 and 103°C. The experimental data collected for SMA copolymers was in the good agreement with Tg provided by supplier. The incorporation of amine to the side chain of the polymers resulted in alternation of Tg. To be more specific, first

modification includes transformation of maleic anhydride to maleimide and incorporation of straight alkane chain terminated with 2°amine (SCII). For the SMA copolymer where 50% and 33% of polymer were modified (FLAKE 1000 and FLAKE 2000, respectively) decrease of Tg was detected. Likely, due to added flexible, short alkane chain. Tg is inversely proportional to flexible moieties within the polymers [106]. Schneider proposed an equation (Eq.10) that represents linear correlation between mass per flexible bond of a polymer repeat unit (M/f) and Tg [107].

$$Tg = A \left(\frac{M}{f} \right)_p + C \quad (10)$$

Where M is the molecular weight of the polymer repeat unit, f is the “number” of flexible bonds in the repeat unit, $(M/f)_p$ is the mass-per-flexible-bond of the (average) repeat unit, and coefficients A and C are described as specific constants polymer class.

For the copolymers EF 40, EF 60 and EF 80 the first modification resulted in the increase of the Tg. This might be due to the difference in the copolymers molecular weights. In Table 4 molecular weights of each copolymer are specified. The copolymers EF 40, EF 60 and EF 80 are of much higher mass than the FLAKE 1000 and FLAKE 2000.

Tg comparison between the products of first modification with the products obtained by second modification show us an increase of the Tg for each case. Those results show clearly that addition of Stenhouse Salt to the side chain of the polymer creates additional intermolecular interactions within the copolymer and possibly

some steric hindrance, hence it disturbs the cooperative segmental mobility and increase T_g .

4.4 Conclusions

We reported on the modifications of the commercially available SMA copolymers. Commercially available SMA copolymers were thoughtfully studied in order to gain insight regarding their molar composition as well as their sequences distributions. Molar composition was confirmed via ^1H NMR, ^{13}C NMR and titration. The results generated by titration and ^{13}C NMR show the closest similarities to the supplier data, while the results obtained by ^1H NMR variate $\pm 3\text{-}10\%$ comparing to the values given by the provider. These differences could be caused by integration error during ^1H NMR spectra elaboration. The copolymers triad sequence distribution was described via ^{13}C NMR spectra analysis. These results brought us to the conclusion that the copolymers have an inclination towards alternating structures. Having better understanding of SMA nature we proceeded with modification reactions. First modification serves to prepare matrices capable of reacting with DASA precursor. Therefore, side chains of the copolymers were decorated with 2° amines. The reaction between maleic anhydride group and primary amines was known in the literature. Its parameters were adjusted to serve our purpose. SMA copolymers modifications with diamine were successfully performed. The products of the second step of the synthetic path were characterized by means of FT-IR and ^{15}N NMR. The modification for each copolymer was successful, and it was calculated that 92% - 95% of the maleic anhydride groups were converted into maleimide. Thus, the obtained poly(styrene-co-maleimide)s were used in the second modification reaction to create copolymers with photosensitive properties (SCIII). The reaction of DASA incorporation within the side chain of the

poly(styrene-co-maleimide) was successful. The structure of obtained SCIII polymers was elucidated by ^1H NMR analysis. It was calculated that DASA modification of poly(styrene maleimide) varies between 5% and 28% according to ^1H NMR quantitative analysis. Photosensitive performance of the final SCIII polymers will be explained in the next Chapter.

5 Photosensitivity studies

5.1 Introduction

In this Chapter an investigation on photosensitive activity of the SCIII polymers will be addressed. As it was described in the previous Chapters the SCIII polymers contain Donor-Acceptor Stenhouse adducts (DASA) photo-sensitive moieties in their structures. DASA compounds were firstly mentioned by Stenhouse in 1850 [88]. The author introduced Stenhouse salts into the science as sensors to detect amines. He discovered that yellow furfural stains were turning to roseate upon addition of few aniline drops onto them. The revived interest in Stenhouse salts appeared with the growing field of photochemistry. Parent DASA molecules were described as photoswitchers i.e. molecules that reversibly alter their geometry, polarity and charge distribution upon light irradiation [108]. Push-pull chromophore of SCIII polymers is presented in Figure 25 and it is highlighted in red.

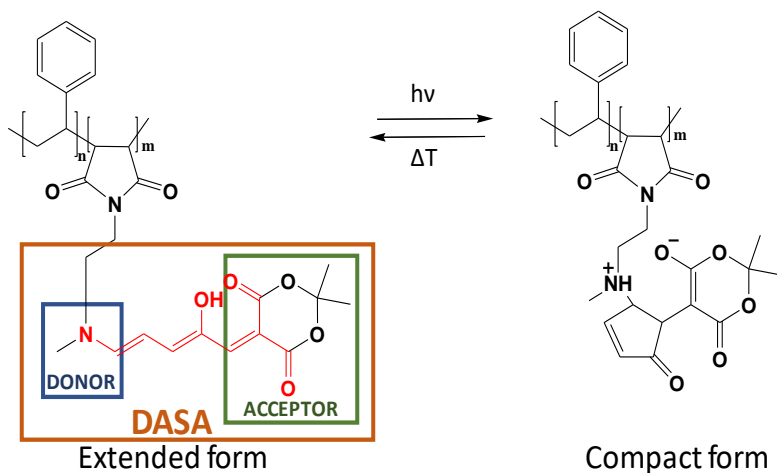


Figure 25. SMA modified with DASA photoswitching scheme.

Triene structure on one end possesses an electron donating group, which is a tertiary amine and on the other end a cyclic acceptor i.e. Meldrum's acid which acts as an electron-withdrawing. Therefore, the extended form of the molecule exhibits strong absorption as a result of a π - π^* transition. DASA molecules in their extended form have a conjugated triene structure that is responsible for a strong absorption band [109]. What is important, the absorption maximum appears in the visible and NIR region of the spectrum, what attracts attention in respect to future possible application for DASA molecules. It is a challenge for scientists to design and synthesise molecules that are photoactive in this particular region of the spectrum. Most of the other known photoswitchers need a specific, tailored modification to achieve this objective. It was investigated before for azobenzenes, diarylethylenes or spiropyrans nevertheless the synthesis might result tedious, time-consuming and of low yields [110-112].

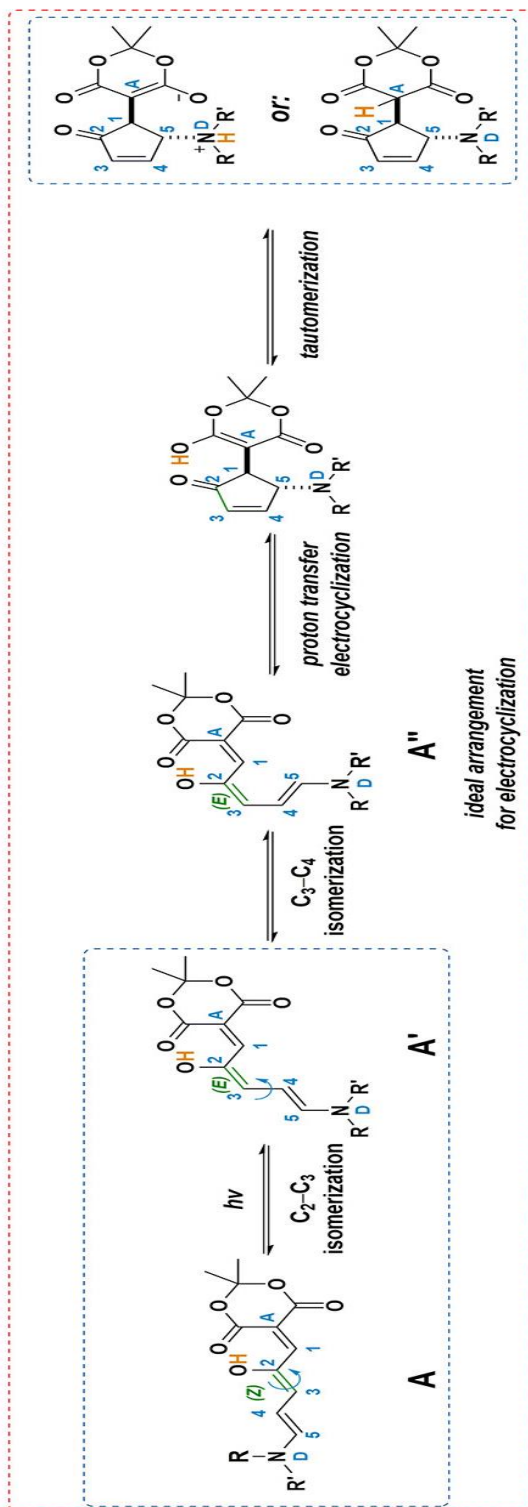
Parent DASA molecules described in the literature have an absorption maximum that fluctuate between 450 and 700 nm [64]. This region of the spectrum is attractive from biological point of view due to its lower energy levels than ultra violet light. Photodamages in biological samples are reduced in comparison with the UV-light activated photoswitchers. Exact absorption maximum of DASA strongly depends on the design of the molecule. The donor and the acceptor part of the molecule can be tailored according to needs. Therefore, absorption maximum depends on the building blocks of the molecule itself, but it is also determined by the environment in which absorption is measured. DASA molecules exhibit solvatochromism. This phenomenon was firstly described in 1922 by Hantzsch and it can be defined as a property of the material to change in electronic absorption spectra with a change in the polarity of the medium [113, 114]. It means that one and the same chromophore could give different

colour depending on the solvent used to dissolve it. The change in colour might be subtle or vast, it is determined by the nature of the chromophore as well as a difference in polarity between the dissolving mediums.

Reversible reactions in case of DASA compounds occur in the dark, therefore they are referred to as a type T photochromes. They exhibit negative photochromism or inverse, what means that their absorption maximum wavelengths are of higher values before irradiation than after [3]. Negative photoswitchers offer advantages over the positive ones particularly at high concentrations. When a positive chromophore is irradiated at high concentration, most of light is absorbed by the outer layer of the sample, due to intensification of colour upon irradiation. This specific constraint is not true for the negative photoswitchers whose undergo photobleaching upon photoswitching to a thermally unstable, colourless state. This characteristic allows for the deeper sample penetration by light, hence increasing light absorption. Photoinduced hypsochromic shift of absorption band can be observed in other organic compounds such as: spiropyrans and spirooxazines, dihydropyrenes, thioindigoid dyes [115].

Structurally DASA molecules are similar to merocyanine dyes. Both can be described as polymethine dyes i.e. chromophoric systems consist of conjugated double bonds (polyenes) located between two end groups: an electron acceptor and an electron donor [13]. What distinct DASA molecules from other polymethine dyes is that they consist of a hydroxy group within polyenes chain. The importance of hydroxy group presence for photochemistry of DASA compound was addressed by Lerch et al. [14]. The significance of the role that hydroxy group plays in DASA compound photoisomerization capacity can be explained using the proposed by Zulfikri et al. mechanism for this transformation.

Figure 26. DASA photoswitching mechanistic proposal. Reprinted from [2].



The scheme of the proposed mechanism is presented in Figure 26 [2]. The authors highlighted that the photoswitching in case of DASA has at least two key steps.

- 1st photoinduced *Z-E* isomerization within the triene chain;
- 2nd 4π thermal electrocyclization followed by a proton transfer and tautomerization.

The actinic step of the reaction is greatly affected by the presence of hydroxy group in the polyene chain. In its absence the *Z-E* isomerization upon photoexcitation can occur in two different locations, and both of them are similarly favoured (C_2-C_3 and C_3-C_4). Further consequences of the existence of hydroxy group in the triene chain appear in the second step of the photoinduced transformation. The authors demonstrated by both theoretical calculation and experimental analysis that the electrocyclization that leads to bleached form of DASA is energetically forbidden. Thus, uniqueness of DASA molecules among other polymethine dyes is justified.

Second key step of the photoinduced transition of DASA cyclization is analogical to the Piancatelli rearrangement and can be also linked to (iso-)Nazarov-type chemistry [116-118]. Actinic step involves *Z-E* photoisomerization that transforms DASA to its intermediate form. It was calculated that this takes place in picoseconds, nevertheless by Evolution-Associated Difference Spectra appearance of a red shifted band corresponding to DASA intermediate could be detected after photoactivation.

Subsequently, rotation between C_3-C_4 is presumed to take place so that the molecule is align in the configuration that favours cyclization. $4-\pi$ conrotatory electrocyclization is followed by proton transfer, what leads to final, compact, colourless form of DASA.

As presented DASA molecules provide an interesting alternative to known photoswitchers. So far they have been used in the wide range of application e.g.: colorimetric method for sensing amines in aqueous media, controlled encapsulation, control over the wettability and contact angle hysteresis on the surfaces, control pull-off adhesion strength, rewriteable data storage, switch permeability of membranes, microfluidics or in drug delivery, photoinducer for creating patterned templates [119-124].

Nevertheless, incorporation of DASA within polymeric matrix might alter aforementioned properties. Therefore, to establish if the photoswitching of DASA was retained after polymer modification series of experiments were performed and analysed.

5.2 Materials and methods

- **Materials**

Five poly(styrene-co-maleic anhydride) (SMA) modified with DASA molecules (SCIII) were synthesised using the procedures described in previous Chapters. Chloroform, dimethylformamide (DMF) were purchased from Sigma Aldrich with purity higher than 98%. All reactants were used without further purification.

- **Characterization**

Photoisomerization was investigated by irradiating samples with visible light emitted by iDual Adaptive LED, 806lm, 11W UV lamp for the desired time. The distance between lamp and sample was 10 cm.

Four different types of experiments involving UV-Vis were designed to investigate the photoswitching of DASA polymers. All UV-VIS spectra were recorded at room temperature (if not

stated otherwise), with a UV-visible spectrophotometer (UV-1800 Shimadzu Spectrophotometer).

1. For the first experiment, polymers were dissolved in chloroform to give concentrations in the range from 0.025 to 0.050 gL⁻¹. Then, the spectra were recorded in the wavelength range 400–700 nm. For each of the polymers the spectra were recorded in the dark at 0, 30 and 60min. Then, samples were illuminated during one hour and spectra were collected at 0, 30 and 60min.
2. Second experiment consisted of recording UV-Vis spectra at 0°C upon light irradiation. SC III EF40 sample was dissolved in chloroform to give a concentration of 0.025gL⁻¹. Next, it was placed in an ice bath and was illuminated as described above for 1 min. Subsequently, sample was placed in spectrophotometer chamber and the spectra was recorded in the wavelength range 400–700 nm.
3. Third experiment was conducted by dissolving SCIII EF 60 copolymer in chloroform to give five samples of concentrations in the range from 0.025 to 0.050 gL⁻¹. Then, samples were illuminated during 10 min and spectra were collected at 541nm each 120s for 1h. Experiments were conducted at different temperatures 10, 15, 20, 25 and 30 °C.
4. Fourth UV Vis experiment included dissolving SCIII EF 60 in five different mediums to give concentrations in the range from 0.025 to 0.050 gL⁻¹. Solvent used were: chloroform, DMF, and their mixtures. Namely: 25 v/v % of DMF and 75 v/v % of chloroform; 50 v/v % of DMF and 50 v/v % of chloroform; 75 v/v % of DMF and 25 v/v % of chloroform. Subsequently, samples were placed in

spectrophotometer chamber and the spectra were recorded in the wavelength range of 400–700 nm.

Fourier transform infrared (FT-IR) spectra of polymer powders were recorded at room temperature with a FT-IR spectrophotometer (Vertex 70, Bruker) with a resolution of 4 cm^{-1} and scanning speed of 2 mm s^{-1} , in absorbance mode. An attenuated total reflection (ATR) accessory with thermal control and a diamond crystal a Golden Gate heated single reflection diamond ATR from Specac-Teknokroma was used to obtain FT-IR spectra. Spectra were elaborated by means of Origin Pro 8.

5.3 Results and discussion

Negative photochromism of polymers modified with DASA was examined by UV Vis spectroscopy. For each of the polymers (SCIII FLAKE 1000, SCIII FLAKE 2000, SCIII EF 40, SCIII EF 60, SCIII EF 80) the spectra were recorded in the dark in order to confirm that the expected absorption band in visible region of the spectra is present and that the absorbance intensity varies due to light exposure the stimuli of the light.

In Figure 27 spectra recorded for all five SCIII copolymers are shown. For all five SCIII polymers spectra recorded in the dark revealed a high intensity absorption band with the absorbance maximum at 541nm. Moreover, all five SCIII polymers spectra recorded in the dark (dark 0min, dark 30min, dark 60min) were almost identical. Meaning that the absorption intensity is not affected without the presence of light. The experiment revealed that for each polymer the absorbance intensity equilibrium was already reached after 30min at room temperature and it was stable after additional 30min at the same temperature in the darkness.

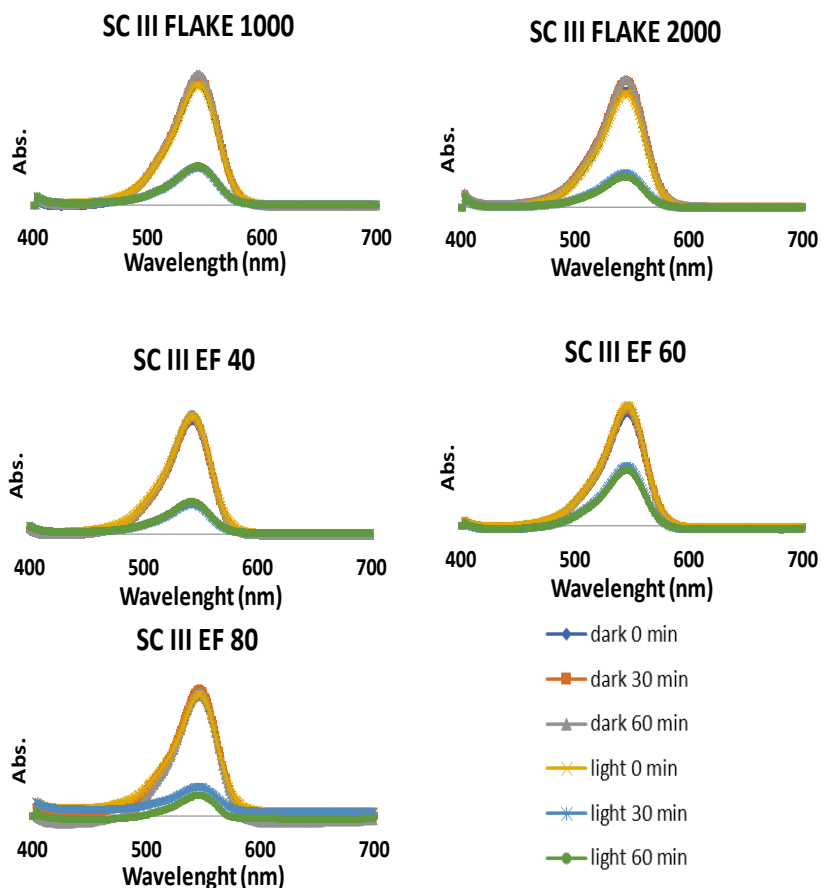


Figure 27. UV-Vis spectra of SCIII polymers in chloroform at RT.

Then, the spectra were recorded after irradiating each sample with light for 30min and 60min (Figure 27, lines: light 0min, light 30min, light 60min). As it is shown in Figure 27, after 30min of sample irradiation with visible light, the band intensity at 541nm decreased for all investigated photosensitive polymers, and remained constant after additional 30min irradiation. From these experiments we concluded that the minimum of the absorbance intensity was reached after 30 min. Samples were additionally irradiated with the light for 30min to confirm that the equilibrium

was reached. Resulted data confirm negative photochromism of obtained material.

Photoisomerization degree was calculated by following equation and the resulted data is gathered in Figure 28.

$$R = \frac{A_0 - A_\infty}{A_0} \cdot 100\% \quad (11)$$

Where, A_0 is the absorption before irradiation and A_∞ is the absorption at the photostationary state.

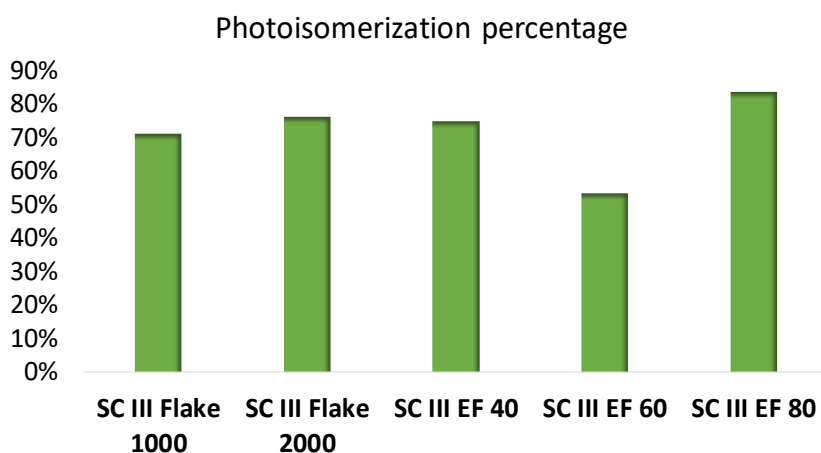


Figure 28. Photoswitching degree of SCIII polymers.

As it is shown in Figure 28, the transformation degree between coloured and colourless SCIII polymers varies between 51% and 83%. The highest value of the photoisomerization degree of SCIII polymers was achieved for SCIII EF80 copolymer with contains 5% of DASA moieties in its structure, and the lowest degree of photoisomerization was detected for SCIII EF60 copolymers which possesses 6% of DASA moieties in its structure. Obtained results put into evidence that the photoswitching degree versus polymer modification degree do not present linear relationship,

what suggests that we cannot directly modify photoswitching degree only by manipulating the content of DASA molecule within material matrix.

To understand the complexity of this transformation and to learn how we can gain more control over it, we decided to investigate furtherly the mechanism of the photoswitching.

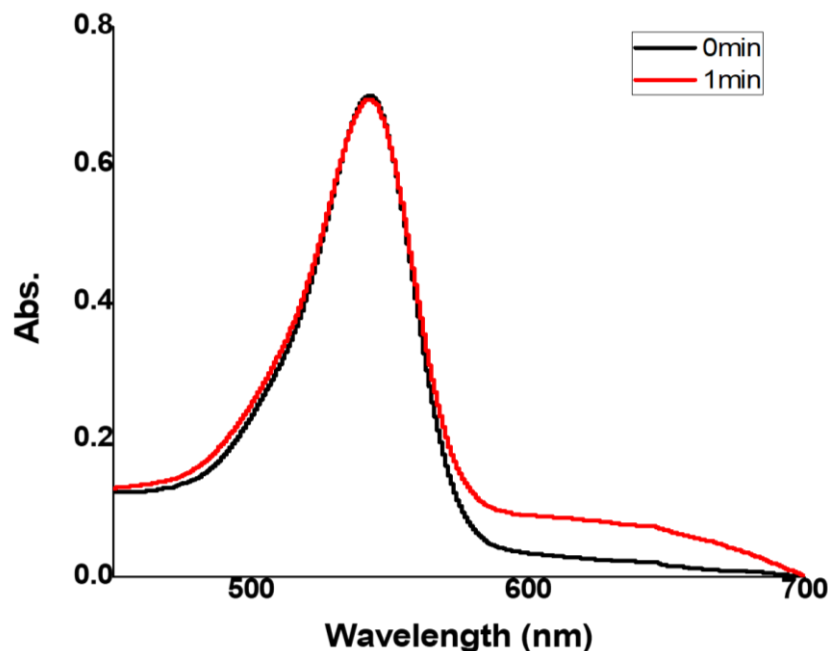


Figure 29. UV-Vis spectra of SCIII EF 40 polymer before (black line) and after (red line) light excitation.

The mechanism of DASA photochromism was described in detail elsewhere [125-127]. Lerch et al. described structural modification of DASA induced by light. Absorption of light causes *Z-E* isomerization of the C₂-C₃ bond of triene structure. Further bond rotation at C₃-C₄ enables formation of an intermediate that favours electrocyclization step to finally obtain compact, bleached form of DASA. Aforementioned intermediate is visible via UV Vis spectroscopy as a red shift from the absorption maximum at 541 nm. Second UV Vis experiment was

designed to detect the presence of this band. As a matter of example Figure 29 shows the spectra recorded of SC III EF 40 at 0°C in darkness (black line) after 1 min of visible light irradiation (red line).

Expected band and slight decrease in absorbance was found. It suggests that the previously described photoisomerization mechanism for the parent DASA molecule might be translated to SC III polymers. In order to gain insight within this transformation kinetics the third UV Vis experiment was performed.

Kinetics experiments of SCIII polymers were performed in chloroform and at the temperature ranges from 10 to 30 °C. As a representation of the results, data obtained for SCIII EF 60 are presented in Figure 30, and obtained plots are given in Figure 31.

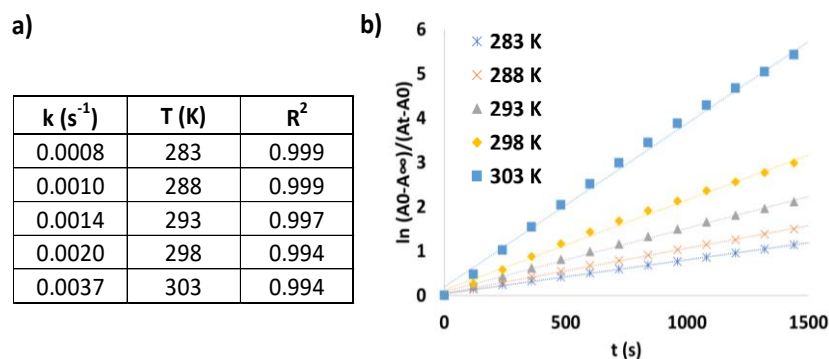


Figure 30. Table with the rate constants of SCIII EF 60 at different temperatures (a) with corresponding spectra (b)

In Figure 30 (a) provides the rates constants of SCIII EF 60 polymer relaxation reaction, along with the temperature at which they were measured and corresponding R^2 . Figure 30 (b) represents how absorption changed in time of relaxation for SCII EF 60 at given temperature. This polymer was found to follow first order kinetics in those specific conditions. To describe changes in the rate of chemical transition against temperature two

separate models were applied: Eyring (Eq.12) and Arrhenius (Eq.13).

$$k = \frac{k_B T}{h} e^{-\frac{\Delta G^\ddagger}{RT}} \quad (12)$$

Where, k is the rate constant; ΔG^\ddagger is the Gibbs energy of activation; k_B is Boltzmann's constant; and h is Planck's constant; T is the absolute temperature (in kelvins); R is the universal gas constant.

$$k = A e^{-\frac{E_a}{RT}} \quad (13)$$

Where, k is the rate constant; A is the pre-exponential factor. According to collision theory, A is the frequency of collisions in the correct orientation; E_a is the activation energy for the reaction; T is the absolute temperature (in kelvins); R is the universal gas constant.

Those equations derived from different statistical considerations. Eyring equation derived from transition state theory, whereas Arrhenius model was formulated by collision theory. Both models are interchangeable upon high temperature ranges. At higher temperatures they differ basing on their foundations. According to the Eyring model rate can continue to rise, while rate described by Arrhenius equation approaches an asymptotic value.[128]

Direct fitting to the Eyring equation gives the entropy of activation of $-82.41 \pm 25 \text{ Jmol}^{-1}$ and the enthalpy of activation of $-63.52 \pm 7 \text{ kJmol}^{-1}$. The enthalpy of activation is approximately equal to the activation energy which was calculated by means of Arrhenius equation and gives $53.40 \pm 8 \text{ kJmol}^{-1}$. Both independent equations are in good agreement.

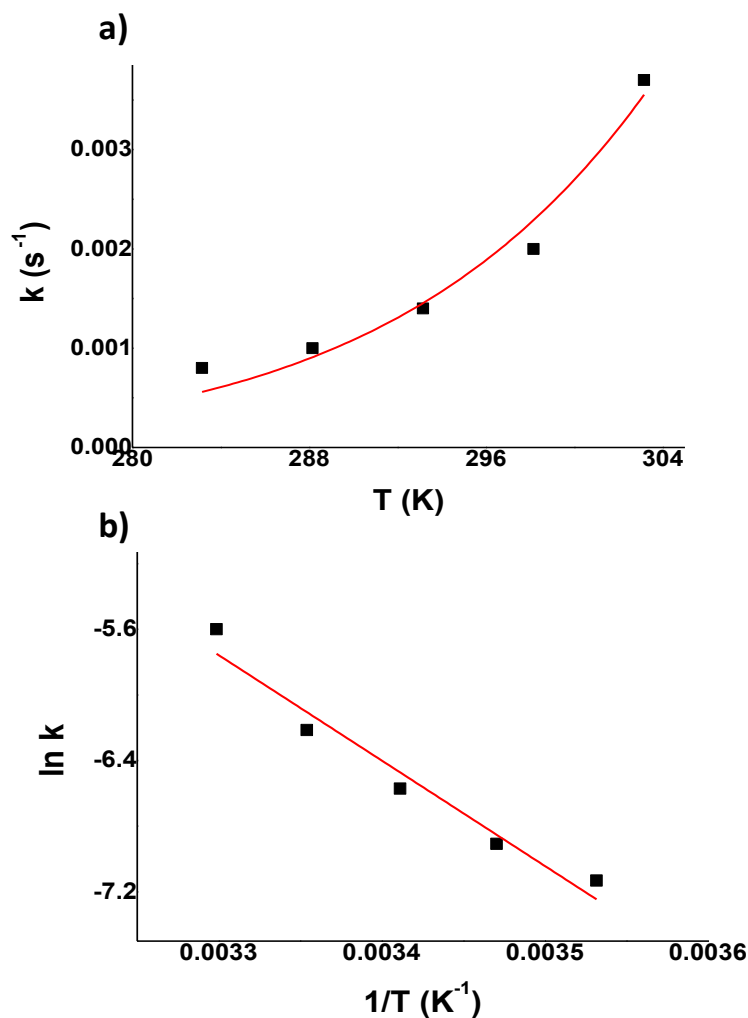


Figure 31. Arrhenius plot with a fitting $R^2=0.95$, (a) and Eyring plot with a fitting $R^2=0.94$ (b) for relaxation of SCIII EF 60 .

Gibbs energy of activation can be also calculated basing on the transition state theory and it gives 87.60 kJmol⁻¹. It is altered to what was provided in the literature for parent DASA molecule. Lerch et al. calculated the Gibbs energy of activation to be 71.17 kJmol⁻¹ [14].

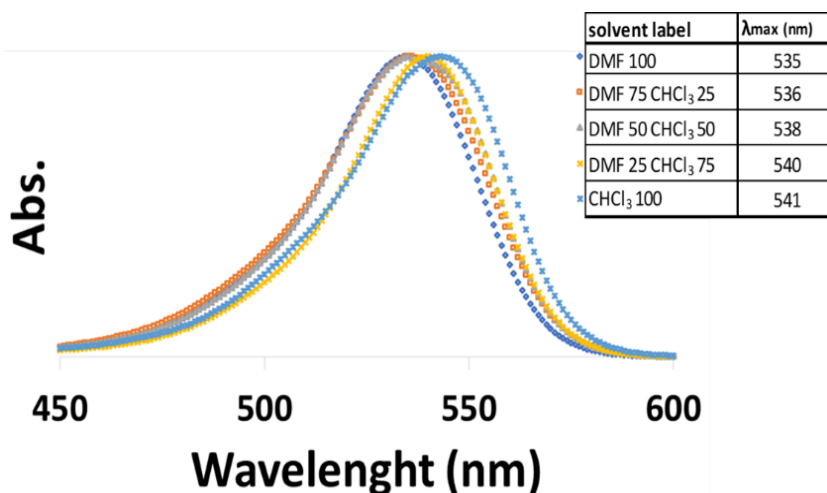


Figure 32. UV-Vis spectra of SCIII in different mediums.

It was described that DASA molecules exhibit strong solvatochromism.[129] To verify if DASA molecule maintains this property while incorporated within polymeric matrix additional experiment was carried out. During this experiment SCIII polymers (SCIII FLAKE 1000, SCIII FLAKE 2000, SCIII EF 40, SCIII EF 60, SCIII EF 80) were dissolved in solvents of different polarity. DMF and chloroform were chosen and their polarity indexes are 6.4 and 4.1, respectively. Then we also used three different binary mixtures of DMF/chloroform (DMF 75 : chloroform 25; DMF 50 : chloroform 50; DMF 25 : chloroform 75) and the spectra were recorded. As a matter of example obtained data for SCIII EF 80 polymer is presented in Figure 32. Spectra recorded in chloroform had absorption maximum at 541nm whereas the other solvents gave red shifted absorption maximums. As expected the DMF present the lowest value of absorption maximum of 535nm, due to its high polarity index. Basing on the results it can be stated that solvatochromism of DASA molecules were retained after its incorporation within SMA structure. This was true for all five SCIII polymers.

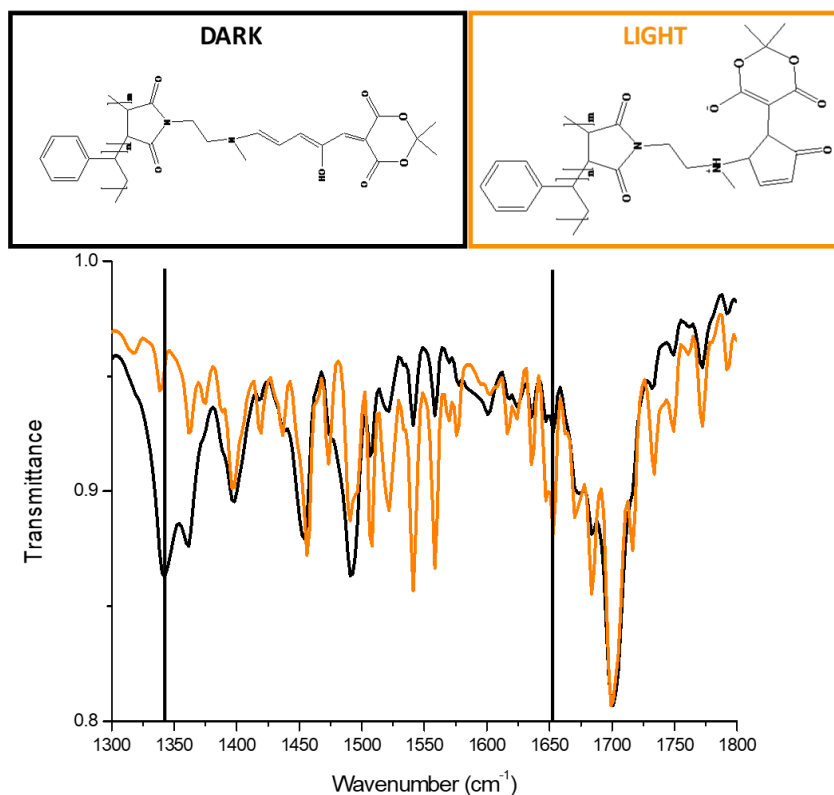


Figure 33. FT-IR spectra recorded at RT in absorption mode of SCIII Flake 1000 before (black line) and after (orange line) illumination.

Then, the photoisomerization of all investigated polymers was also investigated by means of FT-IR spectroscopy. The comparison between the FT-IR spectra of SCIII polymer before (black line) and after (orange line) irradiation with the visible light is shown in Figure 33. As a matter of example one modification was chosen for the experiment as it is representative for all the SCIII polymer family. The spectra confirm photosensitive nature of obtained family of polymers. First detected change, reflected in the spectra as disappearance of the band at 1342cm⁻¹ upon irradiation with the light, was due to transformation that occurs on the carbon atom neighbouring the nitrogen linker group. In the

dark this atom is located in triene chain and is in a sp^2 hybridization and when the copolymer is illuminated electrocyclization of triene chromophore occur, hence the hybridization of said carbon atom rearranges to sp^3 . Moreover, if we focus on the spectra recorded after irradiation we can detect new band at 1652cm^{-1} which is assigned to C=C bond in the cyclopentenone conformation.

5.4 Conclusions

We reported that the negative type T photochromism as well as the solvatochromism of DASA molecules were retained after modification of SMA polymers. The photoisomerization degree between coloured and colourless SCIII polymers varies between 51% and 83%. Photoswitching degree versus polymer modification degree do not present linear correlation. What implies that other parameters needed to be considered in controlling the SCIII polymers photosimerization extent. It is conjectured that the mechanism of the photoswitching was preserved after polymer modification, as described previously in the literature. The alternation of the photoisomerization kinetics between parent DASA and modified polymers was observed and analysed. Two separate models were applied: Eyring and Arrhenius to describe changes in rate of chemical transition against temperature. Eyring model provided Gibbs energy of activation, that gave 87.60 kJmol^{-1} what is a slight increase in comparison to result provided in the literature for parent DASA molecule 71.173 kJmol^{-1} .

6 Applications

6.1 Membranes

6.1.1 Introduction

The main strategic objective of this PhD thesis is focused on the development of novel photosensitive capsules based on the copolymers synthesised by procedures established in the previous Chapters. Before preparing and characterizing microcapsules, we performed an exhaustive characterization of membranes based on the SCIII copolymers. In this way, we tried to simulate the morphology and the behaviour of the microcapsule shell under visible light irradiation. This Chapter describes the SCIII polymeric membranes formation and their behaviour upon light illumination. SCIII polymeric membranes were prepared in order to mimic behaviour of the capsules wall, as the invention of the photoactive capsules are the final objective of this PhD thesis.

In general, membranes can be defined as a selectively permeable barrier between two phases [130]. They are widely used to separate a mixture of different substances, as they permit the passage only of certain species across their structures. The selectivity of membranes depends on various parameters, such as: chemical composition, morphology and methods of preparation. The membranes prepared by us were fabricated by phase inversion process where precipitation occurs by solvent evaporation. In this method polymer is dissolved in suitable solvent and deposited upon a glass plate, or chosen support. Then, solvent is allowed to evaporate, thus solidification of the polymeric structure. In general this method lead to fabrication of dense membranes [131].

DASA moiety was employed recently in various studies to modify the properties of polymeric films [121, 123, 124, 132]. It was

reported that the solid DASA films can change their wettability, adhesive properties and photoisomerization kinetics upon light irradiation.

We employed Atomic Force Microscope (AFM), Contact Angle (CA), and Fourier-transform infrared spectroscopy (FT-IR) to analyse the SCIII films interaction with light.

6.1.2 Materials and methods

- **Materials**

Chloroform was purchased from Sigma Aldrich with purity higher than 98%. SCIII polymers were synthesised in our laboratory by the methods explained in Chapter 3 and 4. Support membranes were acquired from our industrial collaborator (P&G), and were used without any previous preparation. All reactants were used without further purification. Milli-Q water was used in conducted experiments.

- **Membranes preparation**

Membranes were prepared by a solvent evaporation process, in which a homogeneous polymeric solution is cast on a suitable support and placed in a controlled environment until total evaporation of the solvent is reached. In order to prepare photosensitive membranes, the SCIII polymers were dissolved in chloroform by stirring for 24h to obtain a 15 wt % solution. Subsequently, the solution was cast on a supportive membrane which was attached to a glass plate. Then, by means of a custom-made casting knife with a gap of 0.3 mm the solution was homogeneously distributed on the supportive membrane surface. As prepared materials were placed under the fume hood at room temperature for 24h to solvent evaporation. Next, the films were released from the glass plates and stored in a dry, dark box.

- **Characterization**

Photoisomerization of membranes was investigated by irradiating samples with visible light by iDual Adaptive LED, 806lm, 11W UV lamp for the desired time. The distance between lamp and sample was 10 cm. This was true for all below mentioned experiments.

Static contact angles (CA) with water on a membrane surface were measured using an optical contact angle instrument (Dataphysics OCA 15EC) equipped with a motorized pipette (Matrix Technology, Nashua, NH) and Milli-Q water as the probe liquid. The contact angle was calculated immediately after placing the water drop (3 μL) on membranes surfaces, from a digital image by SCA software included in the apparatus. Measurements were repeated five times for each membrane using different areas of the film. Measurements were made for the membranes before and after light exposure. Each sample was illuminated for 30min. ANOVA single factor statistical analysis method available in Microsoft Excel software was applied to verify the statistical significance of obtained results.

Membranes surfaces morphologies were characterized by an atomic force microscopy (AFM). Six measurements were made for each membrane: three before and three after light exposure. Each sample was illuminated for 30min outside of AMF chamber. The AFM images were recorded with an Agilent 5500 Environmental Atomic Force Microscope (Agilent Technology) equipped with an extender electronics module, which enables phase imaging in Tapping Mode. All the images were recorded in tapping mode using Multi 75 (BudgetSensors) silicon cantilevers (length = 225 μm , width = 28 μm , and thickness = 3 μm) with a force constant of 3 N/m and a resonance frequency of 75 kHz. The scan rate was typically 0.7–2 H. All images (2 \times 2 μm) were taken at room temperature, in air without filtering. The microscope was

placed on an active vibration isolation chamber (Agilent Technology), which was further placed on a massive table to eliminate external vibration noise. The Nanotec WSxM 5.0 Develop 4.0 Image Browser Scanning Probe Microscopy was used for the roughness analysis of the images.

Fourier-transform infrared (FT-IR) spectra of membranes were obtained at room temperature with a FT-IR spectrophotometer (Vertex 70, Bruker) with a resolution of 4 cm^{-1} and scanning speed of 2 mm s^{-1} , in absorbance mode. An attenuated total reflection (ATR) accessory with thermal control and a diamond crystal a Golden Gate heated single reflection diamond ATR from Specac-Teknokroma) was used to obtain FT-IR spectra. Spectra were elaborated by means of Origin Pro 8. Measurements were made for the membranes before and after light exposure. Each sample was illuminated for 30min.

Low-to-Mid Range Magnification Digital Microscope Leica DMS1000 (Leica Microsystems) with the built-in HDMI microscope camera provided high definition full colour still images of the membranes surfaces.

6.1.3 Results and discussion

As mentioned before, the final objective of this work was the preparation of the photosensitive capsules. In order to see if the capsules made of SCIII polymer could give significant alteration of the capsule wall upon photoexcitation, we chose to characterize SCIII membranes. We assume that the SCIII flat films will mimic the behaviour of the microcapsule wall.

Membranes were prepared from SCIII polymers by solvent evaporation technique. Firstly, we tried to prepare membranes without any additional support, nevertheless the material resulted to be too brittle, thus homogeneous flat film could not be obtained.

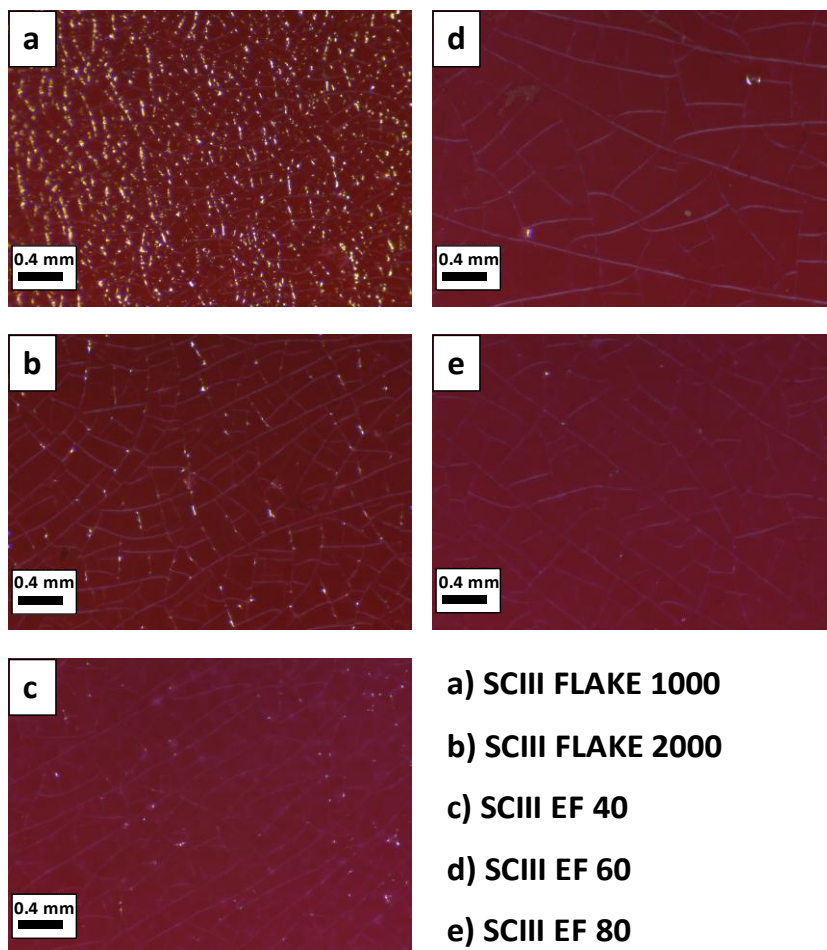


Figure 34. Optical microscope images of the SCIII membranes surfaces.

Moreover, any attempt of membranes manipulation caused total disintegration of the films. Therefore, chemically inert support provided by P&G Company was used to prepare SCIII membranes. Homogeneous solutions of five different modifications of SCIII (SCIII FLAKE 1000, SCIII FLAKE 2000, SCIII EF 40, SCIII EF 60, SCIII EF 80) were casted upon the support. Then, after the solvent evaporation obtained membranes were characterized by optical microscopy, AFM, CA, FT-IR.

The immobilization of the SCIII membranes into the support was successful. The manipulations of obtained membranes were possible. The top surfaces of the membranes were captured by digital microscope and resulted photos are show in Figure 34. Membranes for all the modifications are crimson-purple in colour. The images of Figure 34 reveal that the membranes surfaces are not smooth, many fractures can be observed upon them. The ruptures are randomly distributed through all the surface of the membranes. However, the density of the cracks changes with the modification degree. The membrane SCIII FLAKE 1000 with the highest DASA modification, exhibits much more fractured surface, than the SCIII EF 80 membrane (lowest DASA modification) where the cracks are barely noticeable. To further investigate membranes texture AFM analysis was conducted..

Table 12. RMS roughness of SCIII membranes before light exposure (dark) and after (light).

RMS roughness				
label	dark	error	light	error
SCIII FLAKE 1000	3.2	0.7	2.6	1.4
SCIII FLAKE 2000	3.6	1.4	1.8	0.1
SCIII EF 40	1.8	0.7	0.0	0.0
SCIII EF 60	6.7	2.8	1.1	0.1
SCIII EF 80	8.5	1.8	1.6	0.2

The membranes were further studied by means of AFM. Root-Mean-Squared (RMS) roughness was calculated from topographic images and gave values between $1.8 \pm 0.7\text{nm}$ and $8.5 \pm 1.8\text{nm}$ (Table 12). Corresponding images are shown in Figure 35.

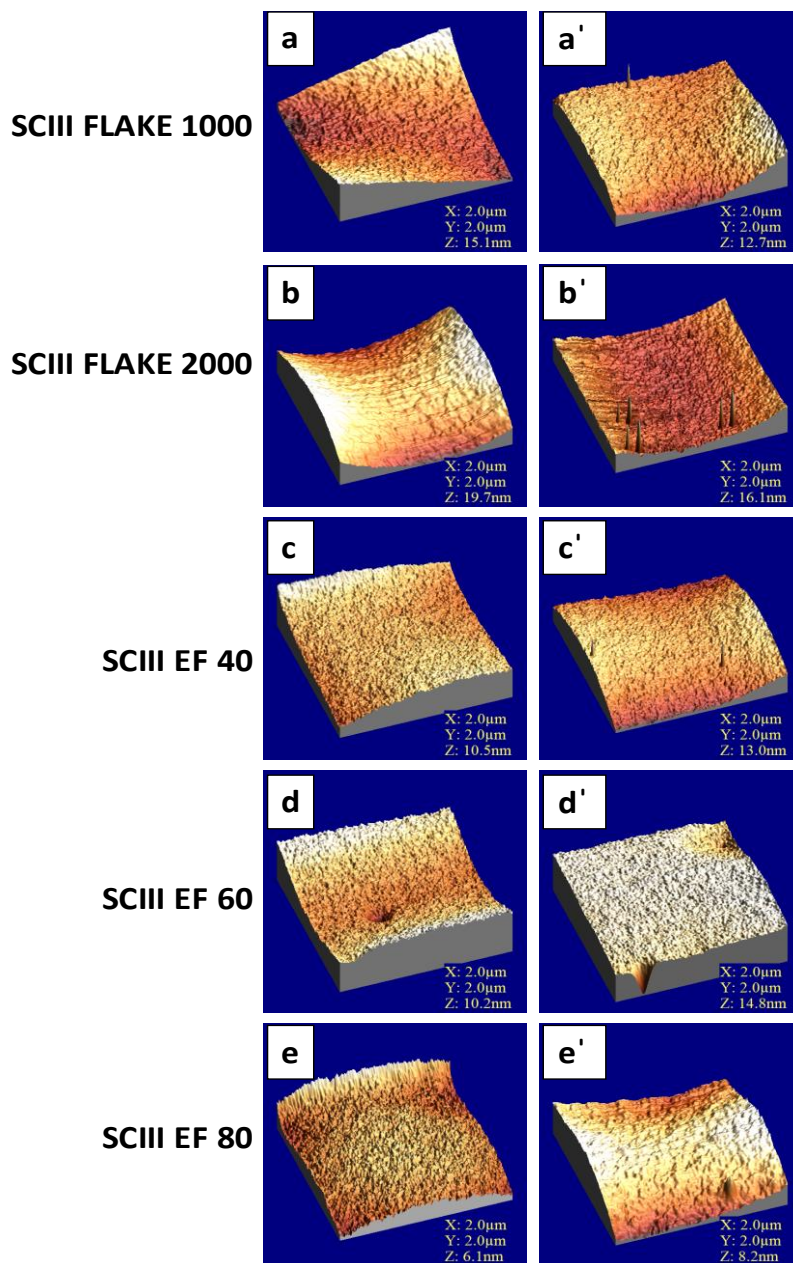


Figure 35. AFM topographic images of membranes that were not exposed to light (a-e) and after 30min of samples irradiation with visible light (a'-e').

The Root-Mean-Squared (RMS) roughness obtained for SCIII Flake 1000, SCIII Flake 2000 and SCIII EF 40 are of similar low values ($3.2 \pm 0.7\text{nm}$, $3.6 \pm 1.4\text{nm}$, $1.8 \pm 0.7\text{nm}$, respectively), whereas for the SCIII EF 60 and SCIII EF 80 membranes the values almost triples, giving $6.7 \pm 2.8\text{nm}$ and $8.5 \pm 1.8\text{nm}$, respectively. Implicating that the membranes with higher amount of photoactive moiety give smoother surface (SCIII Flake 1000, SCIII Flake 2000 and SCIII EF 40); where the membranes with low DASA concentration (SCIII EF 60 and SCIII EF 80) have much rougher surfaces.

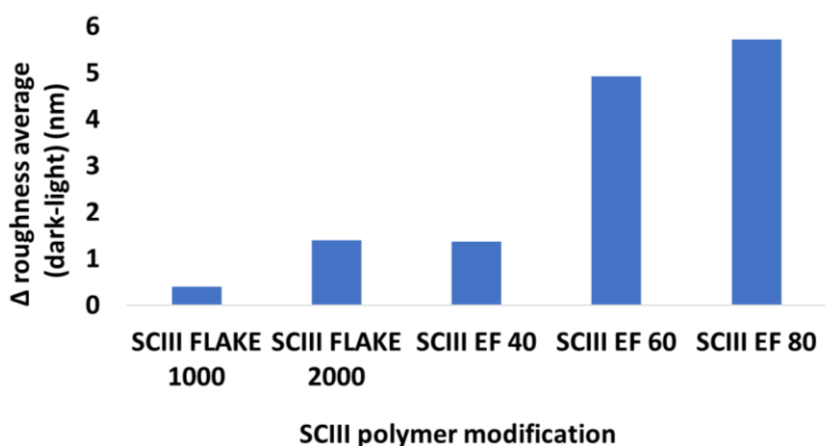


Figure 36. Roughness average change before (dark) light exposure and after (light) for each SCIII membrane.

Light sensitivity of obtained membranes was examined by comparison of the RMS roughness calculated from the images taken after 30min of samples irradiation with visible light and the ones taken for the membranes that were not exposed to the light. In Figure 35 the left column of topographic images corresponds to the samples kept in the dark, and the right column to the irradiated samples. The differences between both are not clear by topographic image examination. However, basing on the images RMS roughness were calculated for each sample and reveal that

the membranes have a tendency to decrease the roughness value after exposure to light. It is true for each SCIII copolymers modifications. Graph that represent this trend is shown in Figure 36.

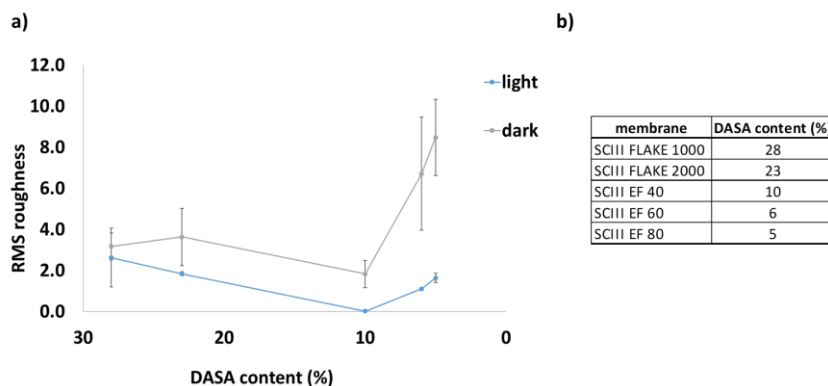


Figure 37. RMS roughness obtained for each SCIII membranes before (dark) light exposure and after (light) (a); Table specifying the content of DASA in each membrane (b).

Further study indicates that the effect of light upon the membranes surface results in roughness changes and it is correlated with DASA concentration of examined sample (Figure 37).

What is surprising is that the membrane with the highest concentration of DASA (SCIII Flake 1000, 28%) provokes the smallest change in the roughness average (0.4nm); and the membrane with the lowest DASA concentration (SCIII EF 80, 5%) triggers the highest change in the roughness average (5.7nm). Similar trend was identified for the degree of photoisomerization versus DASA concentration.

Photoisomerization of membranes was analysed by means of FT-IR analysis. Spectra of each membrane was taken before and after light exposure. Then, the integrations of the band at 1342cm^{-1} were taken. The importance of this band was addressed in Chapter 5. Here it will be shortly discussed. In darkness DASA form contains a triene chain and carbon atoms have a sp^2 hybridization,

what is reflected in spectra as a band at 1342cm^{-1} . When DASA transform upon light irradiation electrocyclicization of triene chromophore occurs, and carbon atom neighbouring nitrogen linker group transform from sp^2 hybridization to sp^3 . In consequence, the aforementioned band recedes.

By way of explanation in Figure 38 spectra collected for membrane made with SCIII FLAKE1000 is shown, and mentioned band as well as the carbon in question are highlighted.

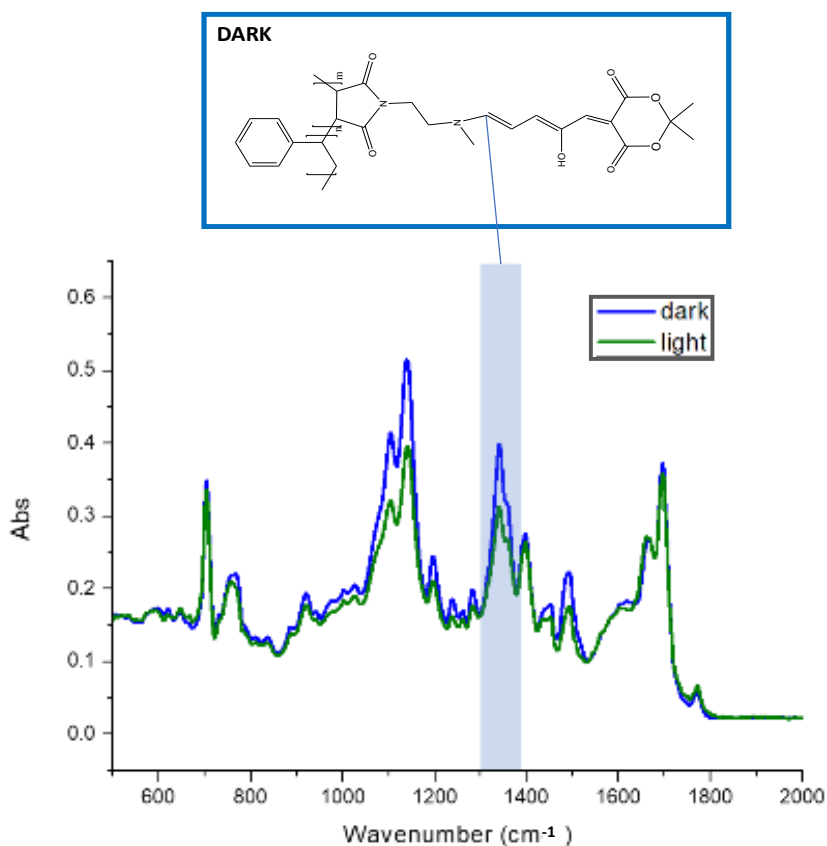


Figure 38. FT-IT spectra of membrane made with SCIII FLAKE 1000. Blue line (dark) corresponds to spectra collected for the membrane before light exposure; and green line (light) for the spectra of the irradiated sample

We measured the differences in the integration of band at 1342cm^{-1} before and after light irradiation and translated it to photoisomerization degree, by means of the equation presented below (Eq.14).

$$\% \textit{photoisomerization} = \frac{A_d - A_l}{A_d} \cdot 100\% \quad (14)$$

Where A_d is the area of the band at 1342cm^{-1} measured on the sample with no light exposure; and A_l is the area of the band at 1342cm^{-1} measured on the sample exposed to visible light. Corresponding data is gathered in Table 13. Then, the photoisomerization degree was plotted against the copolymers modifications (Figure 39).

Table 13. Photoisomerization degree of SCIII membranes.

label	Area _{dark}	Area _{light}	Area _{dark} - Area _{light}	% of photoisomerization
SCIII FLAKE 1000	7.6	4.9	2.7	36
SCIII FLAKE 2000	5.7	3.2	2.5	44
SCIII EF 40	5.6	2.3	3.2	58
SCIII EF 60	4.3	1.7	2.6	61
SCIII EF 80	4.6	1.3	3.3	72

Degree of photoisomerization varies between 36 % and 72 %. Graph shown in Figure 39 displays that the higher DASA concentration the lower % of photoswitching is detected. As mentioned before, similar trend was detected for the roughness of the samples. The differences between the average roughness before and after light exposure were calculated and plotted against the degree of photoisomerization. As a graphical representation imply the change in surface roughness average is driven by

photoisomerization of photoactive moieties (Figure 40). Higher the photoisomerization degree translates to higher change in surface roughness.

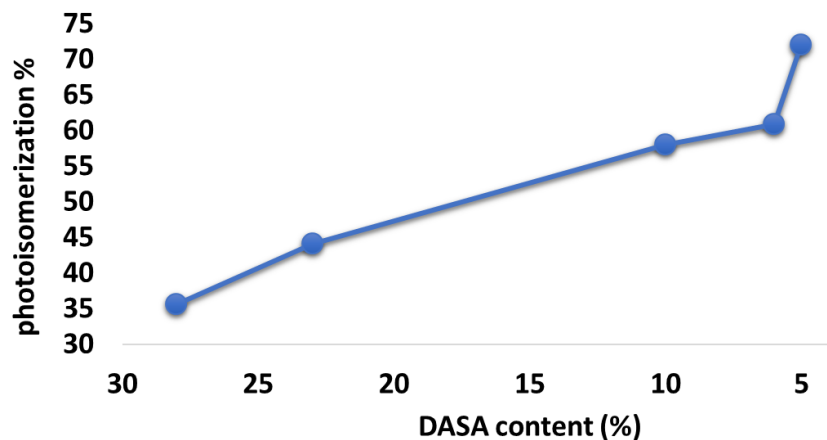


Figure 40. Degree of SCIII membranes photoswitching versus DASA content in each membrane.

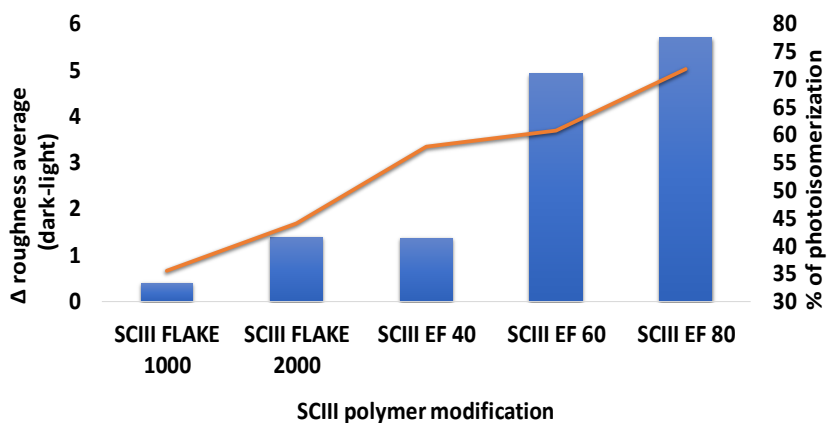


Figure 39. The differences between the average roughness before and after light exposure plotted against the degree of photoisomerization in respect to SCIII polymer modification.

Yap et al. reported that chain length of the polymer modified with DASA might have an impact on its transformation upon light irradiation [132]. In general, it was described that the longer the chain the more restricted DASA movement are, in consequence it

suppresses the photochromic process. We plotted the molecular weight of the copolymers against degree of the photoisomerization (Figure 41). Our findings give a linear correlation between the chain length versus % of isomerization. Nevertheless, it is exact opposite of the Yep et al. conclusions.

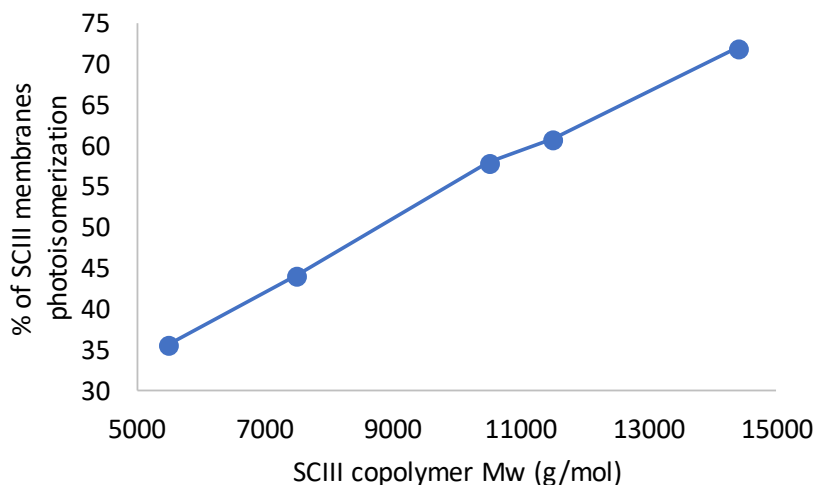


Figure 41. Photoisomerization degree of SCIII polymers plotted against corresponding molecular weight.

The photoisomerization increase proportionally to the chain length.

It was found that the roughness might be linked also to wettability of the films [133]. Commonly known Wenzel model states that the contact angles (CA) are directly correlated with the surface roughness. As a general rule, the rougher surfaces increase the hydrophobicity on hydrophobic surfaces, and enhance the hydrophilicity on hydrophilic surfaces. We measured static CA of each membrane before and after illumination with the visible light and the results are gathered in Table 14.

Table 14. CAs of SCIII membranes measured before (CA dark) and after (CA light) light exposure with corresponding standard deviations.

label	CA _{dark} (°)	error CA _{dark} (°)	CA _{light} (°)	error CA _{light} (°)
SCIII FLAKE 1000	84	3	78	3
SCIII FLAKE 2000	77	2	88	7
SCIII EF 40	95	2	83	3
SCIII EF 60	85	5	96	5
SCIII EF 80	96	4	92	3

As a matter of example images of SCIII 1000 membrane were taken during CA analysis and are shown in Figure 42. Figure 42(a) shows a water drop on the sample surface not irradiated with light, whereas image of Figure 42(b) a water drop on the membrane exposed to light. Careful examination of those images does not reveal any significant difference between them.

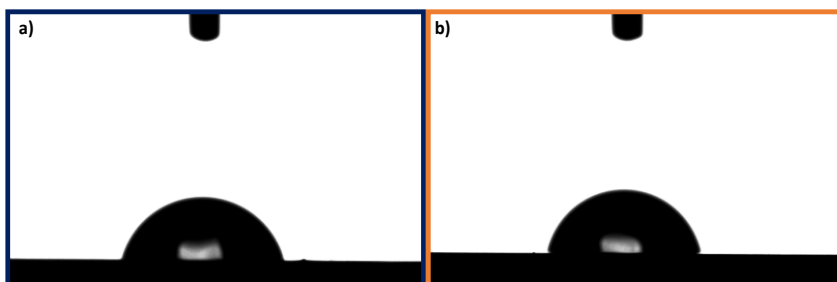


Figure 42. CA images of the SCIII FLAKE 1000 membranes. Image left: water drop on the sample not exposed to light (a); image right: water drop on the irradiated sample (b).

Therefore, to visualize the changes in wettability that occurred during this experiment, obtained CAs were plotted against the polymers modifications and the results are shown in Figure 43.

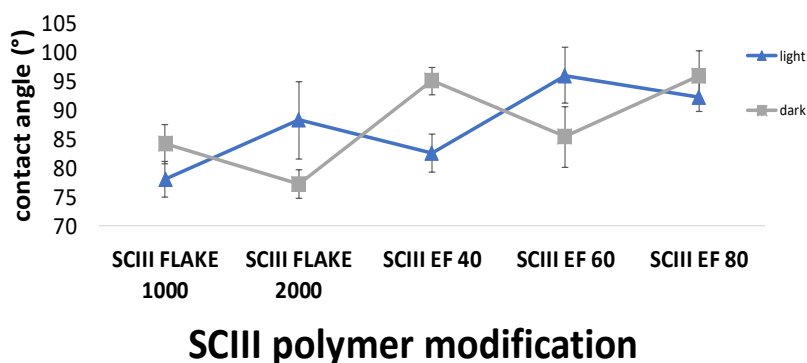


Figure 43. CAs were plotted against the SCIII polymers modifications.

CAs variations do not directly correlate with the differences in surface roughness. We can state that gathered data do not follow Wenzel model [133]. Nogalska et al. stated that the static CA value above 90° indicates a hydrophobic character of the surface, while for the value below 90° the surface is considered hydrophilic [134]. As the present films made with SCIII copolymers balance between the limits of hydrophobicity and hydrophilicity (CA values between $77^\circ \pm 2^\circ$ and $96^\circ \pm 4^\circ$) it is not reliable to apply this model to our system, thus compare them to surface roughness.

We were surprised to see that even the chemical composition seems to not have a direct influence on CA variations. The change in CA before and after light exposure were registered and plotted against the copolymer modification (Figure 44).

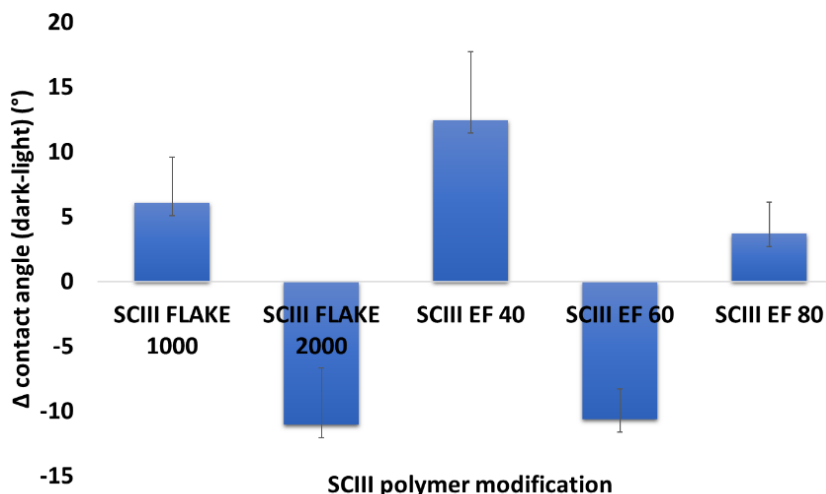


Figure 44. Difference in CAs before and after light exposure were plotted against the SCIII polymers modifications.

For the samples SCIII FLAKE 1000, SCIII EF 40 and SCIII EF 80 the surfaces after illumination became more hydrophilic, giving changes equal to 6° , 12° and 4° , respectively. While the samples SCIII FLAKE 2000 and SCIII EF 60 gave opposite results, becoming more hydrophobic, changing of -11° both of them. Those clear inconsistencies between the samples of the same copolymer but with different chemical composition, made us apply an analysis of variance to confirm the relevance of obtained results [135]. ANOVA statistical technique was employed to compare the differences between groups of data means and state if they are statistically significant or not. We calculated *P-value* that specifies the relevance of the obtained data. In general, if the resulted *P-value* is below 0.05 it means that the obtained results are of relevance, and when they are above of this value it suggest that the data are not significant [136]. We obtained *P-value* of 0.98 for CA measurements before and after irradiation with the light, what statistically made those result not significant, i.e. they are not noteworthy. It means that 98% of the

results are unremarkable in the sense that they occur fairly frequently.

6.1.4 Conclusions

The supported membranes of SCIII polymers were obtained by evaporation of the solvent and characterized. The top surfaces of the membranes images were captured by digital microscope and resulted photos reveal that all membranes were crimson-purple in colour. Their modification upon light exposure were analysed by means of CA, AFM and FT-IR analysis. AFM and FT-IR analysis results imply that the obtained films are in fact photoactive. The alterations detected by those techniques show clear correlation between the roughness, degree of photoisomerization and chemical composition of the material. Degree of photoisomerization was characterized by FT-IR quantitative analysis and varies between 36 % and 72 %. Higher the photoisomerization degree translates to increase in surface roughness. Our findings give a linear correlation between the chain length versus % of photoisomerization. The photoisomerization increase proportionally to the chain length. Contact angles analysis resulted as statistically insignificant.

6.2 Capsules

6.2.1 Introduction

The final objective of this PhD thesis was to create the photoactive capsules with controlled release of encapsulated oil that can be readily applied in P&G company products. This Chapter describes the SCIII polymeric capsules formation and their behaviour upon light illumination. SCIII polymeric capsules were created by means of four techniques: 1) phase inversion precipitation; 2) emulsion crosslinking of partially modified SCIII copolymer (DASA modified polymer, molar ratio ST-styrene, MA-maleic anhydride, MI-maleimide; 4ST : 1MA : 2MI; 3) SMA/SCIII emulsion precipitation in different non-solvents; 4) emulsion crosslinking of SCIII with SMA blend. Each method of preparation as well as characterization of obtained capsules are addressed here.

Encapsulation process is described as the capture of a compound into a coating material [17]. Encapsulation technology is currently the best solution available on the market for the delivery of dedicated components/materials in different applications such as: food ingredients, perfumes, drugs, dyes, acids, pesticides and herbicides, etc [41, 44, 51, 53, 57].

Light sensitive encapsulates would provide release of perfume in absence of external mechanical forces, light being only external stimuli. Thus, the polymeric shell should be designed properly, with the light sensitive moiety incorporated to help the polymeric shell release the encapsulated active when exposed to visible light. Instead of functionalizing an existing polymer, a novel polymer was designed with the intention of making capsules with a compacted shell minimizing leakage in presence of surfactants

and containing DASA light sensitive moiety into the side chain, in order to obtain control on the release. The polymer was designed as a copolymeric chain that contains the side chain modification photosensitive monomer.

The important parameters to consider for the design and the production of the capsules are thus I) the light sensitive behaviour of the photosensitive molecule which will be part of the polymer, II) the light sensitive behaviour of the polymer which will constitute the capsule shell, III) a good flexibility and mobility of the polymeric chain, balanced with a good compactness of the polymer into the shell; in this way the polymer will be capable of undergoing the desired conformational transitions and, in absence of a triggering event, the leakage can be minimized. The parameters I) and II) are addressed in Chapter 5, whereas parameter III) will be shortly addressed here. The final polymer we want to obtain contains flexible spacers between backbone of the polymer and DASA moiety. This allows a higher compaction of the capsule wall and a good mobility of the photosensitive section, which, otherwise, would be too packed. As a flexible spacer, we selected the commercially available N-methylethylenediamine and its amount depends on the amount of maleic anhydride of each SMA copolymer.

6.2.2 Materials and methods

- **Materials**

Chloroform, tetrahydrofuran (THF), n-heptane, hexyl acetate were purchased from Sigma Aldrich with purity higher than 98%. Poly(vinyl alcohol) ($M_w \approx 40000$ g/mol) (PVA) was purchased from Sekisui. SCIII polymers were synthesised in our laboratory by the methods explained in Chapter 3 and 4. Perfume Voyager Zen was acquired from our industrial collaborator (P&G), and was

used without any previous preparation. All reactants were used without further purification. Milli-Q water was used in conducted experiments.

- **Capsules preparation:**

1.Phase inversion precipitation capsules

Capsules preparation MC1 – MC4

Solution of SCIII EF 80 (2.079g) in 20mL of solvent (THF - MC1; Voyager Zen - MC2 and MC3; hexyl acetate – MC4) was prepared by vigorous stirring for 24h. Next day, 4mL of prepared solution was placed into a spray gun and pushed through the nozzle by the force of compressed air ($0.9\text{Nm}^3/\text{h}$) into n-heptane bath (400mL). The distance between the bath and the nozzle was measured to be 30cm. The non-solvent bath was kept at room temperature (RT) for MC1 and MC2; or at 0°C for MC3 and MC4. Produced colloidal dispersion was filtered to collect the capsules. Then, the capsules were dried on air at RT.

2. Emulsion crosslinking of partially modified SCIII copolymer (DASA modified polymer, molar ratio ST-styrene, MA-maleic anhydride, MI-maleimide; 4ST : 1MA : 2MI)

Capsules preparation MC5

First, four solution were prepared:

Solution1:

0.182g of Xantan Gum was dissolved in 60ml of milliQ water by stirring (mechanical stirrer at 400rpm) for 24h.

Solution2:

0.5g of SCIII-15 (DASA modified polymer, molar ratio ST-styrene, MA-maleic anhydride, MI-maleimide; 4ST : 1MA : 2MI) was dissolved in 6mL of chloroform.

Solution3:

0.179g of 1.8-diaminooctane and 0.0279g of NaCO₃ were dissolved in 1ml of milliQ water by stirring for 5min.

Then, 60ml of solution1 was placed under mechanical stirrer (400rpm). Subsequently, solution2 was added in dropwise manner into solution1. After 30min o/w emulsion was created and the speed of agitation was decreased to 150rpm. When the speed of the stirrer was adjusted, 1ml of solution3 was added in dropwise manner to reaction mixture and then was continuously stirred for another 2h.

As prepared slurry was stored.

3. Emulsion precipitation in different solvents

Preparation of MC 6 – MC 10

First, three solutions were prepared:

Solution1:

2.079g of SCIII EF 80 were dissolved in 20mL of perfume Voyager Zen. As prepared mixture was ultrasonicated for 15min and left overnight.

Solution2:

2.062g of SMA EF80 were dissolved in 20mL of perfume Voyager Zen. As prepared mixture was ultrasonicated for 15min and left overnight.

Solution3:

0.992g of PVA was dissolved in 98ml of milliQ water by heating (80°C) and stirring (magnetic stirrer 400rpm) for 2h.

Solution4:

0.502g of Xantan Gum was dispersed in 100ml of milliQ water by stirring for 24h (mechanical stirrer 400rpm).

Solution5:

1ml of solution1 was mixed with 19ml of solution2.

Then, 6ml of solution3 were placed under mechanical stirrer (200rpm) and 2ml of solution5 were added in dropwise manner into it. After 10min 1 mL of o/w emulsion was created and was added in dropwise manner to beaker containing 10mL of methanol (MC6), isopropanol (MC7), n-heptane (MC8), ethanol (MC9) or petroleum ether (MC10). As prepared mixture was stirred magnetically for 1h at 300rpm. After this time, 10ml of solution4 were added in dropwise manner to the system and kept agitated magnetically (300rpm) for another 15min. As prepared slurry was stored.

4.Emulsion crosslinking of SCIII with SMA blend

Preparation MC11

First, four solution were prepared:

Solution1:

0.998g of PVA was dissolved in 98ml of milliQ water by heating ($T \approx 80^{\circ}\text{C}$) and stirring (magnetic stirrer 400rpm) for 2h.

Solution2:

2.072g of SMA were dissolved in 20mL of perfume Voyager Zen. As prepared mixture was heated ($T \approx 60^{\circ}\text{C}$) and stirring (magnetic stirrer 400rpm) for 48h.

Solution3:

2.076g of SCIII were dissolved in 20mL of perfume Voyager Zen. As prepared mixture was ultrasonicated for 15min and left overnight.

Solution4:

0.033g of 1.4-diaminobutane and 0.062g of NaHCO₃ were dissolved in 7.5ml of milliQ water by stirring for 5min.

Then, 16ml of solution1 was placed under mechanical stirrer (720rpm). Separately, 7.5mL of solution2 was mixed with 0.395ml of solution3. Subsequently, mixture of solution2 and 3 were added in dropwise manner into solution1. After 30min o/w emulsion was created and the speed of agitation was decreased to 150rpm. When the speed of the stirrer was adjusted, 7.5mL of solution4 was added in dropwise manner to reaction mixture and then was continuously stirred for another 24h. As prepared slurry was stored.

- **Characterization**

Photoisomerization of membranes was investigated by irradiating samples with visible light by iDual Adaptive LED, 806lm, 11W UV lamp for the desired time. The distance between lamp and sample was 10 cm. This was true for all below mentioned experiments.

The environmental scanning electron microscope (ESEM) FEI Quanta 600 apparatus, applying 15 kV with low-vacuum and without sputter coating was employed to characterize the morphology of obtained capsules.

Optical Microscope Zeiss Axiovert 40C for transmitted light, with the incorporated Invenio3SII microscope camera provided high definition images of the capsules, what give an insight regarding the outer surfaces morphology of obtained capsules.

Gas chromatography (GC) was employed to quantify the encapsulation efficiency and the release of the encapsulated active. Determination of the free perfume composition in the slurry via liquid-liquid extraction and Gas Chromatographic-Mass Spectrometric Analysis was adapted from the method described in patent US2013/0039962A1.

Confocal laser scanning microscopy (NIKON ECLIPSE TE2000-E) was employed to investigate the location of DASA moiety within the capsules structure, utilizing DASA fluorescent response. Optical sections were gathered in $3.65\mu\text{m}$ steps perpendicular to the z-axis (microscope optical axis) using an excitation laser of 543nm and resulted emission was detected in the range $590 \pm 50\text{nm}$. Seven cross-section images were taken, giving a total depth of analysis of $25.55\mu\text{m}$.

6.2.3 Results and discussion

As mentioned before, four generation of capsules were prepared. Primarily, we decided to prepare capsules by a technique commonly used in our research group, i.e.: phase-inversion precipitation [137-140].

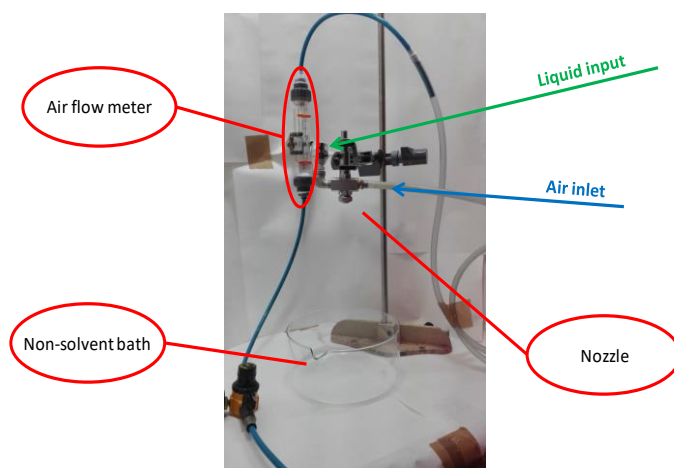


Figure 45. Phase-inversion precipitation technique set-up.

The method comprises mass transfer and phase separation processes which occur when polymeric solution gets in contact with its non-solvent. Process begins by dissolving polymer in the solvent and confining it in the wanted shape, for example film or droplet. The exchange between molecules of solvent and non-solvent takes place on the droplets surface what leads to polymer solidification, thus capsule formation. The experimental set-up of technique used in our laboratory is presented in Figure 45. Initially, as a SCIII solvent for this technique we used THF. As we were sure that it is suitable for SCIII copolymer as well as it is miscible with SCIII non-solvent, i.e. n-heptane. The copolymer modification that we chose was SCIII EF 80, as it has the highest molecular weight of all the SCIII family, and it is expected to exhibit the best mechanical properties among them. Prepared polymeric solution was casted into a non-solvent bath by means of an air-brush device working in semi-continues process which allows to form micro-droplets in fast, one-step manner. Next, the colloidal suspension was collected.

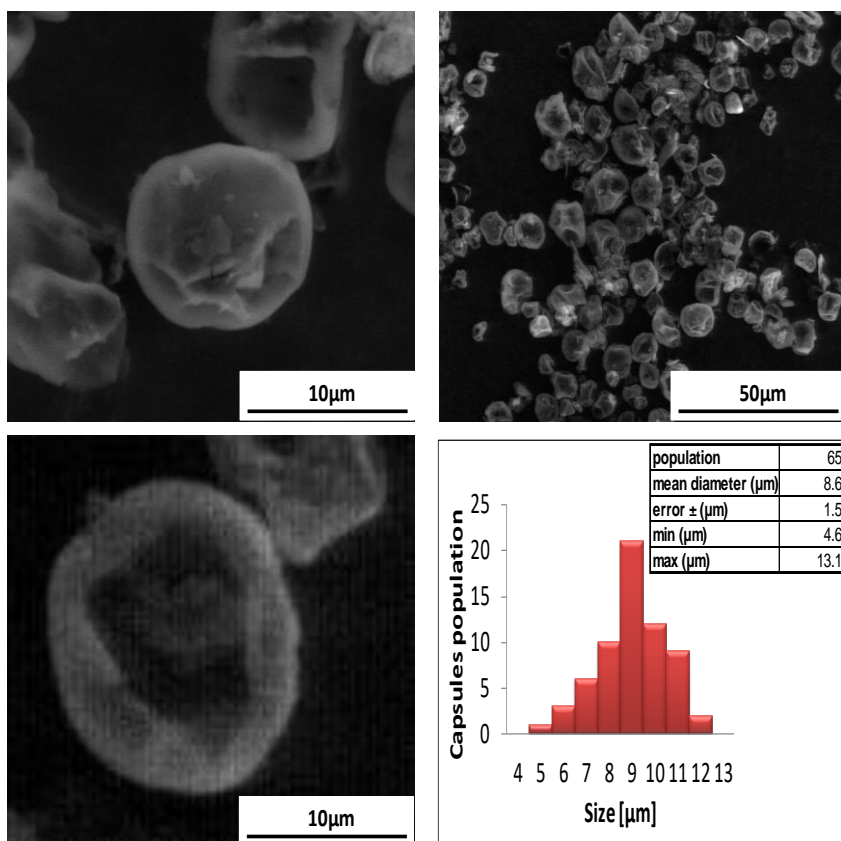


Figure 46. MC1 capsules with encapsulated THF made by PIP method.

Resulted capsules (MC1) were analysed by ESEM micrographs shown in Figure 46. They are round and visibly deflated, what suggests they are of hollow nature (core shell capsules). The microcapsules size distributions was determined by ESEM micrographs examinations. After counting 65 capsules the histograms reveal mean diameters of $8.5 \pm 1.5\mu\text{m}$ for the MC1 capsules with a THF as an encapsulated cargo. Careful examination of the outer surface of the capsules reveals that the surface is not homogeneous, it contains visible pores. This might be due to the encapsulated active. As THF is a good SCIII EF 80 solvent, it can easily penetrate capsules wall, thus creates multiple pores. The final objective of this thesis was fragrances encapsulation, thus in the second approach to make capsules by

PIP method instead of THF we used Voyager Zen perfume as a core material (MC2).

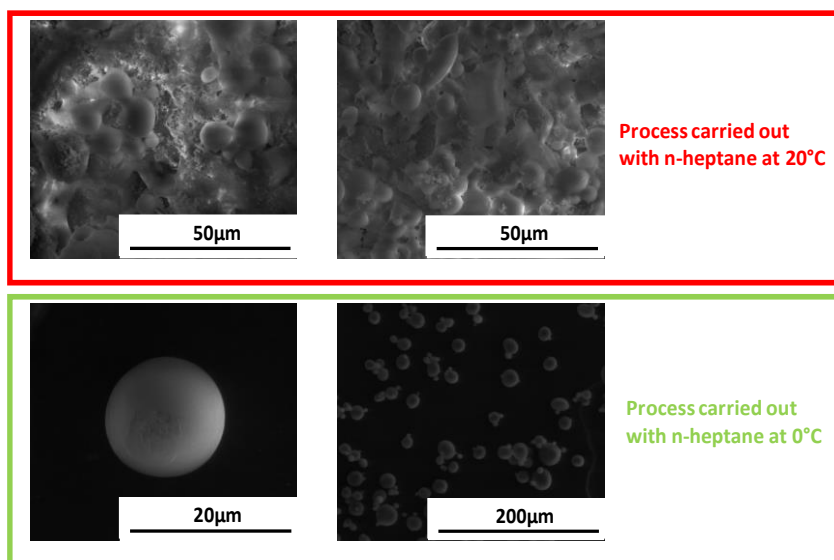


Figure 47. Voyager Zen encapsulated by SCIII EF 80 in PIP method at 20°C (top, red frame) and 0°C (bottom, green frame).

The results obtained for the capsules prepared by PIP method for SCIII EF 80 with Voyager Zen as an active substance were surprising. Desired capsules were not obtained, but a cluster of them, as it is shown in Figure 47 top. The only variable changed in this approach was the solvent of the SCIII copolymer. Thus, it implies that the demixing between the solvent-nonsolvent was disturbed. Instantaneous demixing should occur immediately after the immersion of casted solution into a nonsolvent. Moreover, it was noted that during the process airbrush nozzle was continuously blocked by precipitated SCIII polymer on its tip, due to unwanted saturation of air with n-heptane vapour. Taking both features under consideration, we decided to place a non-solvent bath at lower temperature, thus altering the demixing rate and reducing a density of n-heptane vapour. Thus, the process was repeated and capsules MC3 were prepared. The SCIII EF 80 was dissolved in Voyager Zen and precipitated in cold n-heptane

(0°C). The resulted MC3 capsules are shown in Figure 47 bottom. The comparison of the micrographs taken for the process, where n-heptane was used at room temperature with the process carried out at 0°C, gives clear conclusion. Encapsulation of perfume was successful only in the latter case. Figure 47 top (MC2, red frame, n-heptane at 20°C) reveals aggregations of capsules that form a macroscopic ununiform film, whereas the bottom of this figure (MC3, green frame, n-heptane at 0°C) demonstrates micrographs of uniform, separated, globular capsules. The microcapsules MC3 size distribution was determined by ESEM micrographs examinations (Figure 48)

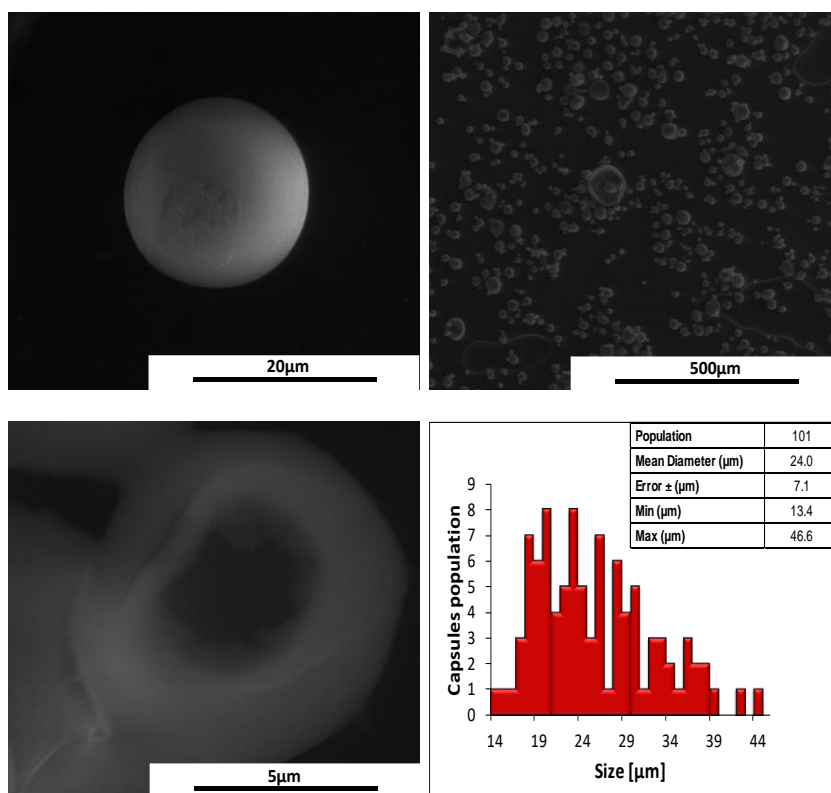


Figure 48. ESEM micrographs of MC3 capsules and corresponding size distributions data.

After counting 101 capsules the histograms reveal mean diameters of $24.0 \pm 7.1 \mu\text{m}$. The mean diameter increased three times in respect to MC1 capsules. Careful examination of the outer surface of the capsules reveals that the surface is mainly dense and homogeneous. As MC1 capsules, MC3 represent core-shell morphology. However, while MC1 appeared to be deflated, in contrast MC3 capsules are round and globular. This might be due to the thickness of the capsules wall. MC3 capsules wall exhibit sponge like structure with dense outer and inner surface (Figure 49), while MC1 capsules wall is of dense nature. MC3 capsule wall is 10times thicker than MC1 capsules wall. This substantial difference between MC1 and MC3 might lie in the nature of the core material used. In case of MC1 it was THF which is a good SCIII EF 80 solvent, and in case of MC3 it was Voyager Zen perfume. Moreover, it is important to mention that due to the reduced n-heptane bath temperature, the solvent-nonsolvent demixing was slower in case of MC3 capsules, what gives more time for the wall to be formed.

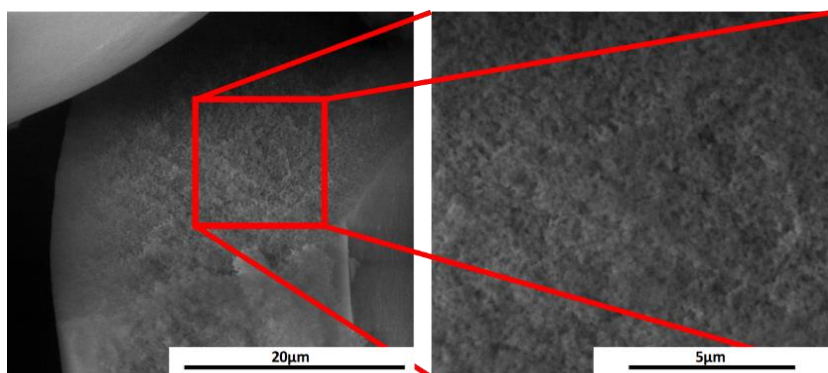


Figure 49. MC3 capsules cross-section ESEM micrograph.

Encapsulation efficiency of MC3 capsules was calculated to be $95.2\% \pm 1.4\%$. It entails that only 4.8% of free perfume were found in the slurry. It was relatively high percentage of successfully entrapped perfume. Therefore, further characterization was performed on those capsules. We selected two equal batches of

the capsules and one was kept in the dark, whereas the other was irradiated with the light. After 48h micrographs of two batches were taken (Figure 50).

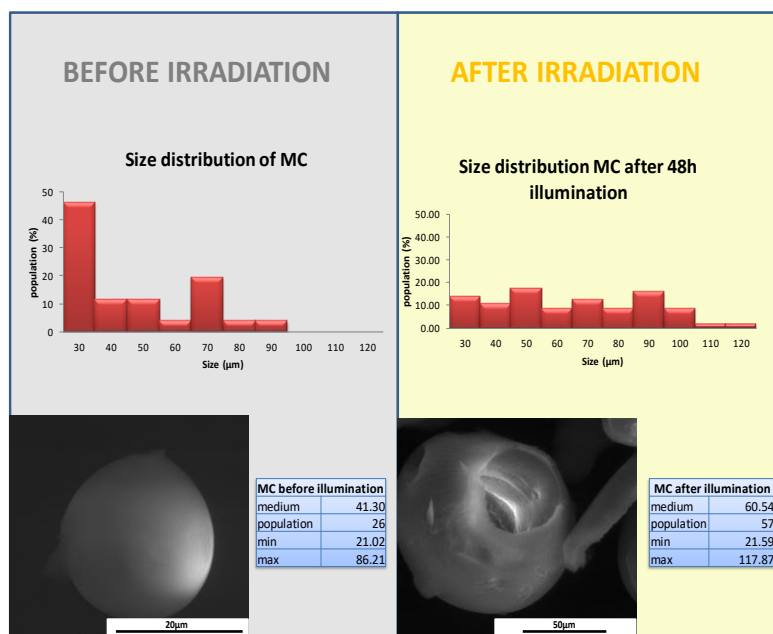


Figure 50. MC3 capsules size distributions and ESEM micrographs before light exposure (left side of the Figure), and after light exposure (right side of the Figure).

The obvious differences in the surface aspect of examined capsules were noted. The capsules before irradiation are globular and of smooth homogenous texture. In contrast, the capsules after light exposure were broken, with visible macropores on their surfaces. Mean diameter of the capsules increased by 46% after light exposure. It might be due to additional pores appearance.

Promising results obtained for MC3 capsules, allow their further characterization at our industrial collaboration facilities. Nevertheless, capsules were found to have weak mechanical

stability and, due to high breakage upon any attempted manipulation, further study upon them was ceased.

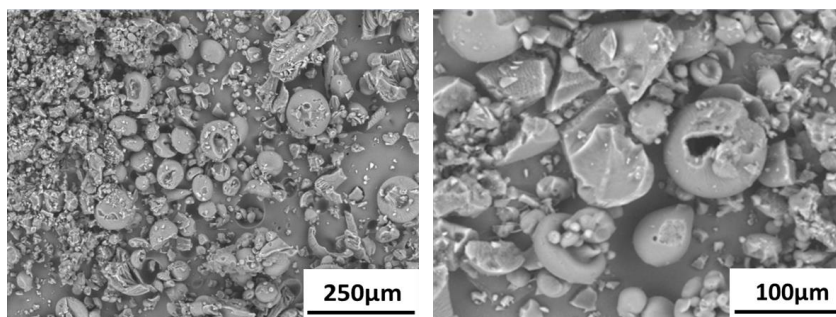


Figure 51. ESEM microscope images of MC4 capsules.

Another attempt to make PIP capsules were pursued, with the use of different core material, in particular hexyl acetate. It was chosen as an active agent, as it was known perfume raw material and SCIII polymers were soluble in it. In Figure 51 resulted MC4 capsules were shown. They were mostly broken and heterogenous in size and shape. Therefore it was concluded that different approach was needed to SCIII capsules. Serval ideas emerged to improve mechanical properties of the capsules. Primarily, we chosen to try an emulsion crosslinking of partially modified SMA FLAKE 1000 with DASA. It was described in the literature that the strain hardening modulus proves to be proportional to the network density created by cross-linking [141].

Therefore, we modified SMA polymer partially with DASA, to obtain terpolymer of molar ratio ST-styrene, MA-maleic anhydride, MI-maleimide; 4ST : 1MA : 2MI (Figure 52). This material was used to create microcapsules wall. As it was mentioned before, the encapsulated active was imposed upon us by industrial collaborator. Thus, firstly the solubility of SMA/DASA terpolymer in the perfume was examined. Unfortunately, the SMA/DASA terpolymer was not soluble in Voyager Zen perfume. However, we decided to make the capsules using this method to evaluate if this technique could give us desired product. Scheme of the encapsulation process is presented in Figure 53.

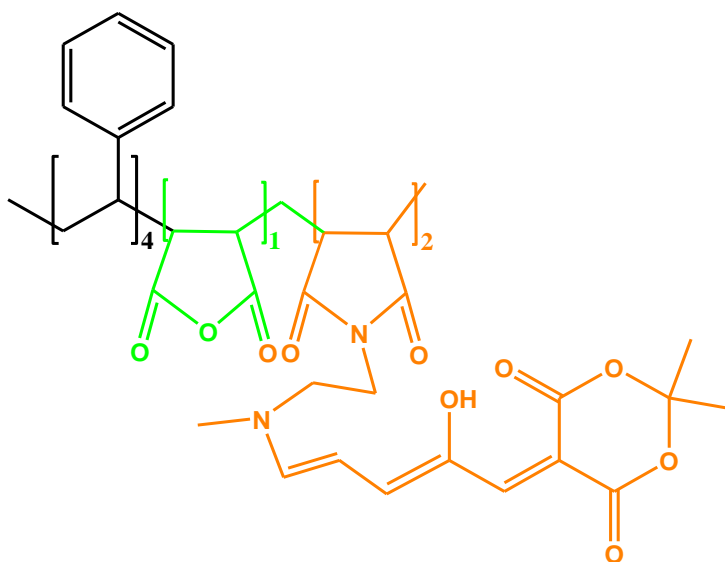


Figure 52. Terpolymer of molar ratio ST-styrene, MA-maleic anhydride, MI-maleimide; 4ST : 1MA : 2MI.

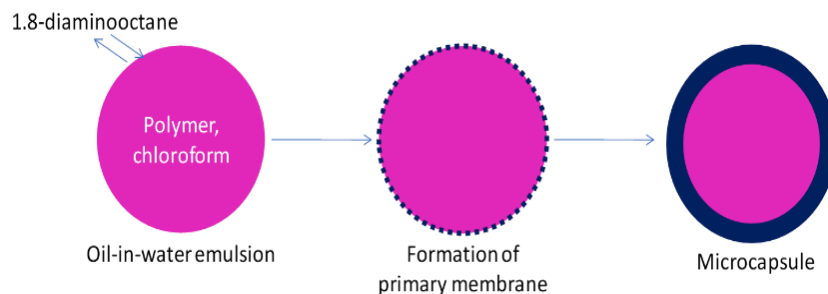


Figure 54. Scheme of MC4 encapsulation process.

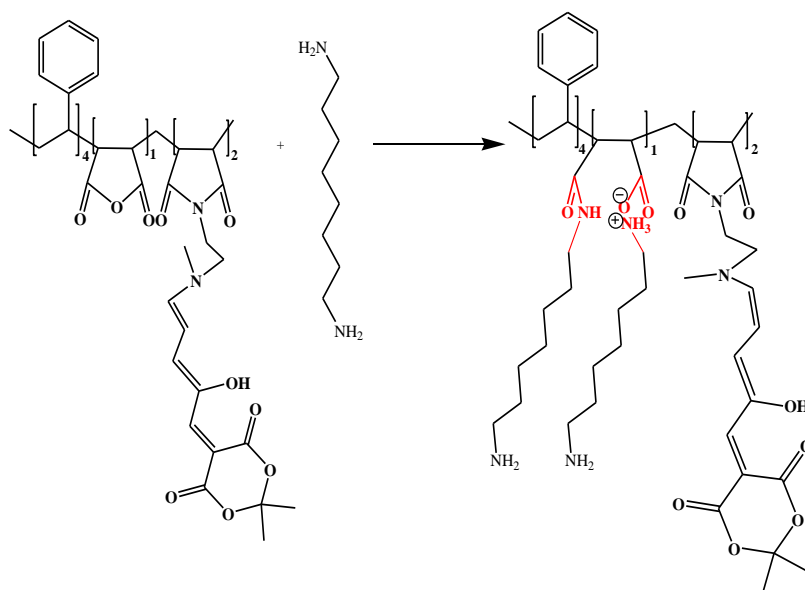


Figure 53. Scheme of the reaction between SMA/DASA terpolymer and 1.8-diaminooctane.

In general, this technique requires to create an emulsion. In our case it was an o/w emulsion, where the dispersed phase was composed by SMA/DASA terpolymer and chloroform, and as a continuous phase aqueous xanthan gum solution was chosen. Then, to solidify the dispersed polymeric droplets, the crosslinker was added. For the function of a linker we used diamine, and the

graphical representation of the reaction between SMA/DASA terpolymer and 1.8-diaminooctane is shown in Figure 54.

Resulted microcapsules (MC5) were characterized by optical microscope and their size distribution was determined by images examinations (Figure 55). After counting 111 capsules the histograms reveal mean diameters of $61.0 \pm 24.7 \mu\text{m}$. The sizes of the capsules fluctuate between $25.6 \mu\text{m}$ and $133.8 \mu\text{m}$, what gives quite heterogenous size distribution. Resulted capsules are globular in shape and they are pale rose in colour.

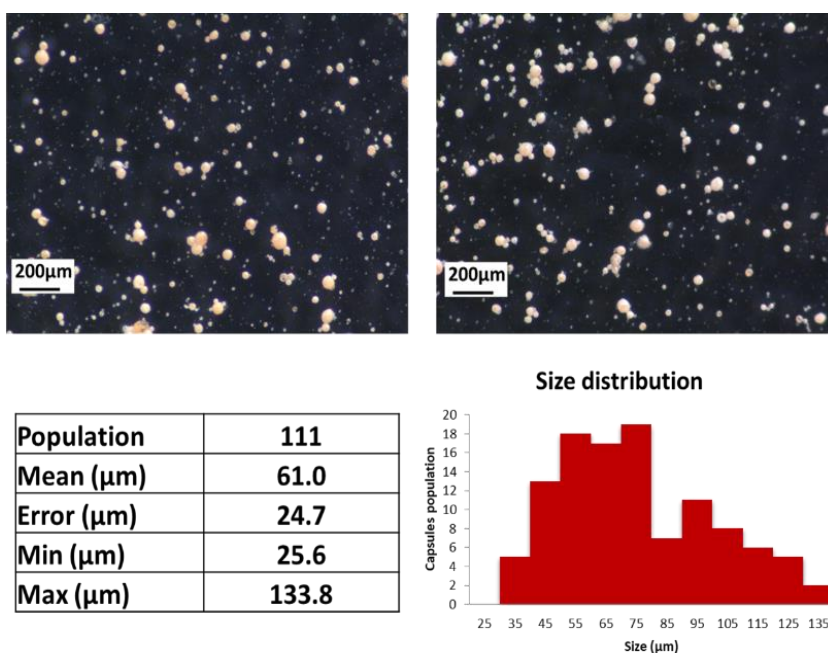


Figure 55. Optical microscope images of MC5 capsules with corresponding size distribution data.

What surprised us was that the resulted capsules change in time, while kept in the dark. After 4 days, micrographs of capsules MC5 were taken, and resulted images are shown in Figure 56.

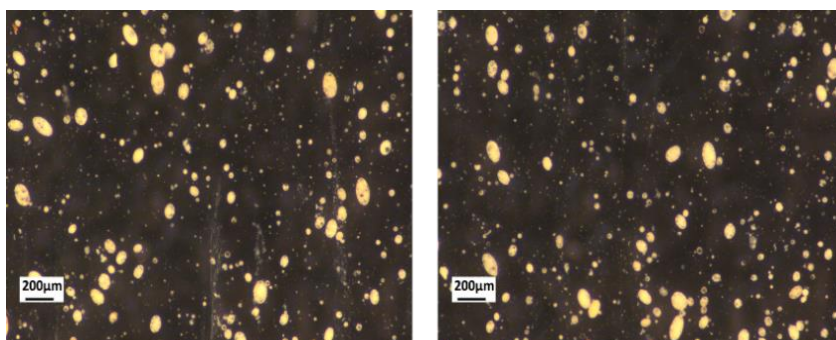


Figure 56. Optical microscope images of MC5 capsules after 4 days of their preparation.

Clear changes in MC5 capsules morphology were noted. The capsules were not globular any more, they change to more prolonged structures. We attributed this change to their loading with chloroform, as it is a solvent of high vapour pressure, its entrapment inside the capsule might have changed the shell shape. We did not pursue additional characterization of MC5 capsules as they were clearly unstable.

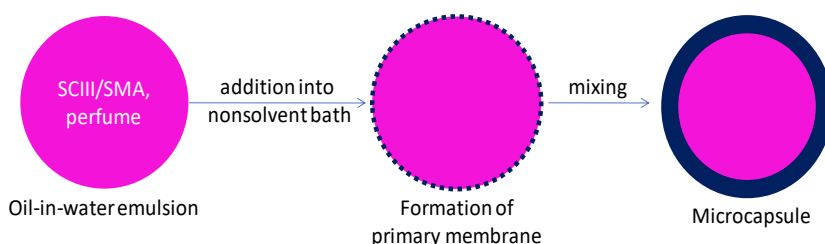


Figure 57. Scheme of MC6-10 encapsulation process.

Another approach to make photoactive capsules includes blends of SCIII copolymers with their precursors SMA copolymers. Here, mixture of SMA and SCIII was dissolved in the Voyager Zen perfume. Subsequently, o/w emulsion was prepared by dispersion of SMA/SCIII solution in aqueous Xanthan Gum. The idea was to precipitate as prepared emulsion in high excess of the SCIII/SMA nonsolvent. To visualize the procedure Figure 57 shows its graphical representation.

For this method we tried to use five different nonsolvents: methanol (MC6), isopropanol (MC7), n-heptane (MC8), ethanol (MC9) or petroleum ether (MC10). This method did not give expected results. Capsules were not obtained, for neither of the method variation. We could observe creation of primary membranes around emulsion droplets in case of MC6, where methanol was used as a nonsolvent (Figure 58).

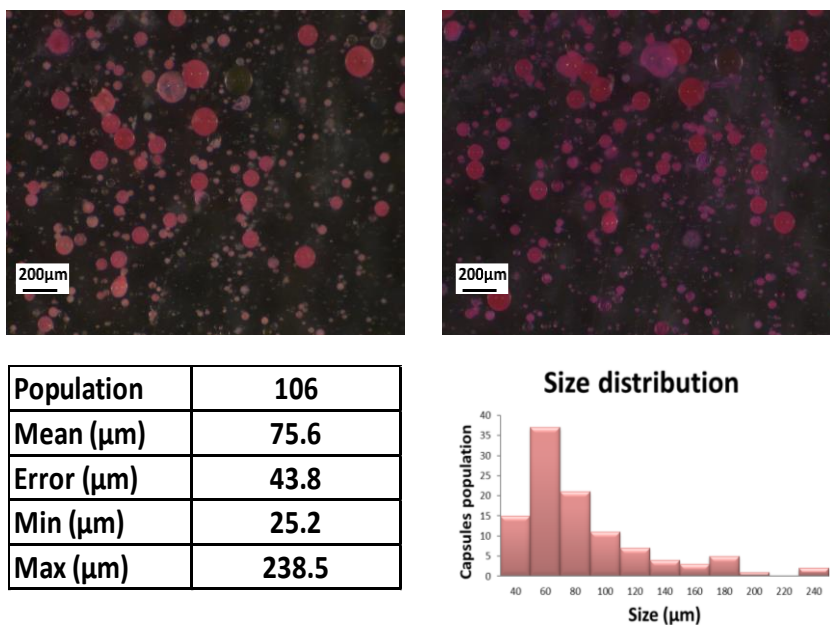


Figure 58. Optical microscope images of MC6 capsules with corresponding size distribution data.

Behaviour upon light irradiation of MC6 capsules was investigated by means of optical microscope (Figure 59). Light of the microscope was focused on the slide with MC6 capsules. As a matter of example one capsule was chosen to observe changes that occur upon light exposure during 6min. The images were captured at 1min, 4min, 5min and 6min of irradiation. Results reveal that light have severe impact on capsule's integrity.

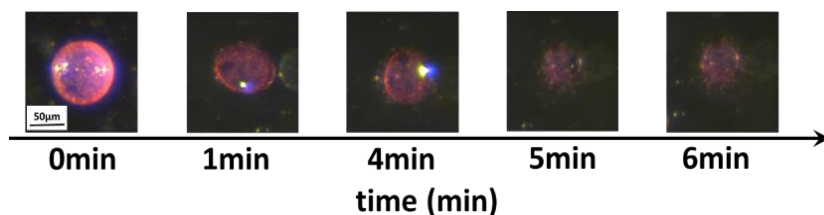


Figure 59. Optical microscope images of MC6 capsule upon irradiation.

Lastly, we decided to use blend of the SCIII/SMA and take advantage of highly reactive maleic anhydride groups within it to form three-dimensional cross-linked network. Shulkin et al. introduced interfacial polyaddition between SMA copolymers and amines to produce microcapsules [142]. The authors reported that in case of this process two mechanisms were responsible for encapsulation: 1) interfacial reaction between maleic anhydride and amines, and 2) solvent-driven phase separation. Moreover, they stated that mainly the reaction-driven process causes the copolymer to form a shell at the interface. Inspired by those findings we adapted the method to our needs. Here, a mixture of SMA and SCIII was dissolved in the perfume. Subsequently, o/w emulsion was prepared by dispersion of SMA/SCIII solution in aqueous PVA. Then, 1,4-diaminobutane the crosslinking agent, was added to as prepared emulsion.

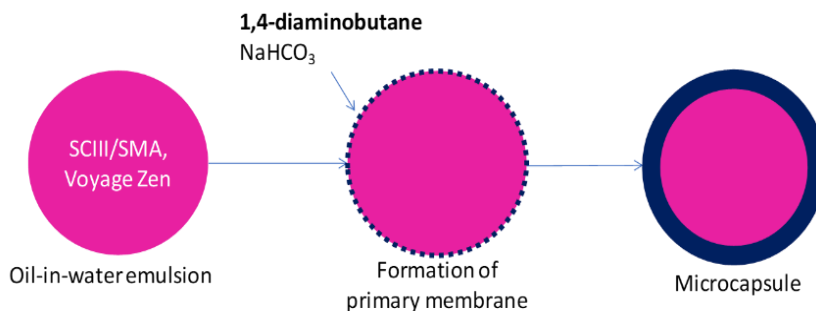


Figure 60. Scheme of MC11 encapsulation process.

In general, dispersed phase of the emulsion is composed of oil droplet that contains SCIII/SMA mixture. As such it poses maleic anhydride groups within its structure that reacts with primary amines of cross-linker. We studied the influence of different SMA/SCIII blends, crosslinkers, and temperature of reaction. Desired results were obtained with a blend SMA FLAKE 2000 and SCIII EF 60 in a ratio 95:5, respectively; crosslinker 1.4-diaminobutane ;and at 25°C. Schematic representation of the MC11 capsules preparation is shown in Figure 60.

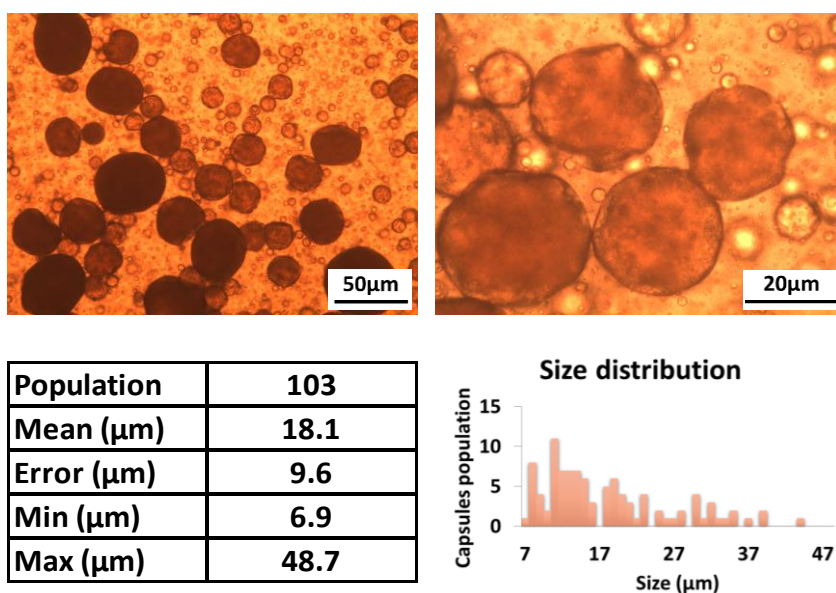


Figure 61. Optical microscope images of MC11 capsules with corresponding size distribution data.

Resulted microcapsules (MC11) were characterize by optical microscope, and their size distribution was determined by images examinations (Figure 61). After counting 103 capsules the histograms reveal mean diameters of $18.1 \pm 9.6\mu\text{m}$. The sizes of the capsules fluctuate between $6.9\mu\text{m}$ and $48.7\mu\text{m}$, what gives quite narrow size distribution. Resulted capsules are suspended in a slurry. Images reveal that the capsules are not perfectly globular in shape and some are not transparent to light.

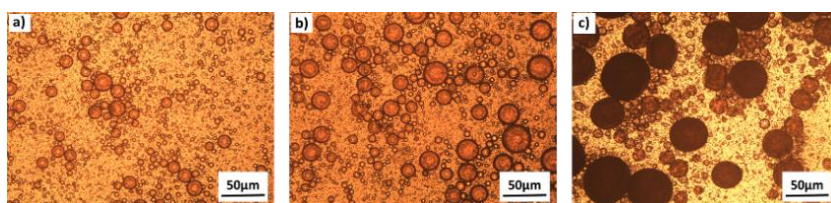


Figure 62. Optical microscope images of MC11. During preparation process; emulsion (a), immediately after amine addition (b), after completion of the process (c).

In order to carefully study the process, the optical images during capsules preparation were taken. Figure 62(a) represent the beginning of the process, where emulsion is created. The image reveal dispersed phase as a perfect, globular particles. Image of Figure 62(b) shows emulsion droplets of more define contours, whereas micrograph in Figure 62(c) demonstrate fully solidified capsules.

MC11 capsules morphology analysis by optical microscope gave promising results, therefore further analysis of the capsules was conducted.

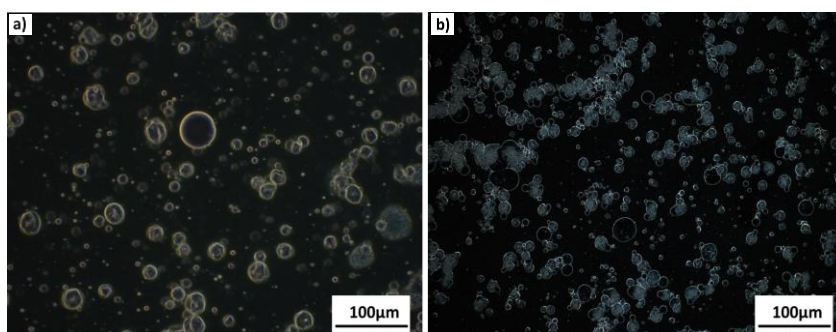


Figure 63. Optical microscope micrographs of MC11 capsules taken at 0min (a) and 80min (b).

First, study of MC11 capsules behaviour upon light irradiation was studied. Capsules were illuminated with microscope light during 80min. Corresponding micrographs were taken at 0min

and 80min and are shown in Figure 63. Within the first 20min no visible structural changes were detected. However, after additional 60min the capsule's morphological changes were noticed. They seem to expand and break, hence in consequence release encapsulated oil.

In order to visualize the release of encapsulated active, one capsule was amplified and over the course of 80min series of micrographs of the capsule were captured (Figure 64). As explained before, capsule seems to visibly swell and in consequence release core material.

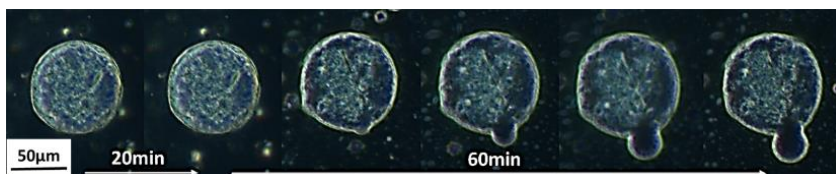


Figure 64. Optical microscope micrographs of MC11 capsule taken during 0min and 80min light irradiation.

For better understanding the release process and quantifying the amount of released perfume upon light irradiation, GC analysis of MC11 capsules was performed. Corresponding data is collected in Table 15.

Table 15. GC analysis of the free perfume content in the MC11 capsules slurry.

label	perfume content in the slurry	
	dark (%)	light (%)
1	24.6	20.0
2	33.1	23.2
3	29.6	22.1
error	4.3	1.6
mean	29.1	21.8

The free perfume content in the slurry before light exposure was 29.1%. It means that 70.9% of the perfume was encapsulated. This result of the amount of the free perfume in slurry after 1.5h light irradiation gave 21.8%. The difference is substantial, and it was calculated to be 25%. What is unexpected is that the amount of free perfume decreases upon light exposure. Our assumption was that the capsules will release the encapsulated active while illuminated. Nevertheless, the GC analysis indicates that the effect of light gives an opposite result. It implies that the capsules adsorbed the oil upon irradiation. The mechanism of this phenomenon is unknown. It is imperative to mention that in the employed GC method to evaluate perfume content, the capsules were exposed to n-heptane. This organic solvent may cause capsules precipitation, therefore by n-heptane-perfume demixing increase of perfume in the slurry may be detected. Moreover, the results obtained by the GC analysis are not in a good agreement with what was concluded basing on the micrographs of those capsules. Images taken of the capsules upon irradiation showed clear oil release (Figure 63 and 64).

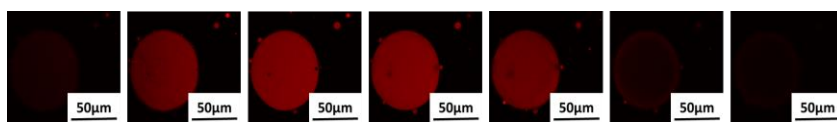


Figure 65. Confocal laser scanning microscope images of MC11 capsule.

Confocal laser scanning microscopy was employed to further investigate the peculiar behaviour of the capsules upon irradiation with light i.e. the amount of free perfume decreases in the slurry upon capsules exposure to light. The technique used to fabricate MC11 capsules left us with doubt where exactly DASA is located within the capsules matrix. Thus, it can have an impact upon final capsules performance upon light irradiation. As the SMA is crosslinked to create capsule wall, SCIII polymer is solubilized in perfume and it is unknown if it's a building block of the capsule

shell or rather it is only present in capsule core. In Figure 65 confocal images were taken of one capsule of MC11 batch. The capsule was excited with green laser beam and responded red fluorescence was assigned to DASA moiety. Thus, the red colour in those images reveal location of DASA. Figure 65 shows different focal planes within the sample and optical cross-sectional micrographs of the same capsules taken at different capsule height. The results showed that DASA moiety was still present within the capsule core as solubilized SCIII polymer, but also it was trapped within the wall of the capsule.

6.2.4 Conclusions

The series of microcapsules containing SCIII polymers were obtained by number of techniques. We reported phase inversion precipitation technique to give desired, globular, homogeneously size dispersed capsules. However, their manipulation became a problem as their shell was highly brittle. Each contact with the capsules powder resulted in the capsule's breakage. Therefore, subsequent techniques were employed to obtain desired capsules: 1) emulsion crosslinking of partially modified SCIII copolymer (DASA modified polymer, molar ratio ST-styrene, MA-maleic anhydride, MI-maleimide; 4ST : 1MA : 2MI; 2) SMA/SCIII emulsion precipitation in different non-solvents; 3) emulsion crosslinking of SCIII with SMA blend. First method i.e. emulsion crosslinking of partially modified SCIII copolymer, did not give anticipated capsules, as the partially modified SMA with DASA oligomer was not compatible with the perfume provided by P&G company. SMA/SCIII blend emulsion precipitation in different non-solvents gave partially created capsule's wall, thus they were not applicable for P&G products. Emulsion crosslinking of SCIII with SMA blend give the most promising results basing on the optical microscope analysis. Therefore, their

modification upon light exposure was analysed by means of optical microscope and GC analysis. Both of them revealed that the obtained capsules are in fact photoactive. However, the effect of light gave an opposite result. Instead of perfume release into the slurry, the free perfume amount decreases upon irradiation, what suggests that the capsules attract the perfume upon irradiation and do not release it into the slurry, as previously thought. It is imperative to mention that the employed GC method to evaluate perfume content may not be suitable for our system. The capsules were exposed to n-heptane in the sample preparation to GC analysis. Therefore, the capsules may precipitate, what implies n-heptane-perfume demixing and subsequent increase of perfume in the slurry.

7 Acrylates

7.1 Introduction

As mentioned before, the final objective of this PhD thesis was to create the photoactive capsules with controlled release of encapsulated oil that can be readily applied in P&G company products. This Chapter describes the polyacrylates capsules modifications with DASA moieties and their behaviour upon light illumination. Capsules described here were created by means of two separate techniques. Their preparation as well as characterization is addressed here. First, we decided to modify existing capsules with DASA molecule. For this reason, polyacrylate capsules with secondary amines in their matrix were employed. Those template capsules were then used to react with SCI (DASA precursor, synthesised in Chapter 3). Polyacrylate template capsules were provided by P&G company. The second approach consist of interfacial polymerization on the oil droplet surface. To introduce photosensitive moiety within the wall of polyacrylate capsule, primarily we synthesised an acrylate monomer containing DASA. 2-(tert-Butylamino)ethyl methacrylate reacted with SCI to get Acrylate/DASA monomer. As such it was used along with two others acrylate monomers to encapsulate perfume oil. In this approach the encapsulation process was adapted from a method previously created and provided to us by P&G company. Nevertheless, the interfacial polymerization was known for many years. As mentioned in Chapter 1 of this thesis, the first one to reported this was a polymer scientists - Morgan and his group at Dupont Nemour in 1959 [143-146]. Not far from it, the process was expanded. In 1983 Beestman et al. patented the basic methodology of this process [147]. Since then the method was improved significantly. One of its major advantages is its controllable character. Capsule mean

size and membrane thickness can be directly designed. In this technique the reaction takes place at the interface between two immiscible liquids, each of the liquids contains reactive monomers and/or initiators that polymerize when get in contact with each other [15]. Here, thermally driven free-radical polymerization was employed to form capsules. As monomers a mixture of acrylates and methacrylate soluble in oil phase were chosen. To trigger the polymerization reaction three azo-radical initiators were selected.

7.2 Materials and methods

- **Materials**

5-(furan-2-ylmethylene)-2,2-dimethyl-1,3-dioxane-4,6-dione (SCI) was synthesised in our laboratory by the methods explained in Chapter 3. Tetrahydrofuran (THF), 2-(tert-Butylamino)ethyl methacrylate (TBA), chloroform, ethyl acetate, silica 40-60 μ m were purchased from Sigma Aldrich with purity higher than 98%. Poly(vinyl alcohol) ($M_w \approx 40000$ g/mol) (PVA) was purchased from Sekisui. PAC Freesia EF5469C, 2-carboxyethyl acrylate, CN975 acrylate, 2,2'-azobis(2,4-dimethylvaleronitrile), 2,2'-azobis(2-methylbutyronitrile), 4,4'-azobis(4-cyanovaleric acid) and Voyager Zen perfume were acquired from our industrial collaborator (P&G). All reactants were used without further purification. Milli-Q water was used in conducted experiments.

- **Acrylate/DASA synthesis**

2.648g of SCI was dissolved in 20 mL of THF. Separately, 2.5mL of TBA was dissolved in 15mL of THF. Then, to begin the reaction both solutions were mixed together by means of magnetic stirrer, in one neck round bottom flask at room temperature. Reaction was carried out during 2h. Subsequently, the solvent was

evaporated by means of rotary evaporator. Obtained solid was dissolved in 5mL of chloroform and obtained reaction mixture was purified by elution chromatography. Stationary bed was composed of 36g of silica 40-60 μ m and as an eluent ethyl acetate was chosen. Fraction of eluent that contained Acrylate/DASA was placed in rotary evaporator to remove the solvent. Yield of the reaction was calculated to be 7.8%.

- **Capsules preparation:**

1. Modification of NH₂ functionalized capsules with SCI

First, two solution were prepared:

Solution1:

25.818g of aqueous 2% PVA was placed in 150mL beaker. Then, 0.536mL of NH₂ functionalized capsules (PAC Freesia EF5469C) were added and stirred (mechanical stirrer 117rpm) for 30min.

Solution2:

0.104g of SCI (DASA precursor) were dissolved in 5.024g of THF.

Then, solution2 was added in a dropwise manner into solution1. After 1.5h reaction was stopped by means of centrifugation. Centrifugation was performed 3 times (conditions: 10min at 6500 rpm). Supernatant was discarded and replaced with water and precipitate was redispersed. As prepared product was stored.

2. Acrylate/DASA capsules preparation

Two phases were prepared. First, the dispersed phase was composed of: 1.5g of chloroform, 1g of Voyager Zen perfume, 0.11g of Acrylate/DASA, 0.014g of 2-carboxyethyl acrylate,

0.385g of CN975 acrylate, 0.043g of 2,2'-azobis(2,4-dimethylvaleronitrile), 0.007g of 2,2'-azobis(2-methylbutyronitrile). Second, the continuous phase: 4.01g of 2% PVA aqueous solution, 0.015g of 4,4'-azobis(4-cyanovaleric acid) and 0.036g of 16% NaOH aqueous solution. Subsequently, the dispersed phase was placed under mechanical stirring (12000rpm) and continuous phase was added to it, in a dropwise manner. After 30 min of emulsification, the stirring speed was decreased to 400rpm and was kept constant during the next 14h of the encapsulation process. The temperature was increased gradually. Reaction mixture was kept at 40°C for 15min, then at 60°C for 75min, next at 75°C for 270min, and finally at 90°C for 480min. As treated reaction mixture was then cooled down to room temperature, and the stirring was turned off. As prepared capsule's slurry was stored.

- **Characterization**

The structure of obtained Acrylate/DASA was characterized by means of ^1H NMR spectroscopy, using deuterated chloroform (CDCl_3) as a solvent with a Varian Gemini 400 MHz spectrometer (^1H – 400 MHz, tetramethylsilane), at room temperature, using a pulse delay time of 5s.

Photoisomerization of Acrylate/DASA was investigated by irradiating samples with visible light by iDual Adaptive LED, 806lm, 11W UV lamp for the desired time. The distance between lamp and sample was 10 cm. This was applied for the below mentioned UV-Vis experiment.

The UV-VIS spectra were recorded at room temperature (20°C) with a UV-visible spectrophotometer (UV-1800 Shimadzu Spectrophotometer).

For the experiment, Acrylate/DASA was dissolved in chloroform to give a concentration in the range of 0.025–0.050 gL⁻¹. Then, the spectra were obtained in the wavelength range 400–650 nm. Then, the spectra were recorded before sample was exposed to light (dark), and after it was illuminated for one hour.

Optical Microscope Zeiss Axiovert 40C for transmitted light, with the incorporated Invenio3SII microscope camera provided high definition images of the capsules, what give an insight regarding the outer surfaces morphology of obtained capsules.

Dynamic headspace–thermal desorption (DHS–TD) combined with gas chromatography–mass spectrometry (GC–MS) was employed to quantify the amount of perfume released form the capsules during controlled release experiment. The procedure used is as follows:

1. Flushing jars of 500mL with N₂ and making 2 holes in the lid.
2. Depending on the touchpoint that is measured the light inside the jar is on or off.
3. 60min waiting for headspace to be formed.
4. Tenax (a porous polymer that absorb volatile substances) trap connected to a pump is inserted through the hole.
5. Headspace is captured for 10 min at a flowrate of 20 mL/min.
6. Tenax (a porous polymer that absorb volatile substances) traps are thermally desorbed into GC-MS.

2 jars 500mL are prepared for sample. In Jar 1 a flashlight is installed, hanging on the lid. Jar 1 and 2 are both covered with aluminium foil. Jar 1 is the sample that was illuminated, while Jar 2 is the sample that was kept in the dark. Two rectangular filter papers were prepared (4x5cm). Then, 100µL of 0.3% capsules aqueous slurry solution were sampled on the filter paper.

Subsequently, the filter papers were placed in the jars. The jars were tightly closed. Then, the flashlight was turned on in Jar 1. After 30 min of exposure Jar 1 and 2 were measured with dynamic HS by the hole that was prepared in the lid. After the measurement the jars were sealed.

7.3 Results and discussion

The synthesis of photosensitive Acrylate/DASA was successful. In Figure 66 the reaction between TBA and SCI is presented. The yield of the obtained product was low (7.8%). Low efficiency of the reaction may be attributed to a high content of by-products, and unavoidable losses during the extensive purification procedure.

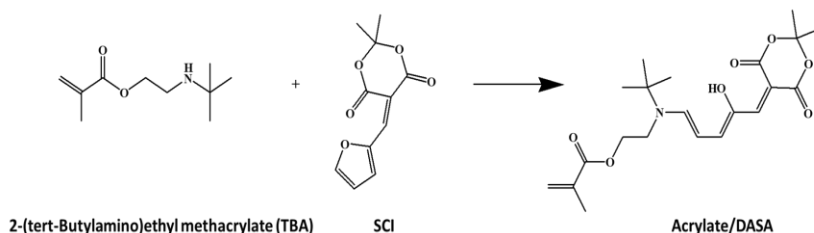


Figure 66. Reaction between 2-(tert-butylamino)ethyl methacrylate and SCI.

The structure was confirmed by ^1H NMR spectroscopy. As the matter of fact, Figure 67(a) provides a ^1H NMR spectra of purified Acrylate/DASA product along with peak assignments (Figure 67(c)).

Photoactive behaviour of Acrylate/DASA is expected. The scheme of anticipated effect of light on Acrylate/DASA structure is presented in Figure 68.

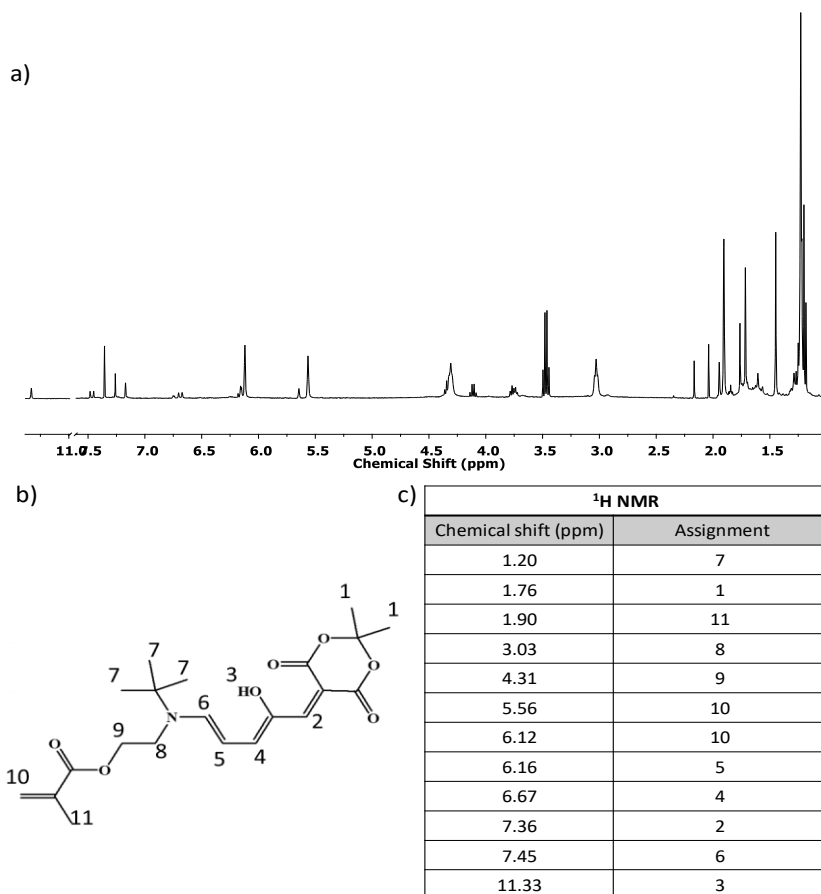


Figure 67. ¹H NMR spectra for Acrylate/DASA. ¹H NMR (400 MHz, (CDCl₃)) (a); generic structure of Acrylate/DASA (b); table of chemical shifts assignments of Acrylate/DASA (c). Additional peaks not include in (c) are assigned to residual solvents.

Photochromism of TBA modified with DASA was examined by UV Vis spectroscopy (Figure 69). The spectra collected for sample before light irradiation (Figure 69, black line) reveal strong absorption band with the maximum at 543nm. This peak is assigned to a π - π^* transition of a conjugated triene structure within DASA molecules extended form [109]. Negative photochromism of Acrylate/DASA molecule was expected. Therefore, spectra upon illumination of the sample was collected

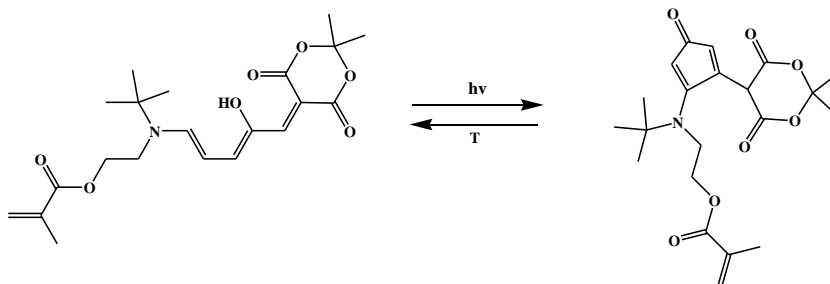


Figure 68. Acrylate/DASA suspected behaviour upon light exposed and corresponding thermal relaxation.

(Figure 69, orange line). The intensity of the band significantly decreases, what confirms photoactive properties of Acrylate/DASA. As mentioned in Chapter 5, the photoswitching in case of DASA occurs due to transformation of the coloured, conjugated triene chain to the colourless, compact form of DASA. As a reminder, in general, DASA photoswitching occurs in two steps: 1) photoinduced *Z-E* isomerization within the triene chain;

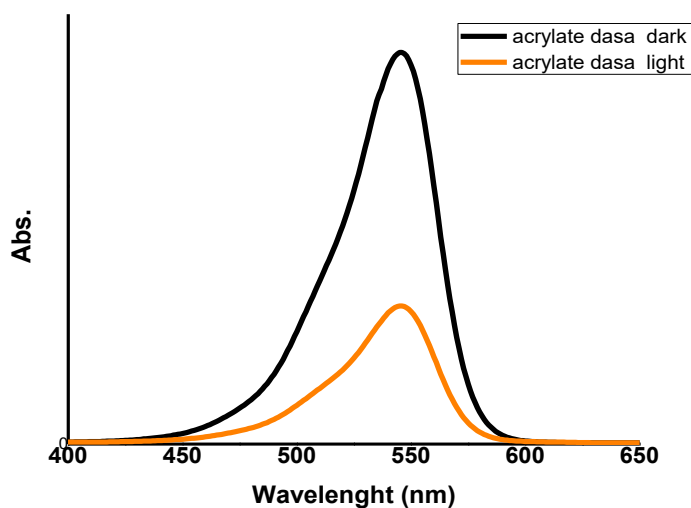


Figure 69. UV-Vis spectra of Acrylate/DASA polymers in chloroform at RT.

2) 4π thermal electrocyclization followed by a proton transfer and tautomerization [2].

Confirming that Acrylate/DASA contains photosensitive properties, two different approaches were developed and implemented to achieve desired capsules with light controlled release.

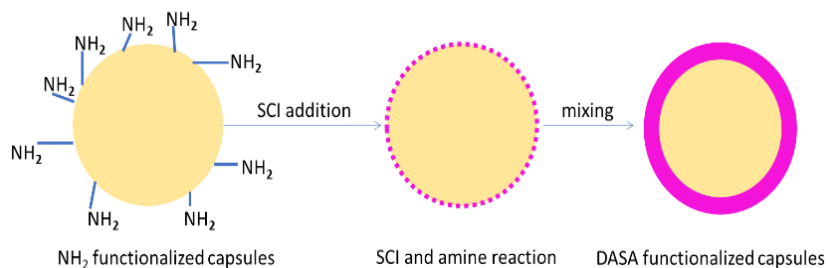


Figure 70. Scheme of NH_2 functionalized capsules modification with SCI.

First, we decided to incorporate DASA in the microcapsule's matrix by reaction on/within existing capsule wall. The graphical representation of the capsules modification is shown in Figure 70. The idea was to integrate DASA into capsule by *in situ* reaction between DASA precursor (SCI, synthesised in Chapter 3) and amine groups, that were randomly distributed on the porous surface of the polyacrylate capsules. The capsules used in the process were PAC Freesia EF5469C. They were synthesised at P&G company and delivered to us. The polyacrylate beads were used as templates for DASA photoactive capsules. The template capsules contained primary amine groups in their matrix, thus it allows the reaction between them and SCI.

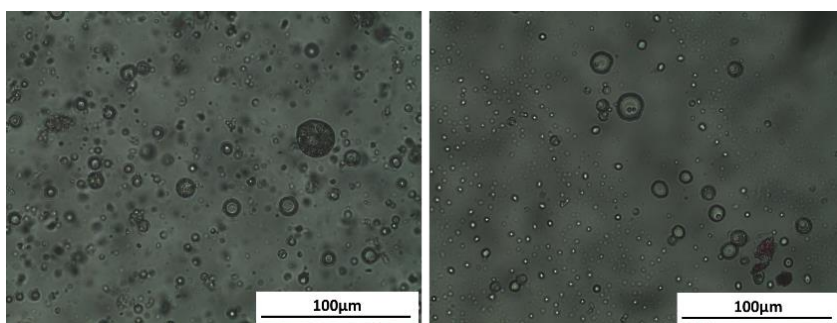


Figure 72. Optical micrographs of NH₂ functionalized capsules modified with SCI.

First indication that the reaction between SCI and secondary amine groups located on the capsule's wall occurred was the change in colour of the reaction mixture. The template capsules were yellow, whereas after SCI addition reaction mixture was pink. Optical microscope was employed to analyse the outer morphology of the capsules and representative results are shown in Figure 71. As it can be seen, capsules were still present after functionalization, however there were some capsules that were broken, some oil drops as well as some pink precipitate could be found.

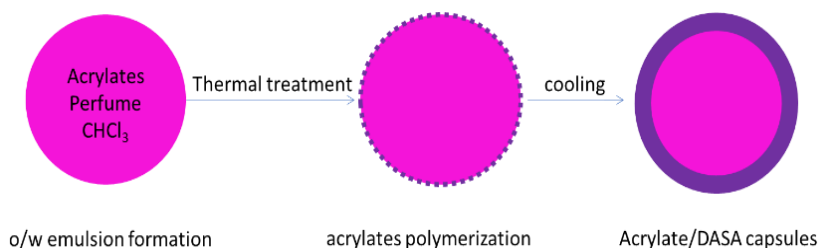


Figure 71. Scheme of the Acrylate/DASA capsules preparation.

Therefore, decision to attempt the second approach was taken. This method included encapsulation of Voyager Zen perfume within polyacrylate polymeric shell. The wall of the capsules was composed from mixture of three acrylate units: Acrylate/DASA, 2-carboxyethyl acrylate, CN975 acrylate. In respect to poor

Acrylate/DASA solubility in Voyager Zen perfume, chloroform as a cosolvent was used. Thus, it was expected that the core of the capsules will be a mixture between Voyager Zen perfume and chloroform. The solidification of the capsules wall was triggered by gradual increase of temperature. Three initiators were selected to begin the polymerization: 2,2'-azobis(2,4-dimethylvaleronitrile), 2,2'-azobis(2-methylbutyronitrile), and 4,4'-azobis(4-cyanovaleric acid). The two former ones are soluble in oil phase, while the latter one is soluble in continuous phase. 10h half-lives for all of them are quite similar, ranging between 51°C and 69°C. Hence, the increase of the temperature caused the acrylates to polymerize on the surface of the spherical droplet. After reaching 90°C the solid, globular capsules were obtained. Scheme of the Acrylate/DASA capsules preparation is shown in Figure 72 and resulted capsules images in Figure 73.

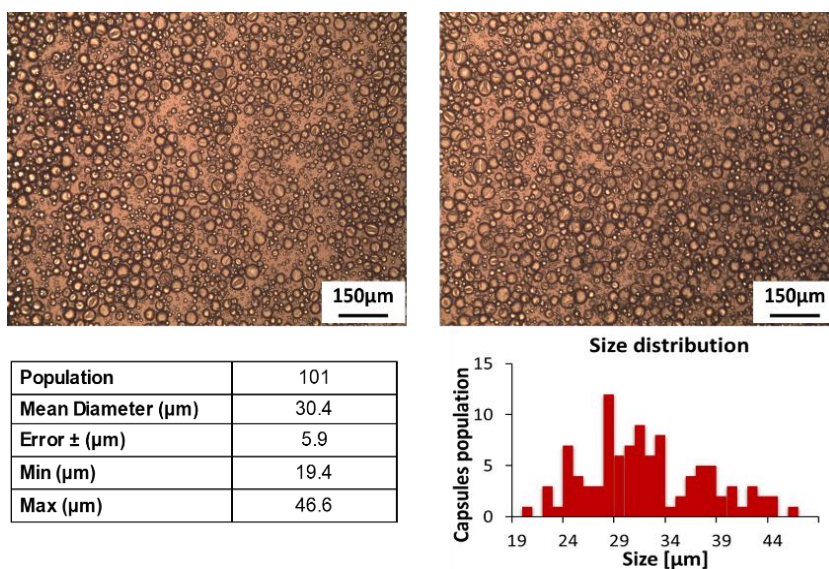


Figure 73. Optical microscope images of Acrylate/DASA capsules with corresponding size distribution data.

Images of Acrylate/DASA capsules presented in Figure 73 revealed round and visibly deflated capsules, what suggests they are of hollow nature (core shell capsules). The microcapsules size

distribution was determined by Optical microscope micrographs examinations. After counting 101 capsules the histograms show mean diameters of $30.4 \pm 5.9 \mu\text{m}$, with the minimum diameter size of $19.4 \mu\text{m}$ and the maximum $46.6 \mu\text{m}$.

Acrylate/DASA capsules morphology evaluation by optical microscope gave promising results, therefore further analysis of the capsules was conducted at P&G company. The quantification of the release of the encapsulated perfume was conducted by dynamic headspace (DHS) combined with gas chromatography. Two vials were examined where one of them was subjected to visible light (light) and the other was kept in the dark (dark). Then, the volatile substances were adsorbed to Tenax (a porous polymer), and subsequently thermally desorbed into GC-MS. The results are shown in Figure 74.

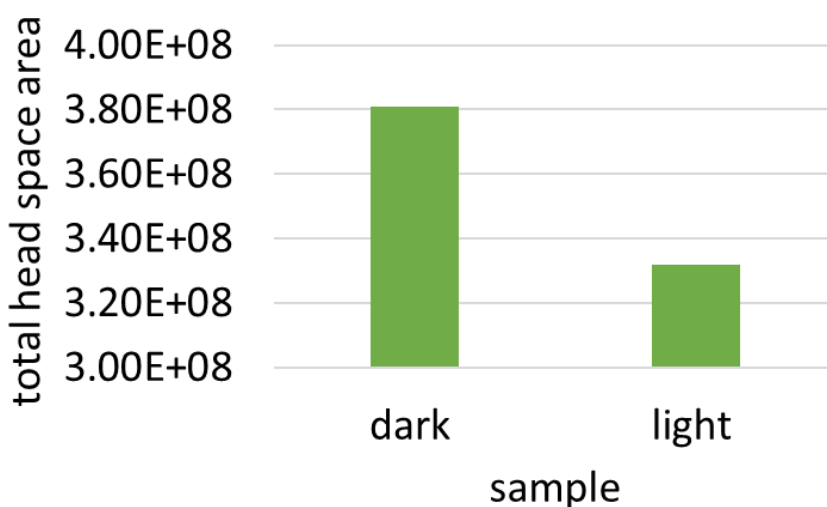


Figure 74. Release of encapsulated perfume analysed by dynamic headspace (DHS) gas chromatography results for Acrylate/DASA capsules. Sample subjected to visible light (light) and sample kept in dark (dark).

Sample that was exposed to light gave lower value of perfume content than the sample that maintained in the dark. It was

expected that the capsules will release encapsulated cargo and therefore the detected perfume content will increase. However, it seems that the capsules, while irradiated, absorb the volatile compound, thus give a decrease value in HS analysis.

7.4 Conclusions

We reported on the synthesis acrylate/DASA molecule, which in our case serves as a one of the component of the polyacrylate capsules shell. Optimization of the preparation procedure needs to be conducted as the yield of the reaction was low (7.8%). Two approaches for the acrylate capsules modified with DASA were attempted. One included modification of the polyacrylate capsules with DASA precursor. This functionalization did not give desired result. The wall of the capsules was not homogenous, many were found broken. It may be due to poor stability of the template capsules. Polyacrylate capsules used in this experiment did not have dense polymeric network formed. In general, template capsules have secondary amine in their matrix, which in order to gain dense capsule shell should be crosslinked. However, secondary amines of template polyacrylate capsules were left unreacted. The presence of secondary amines in the polymeric matrix was needed in order to react with SCI, thus obtaining DASA functionalized capsule wall. In consequence, resulted capsules were of poor stability. Thus, further investigation was ceased and another approach was pursued. Second method included encapsulation of perfume within polyacrylate polymeric shell. The wall of the capsules was composed from mixture of three acrylate monomers, where one of them was synthesised by us Acrylate/DASA. In respect to poor solubility of Acrylate/DASA in Voyager Zen perfume, chloroform as a cosolvent was required. Optical microscope images of Acrylate/DASA capsules analysis reveal that they were globular

in shape and of narrow size distribution. The quantitative analysis of perfume released from Acrylate/DASA capsules kept in the dark and exposed to light was performed. Capsules that were kept in the dark gave higher content of perfume, than the sample that was subjected to visible light. That is exactly the opposite effect to what was expected. Further study is needed to investigate this phenomenon. Our hypothesis is that the capsules while irradiated adsorb the volatile compound, due to change in physicochemical DASA transformation upon illumination.

8 Overall conclusions

- We reported on the synthesis 5-(furan-2-ylmethylene)-2,2-dimethyl-1,3-dioxane-4,6-dione, which in our case serves as a photosensitive precursor used to modify the polymeric matrix. Optimization of preparation procedure previously reported in the literature was successfully performed. Results obtained from this Chapter provide more robust and practical method to gain a high yield of 5-(furan-2-ylmethylene)-2,2-dimethyl-1,3-dioxane-4,6-dione in water without the need of a catalyst. At the small scale, the highest reaction yield of 80 ± 2 % was achieved at 75 °C while at the larger scale the yield of 91 ± 2 % was obtained at room temperature after 3h.
- We reported on the modifications of the commercially available SMA copolymers. First modification serves to prepare matrices capable of reacting with DASA precursor. Therefore, side chains of the copolymers were decorated with 2°amines. The reaction between maleic anhydride group and primary amines was known in the literature. Its parameters were adjusted to serve our purpose and the reaction was successfully performed. Whereas the second modification creates copolymers with photosensitive properties.
- We reported that the negative type T photochromism as well as the solvatochromism of DASA molecules was kept after modification of SMA polymers. It is conjectured that the mechanism of the photoswitching was preserved as described previously in the literature after polymer modification. The alternation of the photoisomerization kinetics between parent DASA and modified polymers was observed and analysed by applying two separate

models: Eyring and Arrhenius. Gibbs energy of activation gave 87.60 kJmol^{-1} which is a slight increase in comparison to result provided in the literature for parent DASA molecule 71.17 kJmol^{-1} .

- The supported membranes of SCIII polymers were obtained by evaporation of the solvent and characterized. Their modification upon light exposure were analysed by means of AFM and FT-IR analysis. Both of them reveal that the obtained films are in fact photoactive materials. The alterations detected by those techniques show clear correlation between the roughness, degree of photoswitching and chemical composition of the material. Contact angles analysis resulted as statistically insignificant.
- The series of microcapsules containing SCIII polymers were obtained by number of techniques: 1) phase inversion precipitation; 2) emulsion crosslinking of partially modified SCIII copolymer (DASA modified polymer, molar ratio ST-styrene, MA-maleic anhydride, MI-maleimide; 4ST : 1MA : 2MI; 3) SMA/SCIII emulsion precipitation in different non-solvents; 4) emulsion crosslinking of SCIII with SMA blend.
- SCIII polymers capsules behaviour upon light exposure were analysed by means of optical microscope and GC analysis. Both of them reveal that the obtained capsules were in fact photoactive. However, the effect of light gave an opposite result. Instead of perfume release into the slurry, the free perfume amount decreases upon irradiation. What suggest that in actual fact the capsules attract the perfume upon irradiation and do not release it into the slurry, as previously thought. It is imperative to mention that the employed GC method to evaluate perfume content may not be suitable for our system. The capsules

were exposed to n-heptane in the sample preparation to GC analysis. Therefore, the capsules may precipitate, what implies n-heptane-perfume demixing and subsequent increase of perfume in the slurry.

- We reported on the synthesis acrylate/DASA molecule, which in our case serves as a one of the component of the polyacrylate capsules shell. Optimization of the preparation procedure needs to be conducted as the yield of the reaction resulted was low (7.8%).
- Two approaches for the acrylate capsules modified with DASA were attempted. One included the modification of the polyacrylate capsules with DASA precursor. This functionalization did not give desired result. Second method included the encapsulation of perfume within polyacrylate polymeric shell. The wall of the capsules was composed from mixture of three acrylate monomers, where one of them was synthesised by us - Acrylate/DASA. Optical microscope images of Acrylate/DASA capsules analysis reveal that they were globular in shape and of narrow size distribution.
- The quantitative analysis of perfume released from Acrylate/DASA capsules kept in the dark and exposed to light was made. Capsules that were kept in the dark gave higher content of perfume, than the sample that was subjected to visible light. That is exactly the opposite effect that was expected. Further study is needed to investigate this phenomenon. Our hypothesis is that the capsules while irradiated adsorb the volatile compound, due to the change in physicochemical DASA transformation upon illumination.

9 References

1. S. Nakamura, H. Hirao, T. Ohwada. *The Journal of Organic Chemistry* **69**, 4309-4316 (2004).
2. H. Zulfikri, M. A. J. Koenis, M. M. Lerch, M. Di Donato, W. Szymański, C. Filippi, B. L. Feringa, W. J. Buma. *Journal of the American Chemical Society* **141**, 7376-7384 (2019).
3. H. Bouas-Laurent, H. Dürr. In *Pure and Applied Chemistry*, p. 639 (2001).
4. V. Malatesta. *Molecular Crystals and Liquid Crystals Science and Technology. Section A. Molecular Crystals and Liquid Crystals* **298**, 69-74 (1997).
5. I. Masahiro, U. Kingo. *Bulletin of the Chemical Society of Japan* **71**, 985-996 (1998).
6. In *Photochromic Materials*, pp. 1-45.
7. B. Tylkowski, M. PREGOWSKA, E. Jamowska, R. Garcia-Valls, M. Giamberini. *European Polymer Journal* **45**, 1420-1432 (2009).
8. H. Tian, S. Yang. *Chemical Society Reviews* **33**, 85-97 (2004).
9. R. Klajn. *Chemical Society Reviews* **43**, 148-184 (2014).
10. T. Sendai, S. Biswas, T. Aida. *Journal of the American Chemical Society* **135**, 11509-11512 (2013).
11. A. A. Beharry, O. Sadovski, G. A. Woolley. *Journal of the American Chemical Society* **133**, 19684-19687 (2011).
12. S. Samanta, A. A. Beharry, O. Sadovski, T. M. McCormick, A. Babalhavaeji, V. Tropepe, G. A. Woolley. *Journal of the American Chemical Society* **135**, 9777-9784 (2013).
13. S. Cha, M. G. Choi, H. R. Jeon, S.-K. Chang. *Sensors and Actuators B: Chemical* **157**, 14-18 (2011).
14. M. M. Lerch, M. Medved', A. Lapini, A. D. Laurent, A. Iagatti, L. Bussotti, W. Szymański, W. J. Buma, P. Foggi, M. Di Donato, B. L. Feringa. *The Journal of Physical Chemistry A* **122**, 955-964 (2018).
15. F. Salaön. In *Encapsulation Nanotechnologies*, pp. 137-173. John Wiley & Sons, Inc. (2013).
16. M. M. Dragosavac, M. N. Sovilj, S. R. Kosvintsev, R. G. Holdich, G. T. Vladislavljević. *Journal of Membrane Science* **322**, 178-188 (2008).
17. C. Thies. In *Encyclopedia of Polymer Science and Technology*. John Wiley & Sons, Inc. (2002).
18. C. Perignon, G. Ongmayeb, R. Neufeld, Y. Frere, D. Poncelet. *Journal of Microencapsulation* **32**, 1-15 (2015).

19. L. Sánchez-Silva, M. Carmona, A. de Lucas, P. Sánchez, J. F. Rodríguez. *Journal of Microencapsulation* **27**, 583-593 (2010).
20. A. Supsakulchai, G. H. Ma, M. Nagai, S. Omi. *Journal of Microencapsulation* **20**, 1-18 (2003).
21. I. Katampe, A. Y. Polykarpov, J. C. Camillus. Google Patents (2005).
22. S. Bonetti, M. Farina, M. Mauri, K. Koynov, H.-J. Butt, M. Kappl, R. Simonutti. *Macromolecular Rapid Communications* **37**, 584-589 (2016).
23. S. Kawaguchi, K. Ito. In *Polymer Particles: -/-* (M. Okubo, ed.), pp. 299-328. Springer Berlin Heidelberg, Berlin, Heidelberg (2005).
24. H. H. Lee, F. L. Schadt, M. S. Wolfe. Google Patents (2014).
25. E. Bourgeat-Lami, J. Lang. *Journal of Colloid and Interface Science* **210**, 281-289 (1999).
26. B. K. Green, S. Lowell. Google Patents (1957).
27. G. Dardelle, P. Beaussoubre, P. Erni. Google Patents (2015).
28. R. Kumar, G. Troiano, J. M. Ramstack, P. Herbert, M. Figa. Google Patents (2008).
29. R. Baker, Y. Ninomiya. Google Patents (1988).
30. P. T. Hammond, Z. Poon. Google Patents (2014).
31. W. Yuan, Z. Lu, C. M. Li. *Journal of Materials Chemistry* **21**, 5148-5155 (2011).
32. M. Björnmalm, A. Roozmand, K. F. Noi, J. Guo, J. Cui, J. J. Richardson, F. Caruso. *Langmuir* **31**, 9054-9060 (2015).
33. B. C. Dave, B. Dunn, J. S. Valentine, J. I. Zink. *Analytical Chemistry* **66**, 1120A-1127A (1994).
34. J. D. Wright, N. A. J. M. Sommerdijk. (1990).
35. I. A. Rahman, V. Padavettan. *Journal of Nanomaterials* **2012**, 15 (2012).
36. L. L. Hench, J. K. West. *Chemical Reviews* **90**, 33-72 (1990).
37. R. Ciriminna, M. Sciortino, G. Alonzo, A. d. Schrijver, M. Pagliaro. *Chemical Reviews* **111**, 765-789 (2011).
38. S. A. Yamanaka, F. Nishida, L. M. Ellerby, C. R. Nishida, B. Dunn, J. S. Valentine, J. I. Zink. *Chemistry of Materials* **4**, 495-497 (1992).
39. L. Ellerby, C. Nishida, F. Nishida, S. Yamanaka, B. Dunn, J. Valentine, J. Zink. *Science* **255**, 1113-1115 (1992).
40. L. J. Juszczak, J. M. Friedman. *Journal of Biological Chemistry* **274**, 30357-30360 (1999).
41. R. B. Bhatia, C. J. Brinker, A. K. Gupta, A. K. Singh. *Chemistry of Materials* **12**, 2434-2441 (2000).
42. M.-L. Zhu, Y.-L. Li, Z.-M. Zhang, Y. Jiang. *RSC Advances* **5**, 33262-33268 (2015).

43. M. Moise, V. Şunel, M. Holban, M. Popa, J. Desbrieres, C. Peptu, C. Lionte. *Journal of Materials Science* **47**, 8223-8233 (2012).
44. A. N. Cadinoiu, C. A. Peptu, B. Fache, J.-F. Chailan, M. Popa. *Journal of Microencapsulation* **32**, 381-389 (2015).
45. E. Dini, S. Alexandridou, C. Kiparissides. *Journal of Microencapsulation* **20**, 375-385 (2003).
46. S. L. Percy. Google Patents (1872).
47. J. O. Dihora, J. R. Cetti, S. E. Witt, J. J. Li. Google Patents (2015).
48. L. S. Cardozo, H. H. Tantawy, J. R. Lickiss, N. P. S. Roberts. Google Patents (2011).
49. Z. J. Hussain. Google Patents (1996).
50. M. Maury, K. Murphy, S. Kumar, L. Shi, G. Lee. *European Journal of Pharmaceutics and Biopharmaceutics* **59**, 565-573 (2005).
51. Y. Zhang, Q. Zhong. *Food Hydrocolloids* **33**, 1-9 (2013).
52. A. Nussinovitch. In *Polymer Macro- and Micro-Gel Beads: Fundamentals and Applications*, pp. 163-189. Springer New York, New York, NY (2010).
53. W. Wang, G. I. N. Waterhouse, D. Sun-Waterhouse. *Food Research International* **54**, 837-851 (2013).
54. F. He, W. Wang, X. H. He, X. L. Yang, M. Li, R. Xie, X. J. Ju, Z. Liu, L. Y. Chu. *ACS Appl. Mater. Interfaces* **8**, 8743-8754 (2016).
55. D. Stéphane, D. Frédéric. In *Handbook of Encapsulation and Controlled Release*, pp. 801-832. CRC Press (2015).
56. K. C. Cochrum. Google Patents (1999).
57. M. Akhtar, B. S. Murray, E. I. Afeisume, S. H. Khew. *Food Hydrocolloids* **34**, 62-67 (2014).
58. C. Frey. In *Microencapsulation in the Food Industry*, pp. 65-79. Academic Press, San Diego (2014).
59. S. K. Ghosh. In *Functional Coatings*, pp. 1-28. Wiley-VCH Verlag GmbH & Co. KGaA (2006).
60. M. Vanderroost, F. Ronsse, K. Dewettinck, J. Pieters. *Journal of Food Engineering* **106**, 220-227 (2011).
61. M. Mulder. In *Encyclopedia of Separation Science* (I. D. Wilson, ed.), pp. 3331-3346. Academic Press, Oxford (2000).
62. C. Panisello, B. Peña, T. Gumí, R. Garcia-Valls. *Journal of Applied Polymer Science* **129**, 1625-1636 (2013).
63. B. Peña, C. Panisello, G. Aresté, R. Garcia-Valls, T. Gumí. *Chemical Engineering Journal* **179**, 394-403 (2012).
64. S. Helmy, F. A. Leibfarth, S. Oh, J. E. Poelma, C. J. Hawker, J. Read de Alaniz. *Journal of the American Chemical Society* **136**, 8169-8172 (2014).

65. A. N. Meldrum. *Journal of the Chemical Society, Transactions* **93**, 598-601 (1908).
66. H. McNab. *Chemical Society Reviews* **7**, 345-358 (1978).
67. E. Fillion, A. M. Dumas, S. A. Hogg. *The Journal of Organic Chemistry* **71**, 9899-9902 (2006).
68. S. M. Senaweera, J. D. Weaver. *The Journal of Organic Chemistry* **79**, 10466-10476 (2014).
69. C. Trujillo, P. Goya, I. Rozas. *The Journal of Physical Chemistry A* **122**, 2535-2541 (2018).
70. E. J. Corey. *Journal of the American Chemical Society* **74**, 5897-5905 (1952).
71. A. M. Dumas, A. Seed, A. K. Zorzitto, E. Fillion. *Tetrahedron Letters* **48**, 7072-7074 (2007).
72. S. Salahi, M. T. Maghsoodlou, N. Hazeri, M. Lashkari, S. Garcia-Granda, L. Torre-Fernandez. *Chinese Journal of Catalysis* **36**, 1023-1028 (2015).
73. J. A. Hedge, C. W. Kruse, H. R. Snyder. *The Journal of Organic Chemistry* **26**, 3166-3170 (1961).
74. D. Tahmassebi, L. J. A. Wilson, J. M. Kieser. *Synthetic Communications* **39**, 2605-2613 (2009).
75. N. B. Darvatkar, A. R. Deorukhkar, S. V. Bhilare, M. M. Salunkhe. *Synthetic Communications* **36**, 3043-3051 (2006).
76. F. Bigi, S. Carloni, L. Ferrari, R. Maggi, A. Mazzacani, G. Sartori. *Tetrahedron Letters* **42**, 5203-5205 (2001).
77. C. F. Jasso-Gastinel, J. F. A. Soltero-Martínez, E. Mendizábal. In *Modification of Polymer Properties* (C. F. Jasso-Gastinel, J. M. Kenny, eds.), pp. 1-21. William Andrew Publishing (2017).
78. C. E. Carraher, M. Tsuda. In *Modification of Polymers*, pp. 1-4. AMERICAN CHEMICAL SOCIETY (1980).
79. J.-C. Soutif, J.-C. Brosse. *Reactive Polymers* **12**, 3-29 (1990).
80. Z. Jin, L. Du, C. Zhang, Y. Sugiyama, W. Wang, G. Palui, S. Wang, H. Mattoussi. *Bioconjugate Chemistry* **30**, 871-880 (2019).
81. Z. Wang, C. Kim, A. Facchetti, T. J. Marks. *Journal of the American Chemical Society* **129**, 13362-13363 (2007).
82. F. Buller, L. Mannocci, Y. Zhang, C. E. Dumelin, J. Scheuermann, D. Neri. *Bioorganic & Medicinal Chemistry Letters* **18**, 5926-5931 (2008).
83. G. Gelbard. *Industrial & Engineering Chemistry Research* **44**, 8468-8498 (2005).
84. C. H. McAteer, R. Murugan, Y. V. S. Rao. In *Heterocyclic Chemistry in the 21st Century: A Tribute to Alan Katritzky* (E. F. V. Scriven, C. A. Ramsden, eds.), pp. 173-205 (2017).

85. M. Ehteshami, N. Rahimi, A. A. Eftekhari, M. Nasr. *Iranian Journal of Science & Technology, Transaction B, Engineering* **30** (2006).
86. S. K. Hota, A. Chatterjee, P. K. Bhattacharya, P. Chattopadhyay. *Green Chemistry* **11**, 169-176 (2009).
87. D. J. Pietrzyk. *Talanta* **16**, 169-179 (1969).
88. J. Stenhouse. *Justus Liebigs Annalen der Chemie* **74**, 278-297 (1850).
89. T. Hofmann. *Journal of Agricultural and Food Chemistry* **46**, 932-940 (1998).
90. S. Helmy, J. R. de Alaniz. *Abstracts of Papers of the American Chemical Society* **244** (2012).
91. N. T. H. Ha. *Polymer* **40**, 1081-1086 (1999).
92. Z. Ai Qin, S. Yinghua, Z. Xiangying, H. Lingcui, W. Zhizhong. *Journal of Polymer Research* **17**, 11 (2009).
93. H. J. Harwood. *Angewandte Chemie International Edition in English* **4**, 394-401 (1965).
94. H. J. Harwood, W. M. Ritchey. *Journal of Polymer Science Part B-Polymer Letters* **2**, 601-& (1964).
95. L. Coleman, J. Bork, H. Dunn. *The Journal of Organic Chemistry* **24**, 135-136 (1959).
96. J. A. Sinegra, G. Carta. *Industrial & Engineering Chemistry Research* **26**, 2437-2441 (1987).
97. N. B. Colthup, L. H. Daly, S. E. Wiberley. In *Introduction to Infrared and Raman Spectroscopy (Third Edition)* (N. B. Colthup, L. H. Daly, S. E. Wiberley, eds.), pp. 327-337. Academic Press, San Diego (1990).
98. N. B. Colthup, L. H. Daly, S. E. Wiberley. In *Introduction to Infrared and Raman Spectroscopy (Third Edition)* (N. B. Colthup, L. H. Daly, S. E. Wiberley, eds.), pp. 289-325. Academic Press, San Diego (1990).
99. N. B. Colthup, L. H. Daly, S. E. Wiberley. In *Introduction to Infrared and Raman Spectroscopy (Third Edition)* (N. B. Colthup, L. H. Daly, S. E. Wiberley, eds.), pp. 339-354. Academic Press, San Diego (1990).
100. P. C. Painter, J. L. Koenig. *Journal of Polymer Science: Polymer Physics Edition* **15**, 1885-1903 (1977).
101. J. L. Koenig. In *Spectroscopy of Polymers (Second Edition)* (J. L. Koenig, ed.), pp. 77-145. Elsevier Science, New York (1999).
102. A. V. Rane, S. A. Begum, K. Kanny. In *Compatibilization of Polymer Blends* (A. A.R, S. Thomas, eds.), pp. 373-390. Elsevier (2020).
103. M. Buback, M. Busch, T. DrÖGe, F.-O. MÄHling, C. Prellberg. *European Polymer Journal* **33**, 375-379 (1997).

104. R. Schaefer, J. Kressler, R. Neuber, R. Muelhaupt. *Macromolecules* **28**, 5037-5042 (1995).
105. G. A. Webb. In *Encyclopedia of Spectroscopy and Spectrometry (Third Edition)* (J. C. Lindon, G. E. Tranter, D. W. Koppenaal, eds.), pp. 274-283. Academic Press, Oxford (2017).
106. J. Schut, D. Bolikal, I. Khan, A. Pesnell, A. Rege, R. Rojas, L. Sheihet, N. Murthy, J. Kohn. *Polymer* **48**, 6115-6124 (2007).
107. H. A. Schneider. *Polymer* **46**, 2230-2237 (2005).
108. M.-M. Russew, S. Hecht. *Advanced Materials* **22**, 3348-3360 (2010).
109. S. Helmy, S. Oh, F. A. Leibfarth, C. J. Hawker, J. R. de Alaniz. *Journal of Organic Chemistry* **79**, 11316-11329 (2014).
110. Y. Kamiya, T. Takagi, H. Ooi, H. Ito, X. Liang, H. Asanuma. *ACS Synthetic Biology* **4**, 365-370 (2015).
111. M. F. Budyka, V. M. Li. *Photochemical & Photobiological Sciences* **17**, 213-220 (2018).
112. A. Kumar, K. Prakash, P. R. Sahoo, S. Kumar. *ChemistrySelect* **2**, 8247-8252 (2017).
113. E. S. Dodsworth, M. Hasegawa, M. Bridge, W. Linert. In *Comprehensive Coordination Chemistry II* (J. A. McCleverty, T. J. Meyer, eds.), pp. 351-365. Pergamon, Oxford (2003).
114. A. Hantzsch. *Berichte der deutschen chemischen Gesellschaft (A and B Series)* **55**, 953-979 (1922).
115. V. A. Barachevsky. *Review Journal of Chemistry* **7**, 334-371 (2017).
116. O. Nieto Faza, C. Silva López, R. Álvarez, Á. R. de Lera. *Chemistry – A European Journal* **10**, 4324-4333 (2004).
117. C. Verrier, S. Moebis-Sanchez, Y. Queneau, F. Popowycz. *Organic & Biomolecular Chemistry* **16**, 676-687 (2018).
118. M. J. Riveira, L. A. Marsili, M. P. Mischne. *Organic & Biomolecular Chemistry* **15**, 9255-9274 (2017).
119. S. Ulrich, J. R. Hemmer, Z. A. Page, N. D. Dolinski, O. Rifaie-Graham, N. Bruns, C. J. Hawker, L. F. Boesel, J. Read de Alaniz. *Acs Macro Letters* **6**, 738-742 (2017).
120. Y. Chen, Z. Li, H. Wang, Y. Pei, Y. Shi, J. Wang. *Langmuir* **34**, 2784-2790 (2018).
121. H. Zhao, D. Wang, Y. Fan, M. Ren, S. Dong, Y. Zheng. *Langmuir* **34**, 15537-15543 (2018).
122. O. Rifaie-Graham, S. Ulrich, N. F. B. Galensowske, S. Balog, M. Chami, D. Rentsch, J. R. Hemmer, J. Read de Alaniz, L. F. Boesel, N. Bruns. *Journal of the American Chemical Society* **140**, 8027-8036 (2018).

123. S. Singh, K. Friedel, M. Himmerlich, Y. Lei, G. Schlingloff, A. Schober. *Acs Macro Letters* **4**, 1273-1277 (2015).
124. S. H. Mostafavi, W. Li, K. D. Clark, F. Stricker, J. R. d. Alaniz, C. J. Bardeen. *Macromolecules* **52**, 6311-6317 (2019).
125. M. M. Lerch, S. J. Wezenberg, W. Szymanski, B. L. Feringa. *Journal of the American Chemical Society* **138**, 6344-6347 (2016).
126. M. Di Donato, M. M. Lerch, A. Lapini, A. D. Laurent, A. Iagatti, L. Bussotti, S. P. Ihrig, M. Medved', D. Jacquemin, W. Szymański, W. J. Buma, P. Foggi, B. L. Feringa. *Journal of the American Chemical Society* **139**, 15596-15599 (2017).
127. S. Helmy, S. Oh, F. A. Leibfarth, C. J. Hawker, J. Read de Alaniz. *The Journal of Organic Chemistry* **79**, 11316-11329 (2014).
128. M. Peleg, M. D. Normand, M. G. Corradini. *Critical Reviews in Food Science and Nutrition* **52**, 830-851 (2012).
129. M. M. Lerch, M. Di Donato, A. D. Laurent, M. Medved, A. Iagatti, L. Bussotti, A. Lapini, W. J. Buma, P. Foggi, W. Szymański, B. L. Feringa. *Angewandte Chemie - International Edition* **57**, 8063-8068 (2018).
130. M. K. Purkait, M. K. Sinha, P. Mondal, R. Singh. In *Interface Science and Technology* (M. K. Purkait, M. K. Sinha, P. Mondal, R. Singh, eds.), pp. 1-37. Elsevier (2018).
131. M. Mulder. In *Basic Principles of Membrane Technology* (M. Mulder, ed.), pp. 71-156. Springer Netherlands, Dordrecht (1996).
132. J. E. Yap, N. Mallo, D. S. Thomas, J. E. Beves, M. H. Stenzel. *Polymer Chemistry* **10**, 6515-6522 (2019).
133. R. N. Wenzel. *Industrial & Engineering Chemistry* **28**, 988-994 (1936).
134. A. Nogalska, A. Trojanowska, B. Tylkowski, R. Garcia-Valls. *Physical Sciences Reviews* (2019).
135. In *Analysis of Variance Designs: A Conceptual and Computational Approach with SPSS and SAS* (A. J. Guarino, G. Gamst, L. S. Meyers, eds.), pp. 21-22. Cambridge University Press, Cambridge (2008).
136. In *Analysis of Variance Designs: A Conceptual and Computational Approach with SPSS and SAS* (A. J. Guarino, G. Gamst, L. S. Meyers, eds.), pp. 34-48. Cambridge University Press, Cambridge (2008).
137. R. Garcia-Valls, C. Panisello. *Microencapsulation by Phase Inversion Precipitation*. Crc Press-Taylor & Francis Group, Boca Raton (2016).
138. B. Pena, C. Panisello, G. Areste, R. Garcia-Valls, T. Gumi. *Chem. Eng. J.* **179**, 394-403 (2012).

139. K. A. Bogdanowicz, B. Tylkowski, M. Giamberini. *Langmuir* **29**, 1601-1608 (2013).
140. C. Panisello, B. Pena, T. Gumi, R. Garcia-Valls. *J. Appl. Polym. Sci.* **129**, 1625-1636 (2013).
141. H. G. H. Melick, L. E. Govaert, H. Meijer. *Polymer* **44**, 2493-2502 (2003).
142. A. Shulkin, H. D. H. Stöver. *Journal of Membrane Science* **209**, 421-432 (2002).
143. E. L. Wittbecker, P. W. Morgan. *Journal of Polymer Science* **40**, 289-297 (1959).
144. R. G. Beaman, P. W. Morgan, C. R. Koller, E. L. Wittbecker, E. E. Magat. *Journal of Polymer Science* **40**, 329-336 (1959).
145. W. M. Eareckson. *Journal of Polymer Science* **40**, 399-406 (1959).
146. P. W. Morgan, S. L. Kwolek. *Journal of Polymer Science Part A: Polymer Chemistry* **34**, 531-559 (1996).
147. G. B. Beestman, J. M. Deming. Google Patents (1983).



UNIVERSITAT
ROVIRA i VIRGILI